Atmospheric Research 252 (2021) 105432

Contents lists available at ScienceDirect

Atmospheric Research

journal homepage: www.elsevier.com/locate/atmosres

Invited review article

A review of the impact of transient luminous events on the atmospheric chemistry: Past, present, and future

F.J. Gordillo-Vázquez [a,*], F.J. Pérez-Invernón [b]

[a] Instituto de Astrofísica de Andalucía (IAA - CSIC), Glorieta de la Astronomía s/n, 18008 Granada, Spain
[b] Deutsches Zentrum für Luft- und Raumfahrt, Institut für Physik der Atmosphäre, Oberpfaffenhofen, Germany

ARTICLE INFO

Keywords:
TLEs
Atmospheric chemistry
Lightning
Streamers
Cloud corona discharges
Greenhouse gases
Imaging
Spectroscopy
Modeling

ABSTRACT

Atmospheric electricity has been intensively studied during the last 30 years after the discovery in 1989 of different forms of upper atmospheric electrical discharges (so–called Transient Luminous Events) triggered by lightning in the troposphere. In spite of the significant number of investigations that led to important new results unveiling how lightning produces a zoo of transient electrical discharges from the upper troposphere to the mesosphere, there is still no clear understanding about how all sort of TLEs – including those that occur inside thunderclouds – can contribute to the chemistry of the atmosphere both at the local and global scale. This review paper aims at presenting a perspective on the TLE atmospheric chemistry research done in the past, in the present as well as to describe some of the challenges that await ahead to find the true scientific importance of the non-equilibrium atmospheric chemistry triggered by TLEs. This review comes to conclude that while the global chemical impact of elves and halos are almost negligible, the large scale chemical impact of sprites, blue jets and blue starters and that of impulsive cloud corona discharges might be non–negligible in terms of their possibly measurable contribution to important greenhouse gases such as ozone and nitrous oxide (N_2O). Being the third strongest greenhouse gas (after carbon dioxide and methane) and by having the ability to deplete ozone, precise determination of atmospheric N_2O sources is of increasing and pressing demand. A new era in atmospheric electricity is just emerging in which dedicated scientific space missions (ISS–LIS, ASIM) together with geostationary lightning sensors (since 2016) and new micro–scale and parameterizations of TLEs in general atmospheric chemistry circulation models will hopefully help to start clarifying the full role of TLEs in the chemistry of the atmosphere.

1. Introduction

Thirty years ago (in July 1990) Franz et al. (1990) announced to the international scientific community the discovery of the so-called sprites that had been originally recorded the year before (1989) as two transient luminous columns of light over a large thunderstorm over the mid-western United States. Prior to 1989 several nonscientific (eyewitness) reports had informed about flashes of light over thunderstorm clouds (Lyons, 2006). Also, some amateur images, taken in 1968 and early 1980s, were published after 1989. Those prior to 1989 images showed exotic atmospheric phenomena, the so-called blue jets later on associated with stratospheric electric discharges officially discovered in 1994 and that can reach terminal altitudes of 30–45 km (Wescott et al., 2001a). Both sprites and blue jets belong nowadays to a new type of atmospheric electricity phenomena named Transient Luminous Events (TLEs).

Franz et al. (1990) estimated that the flashes of light they discovered extended from the cloud tops at ~14 km to the lower stratosphere. However, three years later Sentman and Wescott (1993) demonstrated that sprites were not stratospheric phenomena. They provided the first reasonable estimates of sprite terminal heights (65–90 km) derived from data obtained with an all-sky TV camera aboard a NASA aircraft flying around large thunderstorms over Iowa in 1993. A bit later Sentman et al. (1995) made the first accurate two-station, three-dimensional triangulation of sprites from two aircrafts flying at 12.2 and 12.8 km altitude, respectively. They demonstrated conclusively that sprites are mesospheric phenomena with tops reaching over 90 km, essentially reaching to the base of the ionosphere (Wescott et al., 2001a).

Why did sprites occur in the mesosphere and blue jets in the stratosphere? How were they produced? What was the nature of sprites

* Corresponding author.
E-mail address: vazquez@iaa.es (F.J. Gordillo-Vázquez).

https://doi.org/10.1016/j.atmosres.2020.105432
Received 31 August 2020; Received in revised form 30 November 2020; Accepted 23 December 2020
Available online 4 January 2021

and blue jets and what was their chemical influence in the global atmospheric chemistry? What other types of TLEs could exist? These questions started to be answered step by step and in order of complexity. However, a number of unknowns remain, especially regarding the comprehensive understanding of the chemical influence of TLEs in the atmosphere.

Some of the questions posed above started to receive answers after the revision of C. T. R Wilson's considerations (Wilson, 1924) about the existence of an altitude in the atmosphere where the transient quasi-electrostatic electric field induced by electric charges in thunderclouds should exceed the conventional local air breakdown electric field (E_k) that is proportional to the air density. Therefore, sprites would initiate at altitudes between 75 and 85 km where the electric field can be sustained against the fast relaxation time typical of the highly conducting upper mesosphere and where the air density is sufficiently low (Pasko et al., 2012).

A number of space, balloon, aircraft and ground-based instruments have been designed and operated for the observation of TLEs since their discovery in 1989. TLEs emit flashes of light, radio (Inan et al., 2010) and acoustic signals in the form of infrasound (Farges et al., 2005). All these different types of signatures have been used to detect and understand all sort of TLEs during the last 30 years. In particular, long term space instruments have been developed to study the frequency of occurrence, global distribution and key optical emissions from TLEs. These space instruments are the Imager of Sprites and Upper Atmospheric Lightning (ISUAL) (Chern et al., 2003) on board the FORMOSAT–2 satellite operated between 2004 and 2016 (different types of TLEs observed by ISUAL are shown in Fig. 1), the Japanese Experiment Module – Global LIghtning and sprite MeasurementS (JEM-GLIMS) (Ushio et al., 2011; Sato et al., 2015) between 2012 and 2015 and the Atmosphere Space Interaction Monitor (ASIM) (Neubert et al., 2019) launched in April 2018 and presently in operation. Both JEM-GLIMS and ASIM were on board the International Space Station (ISS). Several Russian space missions were devoted to study transient events in the atmosphere of the Earth. Those missions were the Tatyana–2 satellite (Garipov et al., 2013), launched on September 20, 2009, the Vernov satellite (Panasyuk et al., 2016a, 2016b), launched on July 8, 2014 and the Tracking Ultraviolet Setup (TUS) aboard the Lomonosov Satellite (Khrenov et al., 2020), launched on April 28, 2016. The missions were planned for several years in orbit but, due to technical problems, their lifetimes spanned only for 3 months (Tatyana–2), 5 months (Vernov) and a bit less than 18 months (TUS).

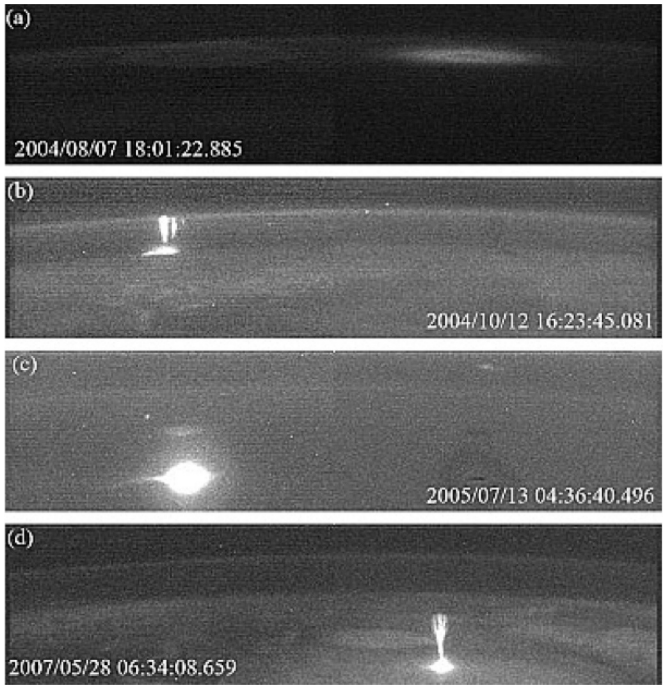

Fig. 1. ISUAL recorded images of different types of TLEs: (a) elve, (b) sprite, (c) halo and (d) giant blue jet. Image reproduced from Chen et al. (2008). (For interpretation of the references to colour in this figure legend, the reader is referred to the web version of this article.)

There were also other important short period space missions aimed at observing TLEs from space such as the early Lightning and Sprite Observation (LSO) experiment on board the ISS (Blanc et al., 2004; Farges and Blanc, 2016), the sprite observation campaign from the space shuttle during the Mediterranean Israeli dust experiment (MEIDEX) (Yair et al., 2003), and the recording of color images of sprites from the ISS in the framework of the NASA Crew Earth Observation (Jehl et al., 2013) and during the JAXA Cosmic Shore program (Yair et al., 2013).

In the following we will briefly introduce some observational and model descriptions of TLEs originated in the mesosphere, that is, TLEs clearly associated to parent lightning. We will start with sprites (the first discovered TLE) and will follow with introductory comments about elves and halos. Other TLEs originated in the upper troposphere like blue jets, blue starters (or cloud corona discharges) and giant blue jets are left aside in this introduction and will be discussed in later sections.

Sentman et al. (1995) showed that sprites are loosely correlated with positive cloud to ground (+CG) lightning occurrences in the decaying portion of a thunderstorm. Boccippio et al. (1995) demonstrated with more examples that sprites are associated, within a few milliseconds, with +CG flashes. Later, Barrington-Leigh et al. (1999) showed that sprites may also be occasionally produced by -CG flashes. After the realistic determination of sprite altitudes and their connection to lightning, a number of studies followed to understand sprite characteristic nature. In this regard, the first real color image and spectra of sprites were published by Sentman et al. (1995), and Hampton et al. (1996) and Green et al. (1996), respectively.

Theoretical models by Pasko et al. (1995, 1997, 1998) showed that the electric field responsible for the quasi-electrostatic heating, ionization, and optical emissions of sprites is caused by the charge moment changes associated with the movement of large thundercloud charges during +CG or -CG discharges. These models predicted a diffuse region near the top of sprites, which was identified with the observations and triangulation of halos reported by Wescott et al. (2001b).

A number of early sprite observations carried out during the mid 1990s detected intense blue optical emissions with highly localized filamentary structures appearing in the initial stages of sprite formation (Sentman et al., 1996; Stanley et al., 1996; Taylor and Clark, 1996; Armstrong et al., 1998; Suszcynsky et al., 1998). This was an indication that, in addition to the upper diffuse glowing sprite structure, sprites were also formed by the so-called streamers which are filamentary plasmas driven by highly nonlinear space charge waves (Raizer, 1991). This fast moving ionization fronts can produce complex filamentary structures that can divide into different branches and can interact among them (Luque and Ebert, 2014). More recently Ihaddadene and Celestin (2015) have used a fluid model to investigate the production of X–rays emissions associated to head–on collisions between negative and positive streamer discharges that could produce high electric fields leading to X–rays emissions.

The first model that investigated the spatial and temporal scales of sprites including their streamers was published by Pasko et al. (1998). This study found that the appearance of sprites was dictated by the relative importance of key characteristic times such as the attachment time scale (τ_a), the ambient dielectric relaxation time (τ_σ) connected with the air electrical conductivity or the time for the development of an individual electron avalanche into a streamer (t_s)(Pasko et al., 1998).

Pasko et al. (1998) found three distinct altitude regions: (1) The diffuse region ($>$ 85 km, $\tau_\sigma < \tau_a$, $\tau_\sigma < t_s$) characterized by collective multiplication of electrons (Townsend mechanism); (2) the transition region (between 75 and 85 km, $\tau_\sigma > \tau_a$, $\tau_\sigma \leq t_s$) characterized by strong

attachment of ambient electrons before the onset of the electric breakdown and (3) the streamer region (<75 km, $\tau_\sigma > \tau_a$, $\tau_\sigma > t_s$) also characterized by strong attachment as well as by individual electron avalanches evolving into streamers. The distinction between an upper region with diffuse appearance and the lower filamentary region was observationally confirmed in the beginning of the XXI century (Stenbaek-Nielsen et al., 2000; Pasko and Stenbaek-Nielsen, 2002; Gerken, 2002; Gerken and Inan, 2003).

As commented in Pasko et al. (1998), the idea of streamer electric breakdown as an essential part of sprite development agreed with previous observations of sprite fine structure going well below the, by that time, good video spatial resolution of ≤ 100 m (Fukunishi et al., 1996; Sentman et al., 1996; Stanley et al., 1996; Taylor and Clark, 1996). Subsequent telescopic imaging of sprites revealed a variety of vertical fine structure with transverse spatial scales ranging from tens to a few hundreds of meters (Gerken et al., 2000; Gerken, 2002; Gerken and Inan, 2003).

The so–called elves (Emissions of Light and Very Low Frequency Perturbations from Electromagnetic Pulse Sources), which are the most frequent type of TLEs, were predicted by Inan et al. (1991) as the manifestation of the impulsive (radiative) electric field component of lightning. The first observation of elves from space was accomplished by the Space Shuttle (Boeck et al., 1992). Elves were first detected from ground by Fukunishi et al. (1996) as diffuse optical flashes with a duration of < 1 ms occurring just after the onset of CG lightning. Elves are a consequence of the heating of electron produced by lightning-generated electromagnetic pulses (EMPs) (Inan et al., 1991, 1997; Moudry et al., 2003). This type of TLE is usually observed in a thin layer of the upper atmosphere usually located at ~ 88 km of altitude (van der Velde and Montanyà, 2016), with a radius of more than 200 km. Barrington-Leigh and Inan (1999) showed that elves may be caused by both positive and negative CG strokes. Lightning detection networks associate most observed elves with CG lightning discharges with peak currents above ~ 88 kA (Blaes et al., 2016) and whose electromagnetic emission pattern produces toroidal light emissions in the lower ionosphere (Moudry et al., 2003; van der Velde and Montanyà, 2016). However, elves can also exhibit a non donut–like shape when their parent lightning are not vertically oriented (Pérez-Invernón et al., 2017).

Sprite halos, a distinctive type of TLE, are diffuse optical emissions associated with lightning discharges that initially looked like elves but upon close examination were revealed to be a separate lower altitude phenomenon from elves (Barrington-Leigh and Inan, 1999; Barrington-Leigh et al., 2001). The investigations of Barrington-Leigh and Inan (1999) and Barrington-Leigh et al. (2001) presented evidence from a high–speed imager (recording at 3000 fps) and a photometer array that true elves are observed at higher altitudes than halos occurring at 70–80 km (when the reduced electric field created by lightning reaches the air breakdown value of ≃ 120 Td) and with a much larger diameter (300 km) and shorter duration (< 1 ms) than sprite halos with typical diameters of 100 km and durations between 1 and 3 ms. Halos are usually seen accompanying sprites but are also seen to appear alone (Wescott et al., 2001b; Marshall et al., 2006; Kuo et al., 2013). Halos are frequently associated with negative or positive CG lightning discharges (Bering et al., 2002, 2004b; Bering et al., 2004a; Frey et al., 2007), since the return stroke stage of the CG lightning can transfer more total charge than intracloud or cloud-to-cloud lightning discharges (Maggio et al., 2009; Rakov and Uman, 2003).

Similarities between spectra of sprites recorded by Hampton et al. (1996), Mende et al. (1995) and Green et al. (1996) and those of sprite halos (Heavner, 2000) and halos (Wescott et al., 2001b) suggested that sprites and halos shared a common mechanism for the excitation of molecular optical emissions.

In regard to the chemistry of the atmosphere, the presence of streamers as a consequence of the triggering process of sprites in the mesosphere is a key discovery that, as we will explain later, is crucial for unveiling the full chemical influence of some TLEs – like sprites, blue jets, blue starters and transient coronas in thunderclouds – in the global atmospheric chemistry.

In the following sections of this review we will first comment key differences between lightning and TLE chemistry in Section 2. Section 3 will be devoted to discuss what we know to date about the atmospheric chemical effects of a variety of TLEs occurring in the different layers of the atmosphere from the mesosphere to the upper troposphere. Later, in Section 4, we discuss some key past, present and future space, balloon, aircraft and ground-based instruments that have contributed, are contributing or have the potential to contribute to increase our knowledge about the nature of TLEs and their influence on the atmospheric chemistry.

The last two sections before the conclusions deal with some of the challenges (that in our view) are facing present day microphysical modeling of streamer containing TLEs (Section 5), and how the implementation of TLEs in general circulation models (GCM) (Section 6) can help to shape and constrain the chemical effects of some TLEs on the concentration and geographical distribution of key greenhouse gases like ozone (O_3) and nitrous oxide (N_2O). We will finalize the paper with some conclusions and considerations on possible future research avenues aimed at quantifying and clarifying the true role and possible contribution of the chemical output from TLEs in the context of the global atmospheric chemistry.

2. Atmospheric chemistry of lightning and transient luminous events: key features

In contrast to hot channels of ordinary lightning, which can reach equally high gas and electron temperatures (≃ 1000–40,000 K, ≃ 3.5 eV (Walker and Christian, 2019)), the filamentary region of some TLEs such sprites in the mesosphere, blue jets and blue starters in the upper troposphere and stratosphere and corona discharges in thunderclouds in the troposphere are made of many cold filaments, called streamers (already mentioned above), with a non-uniform electric field several times larger in the streamer head than in its body. This streamer head transmits a considerable amount of energy to ambient electrons that become "hotter" (≃ 8–10 eV) than the surrounding heavy (gas) particles. While normal lightning is a hot and thermal plasma (gas and electron temperatures are high and similar), streamer discharges are cold and non-thermal plasmas (heavy particles are cold while electrons are very hot), and this underlies their different efficiency in producing key chemical species.

State-of-the-art laboratory studies show that ordinary lightning channels produce high amounts of nitrogen oxides NO_x ($NO+NO_2$), but their direct O_3 and N_2O production is small (Wang et al., 1998; Schumann and Huntrieser, 2007). In contrast, streamers in laboratory corona discharges effectively produce considerable O_3 and N_2O, but only negligible amounts of NO (Levine et al., 1979, 1981; Peyrous and Lapeyre, 1982; Brandvold et al., 1989, 1996; Simek, 2002; Pontiga and Castellanos, 2006; Hill et al., 1988; Ridley et al., 2006; Simek et al., 2002; Zahn et al., 2002). The global occurrence rate of all types of TLEs is still not completely known in spite of recent observational results (Chen et al., 2019). Thundercloud corona discharges are now known to be much more common than previously understood, due to recent instrumental advances (Rison et al., 2016) but their global occurrence rate is not yet known. Thus, some types of TLEs in the upper atmosphere and cloud corona discharges, which can occur continuously in the vicinity of ordinary lightning, but also by themselves, may be a critical additional source of O_3 and N_2O in convectively active areas.

Being the third strongest greenhouse gas (after carbon dioxide and methane) and by having the ability to deplete O_3 (Portmann et al., 2012), precise determination of atmospheric N_2O sources is of increasing and pressing demand. Besides the N_2O production by some TLEs and corona discharges, further N_2O emissions from the boundary layer can be rapidly transported upward by deep convection as observed for other gas tracers as CO (Huntrieser et al., 2016). If storms originate

over extended agricultural areas, significant amounts of N_2O from soils, resulting from the increased use of fertilizers (Mosier et al., 1997; Battye et al., 2017; Tian et al., 2018), may be transported to the upper troposphere –lower stratosphere region. Thus, current research emphasizes the need for an identification and quantification of all N_2O sources and sinks with corresponding assessment of their importance in relation to the atmospheric N_2O budget in this highly climate-sensitive region.

3. Atmospheric chemical effects of TLEs

The generic name Transient Luminous Events (TLEs) is applied to the new types of thunderstorm related upper atmospheric electricity phenomena discovered between 1989 and 2002. TLEs are characterized by exhibiting short ($\leq$1 s) duration optical flashes varying between submilliseconds (in the case of elves), a few milliseconds (in the case of sprites and halos) and tens to hundreds of milliseconds for blue jets, blue starters and giant blue jets. Added to the generic TLEs, there are cloud corona discharges. Cloud corona discharges are another type of frequent and potentially important transient electrical phenomena (Wiens et al., 2008) that occur in thunderclouds and which contribution to atmospheric greenhouse gas chemistry could be critical.

A unique feature of TLEs is the transient (impulsive) nature of the high (between 100 Td and 500 Td; 1 Td = 10^{-17} V cm^{-2}) reduced electric fields (E/N) that drives them. This fast (some microseconds) non-thermal electric injection of energy to atmospheric electrons allows TLEs to activate non-equilibrium atmospheric chemical reactions that would not be possible otherwise. Examples of chemical reactions of atmospheric importance are the limitation of the natural concentration of stratospheric ozone due to the action of nitride oxide (NO) and nitrogen dioxide (NO_2) through the reactions $NO + O_3 \rightarrow NO_2 + O_2$ and $NO_2 + O \rightarrow NO + O_2$ operating at ambient temperatures (Crutzen, 1970). Another example is the so-called basic Zeldovich mechanism (underlying NO formation in ordinary lightning) that comprises a slow $N_2 + O \rightarrow NO + N$ and a fast $N + O_2 \rightarrow NO + O$ chemical reaction that are efficient only for temperatures of about 1500 K.

Recent results of upper troposphere NO_x chemistry indicates that the day time lifetime of upper troposphere NO_x is $\simeq$ 3 h near thunderstorms and $\simeq$ 0.5–1.5 days away from thunderstorms (Nault et al., 2016; Nault et al., 2017). This results in enhanced O_3 production in the cloud outflow of active convection (Pickering et al., 2016; Hauglustaine et al., 2001; DeCaria et al., 2005; Ott et al., 2007; Finney et al., 2016; Allen et al., 2010). As O_3 is known to be a greenhouse gas and a strong oxidant and absorber of ultraviolet radiation (Myhre et al., 2017), the contributions of lightning produced NO_x (LNO_x) to O_3 production also have an effect on climate forcing (Zhang et al., 2020).

In the case of TLEs, energetic (non-thermal) electrons can lead to a diversity of kinetic processes like excitation, dissociation, attachment, detachment and ionization that provide additional sources of NO and other key atmospheric species like the greenhouse gases N_2O or O_3. Careful evaluation of the global occurrence frequency of TLEs in the atmosphere and their thermal non-equilibrium chemical activity is needed to have a complete and comprehensive understanding of their full chemical impact on the atmosphere.

The types of TLEs occurring in the atmosphere can be primarily classified as those appearing diffusive like elves and halos, those combining an upper diffusive glow and a lower filamentary region like sprites, those like blue jets including many streamers and a leader stem resembling an upward moving lightning and, finally, those mainly formed by streamers like blue starters and thundercloud coronas. Each of these TLEs can trigger a variety of non-thermal chemical processes in the atmosphere whose importance is mainly determined by the frequency of the different types of TLEs, and the magnitude and duration of the underlying electric fields.

3.1. Mesosphere: sprites

The initial research efforts to understand sprites after their official discovery by Franz et al. (1990) were mainly devoted to determine the physical mechanisms that originate them. Therefore, most investigations were oriented to unveil the relationships of sprites with causal electrical processes in thunderstorms and lightning occurring in the troposphere. No much attention was paid in the early sprite research years to explore the possible local and/or global impact of the new atmospheric electricity phenomena in the chemistry of the atmosphere. The first real color image of a cluster of sprites shown in Fig. 2 was recorded in 1994 (Sentman et al., 1995). Soon after the discovery of TLEs in North America, different studies and observations started in Europe (Neubert et al., 2001), the eastern Mediterranean (Ganot et al., 2007), China and oceans around Taiwan (Su et al., 2002; Yang et al., 2008, 2020), Japan (Suzuki et al., 2006) and South America (Pinto et al., 2004).

The paper by Sentman et al. (1995) was the first to alert the scientific community about the importance of possible long term consequences of sprite and blue jet occurrence within the mesosphere and stratosphere. They were calling the attention on the possibility of electrochemical modifications to the ambient atmosphere and the creation of long-lived chemical by-products that would otherwise be absent in the upper atmosphere. The production of ionized and/or electronically excited species could conceivably lead to the creation of reactive species, which could in turn initiate chains of free radical chemical reactions. Similarly, one might consider the electrochemical production and/or activation of catalytic species in the atmosphere locally produced by sprites and blue jets that could subsequently lead to possible global chemical effects of some importance.

The full understanding of the atmospheric chemical processes produced by sprites requires in-situ and/or remote diagnostics. Also of key importance is to have a precise knowledge of the inception, propagation and branching dynamics of sprite streamers, as well as their transient internal structure in terms of electric field, charge distribution and

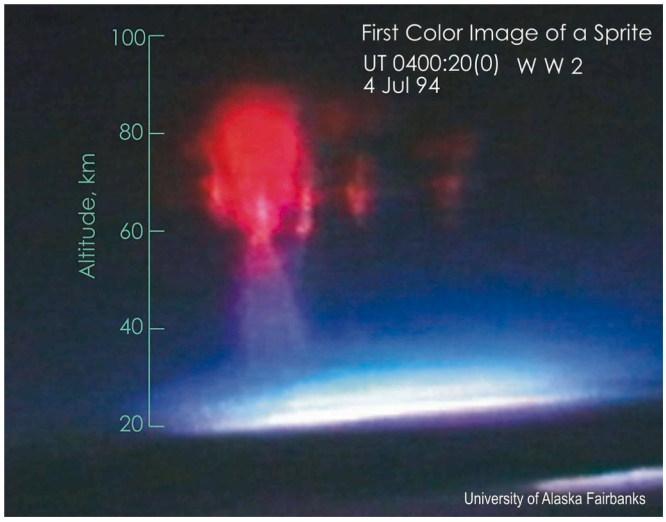

Fig. 2. First color image of a cluster of sprites recorded on July 4, 1994. Observations were conducted at altitudes between 12.2 and 12.8 km during the Sprites94 aircraft campaign of June-July 1994. The red and blue colors correspond to optical emissions of the first and second positive systems of N_2 from the excited electronic states N_2 (B $^3\prod_g$) and N_2 (C $^3\prod_u$), respectively. The lifetime of the electronic molecular level N_2 (B $^3\prod_g$) emitting red light is much longer than that of the electronic level N_2 (C $^3\prod_u$) responsible of blue emissions. At lower atltitudes the pressure is higher and collisional deactivation is more efficient. Consequently red light is quenched (collisionally deactivated) at lower altitudes (high pressure) more efficiently than blue optical emissions. Image reproduced from Sentman et al. (1995).

chemical reactivity. One unique feature of sprite streamers is that they propagate through a varying density environment (Luque and Ebert, 2010; Qin and Pasko, 2015). Contrary to sprite streamers, laboratory streamers are commonly generated under a uniform and constant (ambient or low) pressure environments. However, some researchers have carried out experiments with sprite-like streamer in low-pressure air under the influence of an extended density and pressure gradient (Strikovskiy et al., 2017; Evtushenko et al., 2020). These experiments represent a significant advance in the study of laboratory produced sprite-like streamers. This topic was initiated by Opaits et al. (2010) that created a variable air density environment at constant (atmospheric) pressure to investigate sprite streamer analogues. However, in all these experimental setups the electrodes were in contact with the discharge whereas this is not the case in nature.

Several other types of laboratory produced discharges (Williams, 2001; Williams et al., 2006; Peterson et al., 2009; Nijdam et al., 2010; de Urquijo and Gordillo-Vázquez, 2010; Dubrovin et al., 2010; Parra-Rojas et al., 2013b) have been used since the early 2000s as analogues of TLEs with the goal of investigating their inception, morphology and optical emissions and to establish connections with different types of TLEs such as blue starters, blue jets, giant blue jets and sprite streamers. In some cases dielectrics instead of electrodes were also used to initiate laboratory analogues of TLEs (Robledo-Martinez and Garcia-Villareal, 2016; Robledo-Martinez et al., 2017).

An interesting new discharge, so-called apokamp discharge, first reported in 2016 (Tarasenko et al., 2016) is distinguished from previous discharges by two features: First, its streamer escape from the bend of the discharge channel rather than from the high-voltage electrode. Second, both the electrodes and the discharge channel are at a potential of several kilovolts with respect to ground (Sosnin et al., 2019). Apokamp discharges seem to exhibit interesting features (like the electrodeless emergence of streamers) that mimic the structure of blue jets and blue starters and could be a candidate for laboratory studies of such natural discharges.

3.1.1. Key sprite imagery

The true nature of sprites started to be unveiled in 1999 and the early years of XXI century when telescopic imaging – recorded at 30/60 frames per second (fps) – of sprites revealed the first size estimation of sprite streamer heads initially indicating tens of meters (Gerken et al., 2000). Added to this, high speed imagery of sprites became possible. First between 1000 fps and 4000 fps (Stanley et al., 1999; Stenbaek-Nielsen et al., 2000; Moudry et al., 2003), and later with intensified cameras recording at 10000 fps (Cummer et al., 2006; McHarg et al., 2007) achieving pixel resolution of 140 m (see Fig. 3). This unique sprite streamer imagery started to have enough time resolution to resolve the development and dynamics of sprite streamers. Streamer diameters of hundreds of meters were later derived from the 10 kfps imagery of sprite streamers (Cummer et al., 2006; Kanmae et al., 2012; Stenbaek-Nielsen et al., 2013). Recent video recordings on 2 and 3 June 2019 from Langmuir Laboratory (New Mexico) of sprite streamers at 100 kfps (with pixel resolution of 40 m) have revealed very complex streamer activity not observable in earlier recordings at lower frame rates. Many streamers only last a few frames, and the streamers move in very dynamic patterns. The recordings show streamer path merging, collisions of upward and downward streamers, and streamer rebounding, all indicative of highly structured local electric fields produced by the sprite and independent of the larger, global quasi-electrostatic field (McHarg et al., 2019).

3.1.2. Parameters controlling sprite polarity, morphology and streamer altitude

When ″strong″ (with peak currents above 80 kA, see below) CG lightning occurs, elves can appear afterwards. Following the brief (≤1 ms) optical excitation pulse of an elve, a sprite halo and/or sprite streamers sometimes appear. For some lightning both are present, but

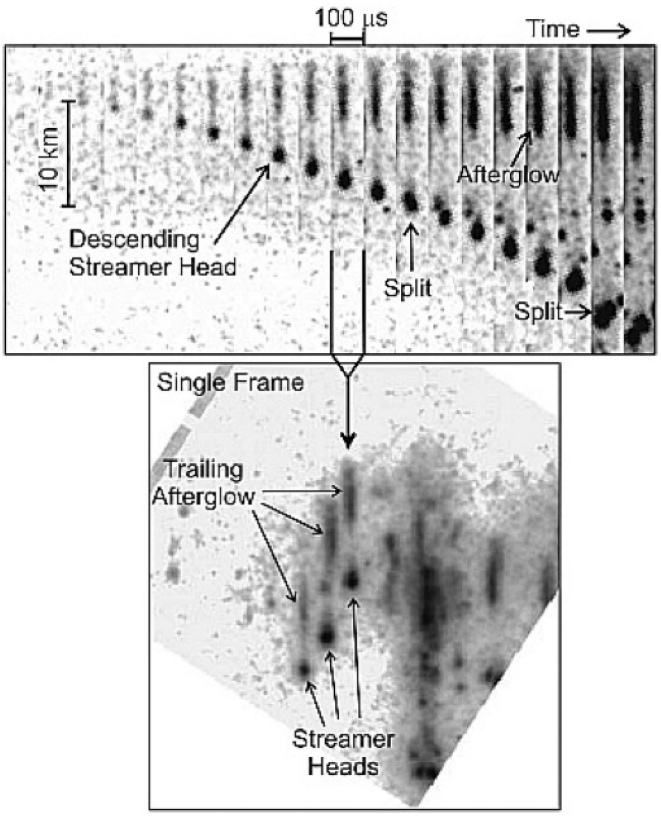

Fig. 3. (Top panel) Time and spatial development of a single sprite streamer observed at 10 kfps with 50 μs exposure time (McHarg et al., 2007). The streamer head and trailing glow are perfectly visible. (Bottom panel) A single frame from the observations showing multiple streamers. The streamer indicated by the arrow in the bottom panel is shown in the top panel in 100 μs time slices. Note that the frame rate required to observe streamers such these of sprites at ground pressure at equivalent temporal resolution (~1 ns) is about 1.5 Gfps. Image reproduced from Sentman et al. (2008b).

there are many in which only the halo or the sprite streamers appear. Strokes produced by CG lightning discharges lower electric charge to the ground, accumulating the same amount of opposite sign charge Q_{max} at thundercloud altitudes (h) originating transient quasi-electrostatic electric fields. The charge moment change (CMC), given by the product hQ_{max} determines both the electric field imposed on the ionosphere and its strength.

The majority of sprites are produced by positive CGs characterized by large peak currents and associated with $hQ_{max} \geq 600$ C km up to thousands of C km (Hu et al., 2002; Cummer and Lyons, 2005). However, Hu et al. (2002) also indicated that +CGs associated with $hQ_{max} \leq 600$ C km still have ≤10% probabilities to produce sprites, and most surprisingly that sprites can be exceptionally initiated by +CGs associated with hQ_{max} as small as 120 C km, whereas as pointed out by Qin et al. (2012) $hQ_{max} \simeq 200$ C km are repeatedly observed in North America (Hu et al., 2002), as well as at other locations, such as in the Hokuriku area of Japan (Hayakawa et al., 2004). Though rare, negative CG lightning can also trigger sprites.

According to the largely accepted conventional breakdown model (Pasko et al., 1997), both halos and sprites are produced by high altitude lightning-driven electric fields. This modeling also pointed out the difference in the initiation mechanism of halos and sprites. Halos are promptly produced when the normalized electric field (E/E_k) is high enough to produce diffuse optical emissions, where E_k is the local air breakdown field (Wilson, 1924). Initiation of a sprite requires both a high field region of $E \geq E_k$ and the persistence of this high field to form the streamer structure (Liu and Pasko, 2004).

Modeling by Qin et al. (2012) indicates that the initiation mechanisms for negative and positive halos are the same but that the streamer initiation region is different for −CGs and + CGs due to their different electric field polarities. This model also predicts that downward streamers in negative sprites (produced by −CGs) should be dimmer than upward streamers due to a higher critical field and thus a smaller development region comparing with positive sprites (produced by +CGs).

Numerical simulations by Li et al. (2012) show that the lightning discharging timescale has substantial impact on the ambient electric fields and thus the negative sprite initiation and morphology. With the same amount of charge transfer, a more impulsive current source can produce higher electric fields of shorter duration at halo and sprite altitudes. The short timescale may explain the higher CMC threshold ($\geq$ 300 C km) required to initiate negative sprites than short-delayed positive sprites (CMC $\geq$ 200 C km, see below), whose parent lightning source is usually less impulsive (Qin et al., 2012).

Comparing narrow (0.5 ms) and wider (2.0 ms) source pulses with the same charge moment change, numerical simulations show that a 0.5 ms pulse produces a very high peak electric field at 75–90 km altitudes, which is the reason that all negative sprites are accompanied with halos. On the other hand, the high fields produced by a fast source also relax more quickly due to extra ionization created by the high fields. Thus the high field may not be able to persist long enough to form sprite streamers (Li et al., 2012).

In contrast, the slower pulse can produce a high field region of $E \geq E_k$ with a longer persistence time, which provides a more favorable condition to initiate sprite streamers. According to Li et al. (2012) this could be the reason that positive sprites are easier to initiate and more often develop into complicated structures. Although the field amplitude and duration are critical in sprite streamer initiation, formation of sprite streamers also depends on other highly nonlinear processes like local ionization patches (Liu and Pasko, 2004; Qin et al., 2012; Liu et al., 2012; Qin et al., 2014) that could be caused by the presence of gravity waves (Sentman et al., 2003).

Interestingly, the study by Li et al. (2012) also indicates that the much less observed negative sprites show remarkably similar morphology, including an accompanying bright halo, relatively simple streamer structure, and streamer termination altitudes measurably higher (at and above 55 km) than for positive polarity sprites (40–50 km). All negative sprites occurred within a few ms from their parent lightning discharge. The sprite images show that all negative sprites are followed by halos with a remarkably consistent structure, unlike the more variable structure (appearance) of positive sprites. These observations suggest that negative sprites may always look like this and may not exhibit the variable spatial structure of their positive counterparts (Li et al., 2012).

The strength of the lightning-induced electric field at sprite altitude also determines the carrot-like or column-like appearance of sprites as shown in the modeling study by Qin et al. (2013). According to Qin et al. (2013), carrot-like sprites with upward negative streamers are produced for lightning with CMCs >500 C km, while column sprites dominated by downward positive streamers occur when causative lightning have CMCs <500 C km under typical nighttime conditions. A recent paper has described the microphysics underlying the emergence of carrot-like sprites (Malagón-Romero et al., 2020).

3.1.3. First laboratory and sprite streamer models

The physics of streamers is complex and has been a matter of fundamental research since the 1930s (Raether, 1939; Loeb and Meek, 1940). Streamers are precursors of sparks (Loeb and Meek, 1940; Marode, 1975; Gallimberti, 1979). They generate the initial ionized paths that facilitate the emergence of the hot spark channel. Streamers are also present in thundercloud large corona discharges and also take active part in the initiation and propagation dynamics of lightning leaders whose behaviour is not yet fully understood.

Streamers transmit a considerable amount of energy to ambient electrons that become "hotter" (~8–10 eV) than the surrounding heavy (gas) particles. Thus, streamer discharges are cold and non-thermal plasmas (heavy particles are cold while electrons are very hot), and this underlies their different efficiency in producing key chemical species. Most technological applications of streamers rely on the distinct chemical properties of such cold filamentary plasma discharges.

The unique non-thermal equilibrium nature of streamers enables efficient chemical reaction pathways that are impossible with thermal plasmas and/or conventional hot reactors (such as, for instance, industrial ovens). In air or air mixtures streamers can greatly enhance the chemical reactivity by the activation of radical chemistry, complex chain reactions and catalytic cycles involving radicals (O_2, OH, HO_2, NO, NO_2), excited and positive and negative ions.

Due to the above mentioned unique chemical activation properties, streamer discharges are of interest for applications in air, water and waste purification technologies, surface treatment, agricultural technologies (seed activation), plasma medicine and, among others, aerospace applications such as plasma assisted combustion and propulsion.

The interest in many of the streamer applications mentioned above emerged during the 1980s but there was a lack of realistic theoretical models of streamers that could describe the dependence of the parameters of the streamer on the applied voltage, on the electrode geometry and polarity, and on the other physical and chemical characteristics of the propagating medium. In this context, the first 2D model able to self-consistently determine the radial structure of streamers was published by Vitello et al. (1994) for negative streamers. They found that at least two characteristic radii are required to describe the streamer structure in the filamentary streamer phase, which self–consistently emerged in their simulations. These length scales corresponded to the space-charge shielding radius and the electron density e-folding radius. This model had a good spatial resolution of $\leq$5 μm that allowed to accurately determine for the first time the axial and radial structure of streamers. Vitello et al. (1994) neglected photoionization since this process was not well known by that time (the effect of photoionization in sprite streamers was first introduced by Liu and Pasko (2004)). For negative streamers the 2D model by Dhali and Williams (1987) used a grid spacing with axial and radial resolution of $\geq$25 μm and $\geq$ 50 μm, respectively.

In this context, the first sprite streamer models were published in 1998 (Pasko et al., 1998; Raizer and Simakov, 1998). The model by Pasko et al. (1998) was the first 2D model to describe sprite streamers occurring in the mesosphere. This model was inspired by previous 2D models of laboratory produced streamers at ground level pressure (Dhali and Williams, 1987; Vitello et al., 1994). Pasko et al. (1998) simulated negative sprite streamers which did not include neither photoionization nor an extensive air kinetic scheme except for the optical emission coefficients of N_2, O_2 and N_2^+ and the two basic electron impact ionization and attachment processes needed to resolve the electric field streamer dynamics.

Though an almost inevitable basic chemical kinetics was implemented, the model by Pasko et al. (1998) was an important step forward for the understanding and successful explanation of the observed sprite spatial structure clearly divided between an upper ($\geq$85 km) diffuse region and a lower ($\leq$75 km) filamentary (streamer dominated) region (see details above). The results obtained from this model for ground level pressure were in agreement with previous streamer simulations (Dhali and Williams, 1987; Vitello et al., 1994). At higher altitudes (lower pressures) the streamers seemed to preserve similarity laws and differed only in spatial and temporal scales. Finally, Pasko et al. (1998) estimated an unimportant ($\Delta T/T \sim$ 2–0.2%) heating of neutrals at lower sprite altitudes (50–60 km) during typical time scales of sprites meaning that a streamer to leader transition was not feasible in sprites. This low sprite streamer heating was later suggested as the source of sprite infrasound (Farges et al., 2005; Farges and Blanc, 2010; de Larquier et al., 2010) and confirmed with remote high spectral resolution sprite

spectroscopy (Gordillo-Vázquez et al., 2018).

So, 10 years after the discovery by Franz et al. (1990), many new and interesting features of sprites had been investigated, and even a first model for the complex sprite streamers was developed. All these findings were needed before studies of the sprite chemistry could be possible.

3.1.4. Initial sprite chemistry investigations: from 1997 to 2007

We comment below some early (1997–2007) observational and modeling investigations that searched for indirect indications of chemical fingerprints of TLEs in the upper atmosphere. Some of the first indirect observations motivated early modeling of sprite chemistry. Apart from a few sporadic reports, neither observational nor experimental investigations have been systematically undertaken to determine the overall magnitude and extent of possible chemical effects of TLEs on the atmosphere.

Soon after the first spectroscopic observations of sprites (Mende et al., 1995; Hampton et al., 1996) in the visible and near infrared (IR) spectral ranges, Inan et al. (1996a) had suggested the possibility that sustained heating of lower ionospheric electrons by thundercloud electric fields could lead to the production of IR emissions, in particular 4.3 μm CO_2 emission. It was also possible that sprites could activate ambient CO_2 molecules and produce transient IR glows potentially detectable from space. The study of Picard et al. (1997) investigated the excitation rate of N_2 ($X^1\Sigma_g^+$, v) via electron collisions by using a, by that time new, steady-state two-dimensional electrostatic-heating model of the upward coupling of the thundercloud electric fields proposed by Pasko et al. (1996b). The vibrational energy transfer to CO_2 and 4.3 μm radiative transfer were computed using a line-by-line non-LTE (non-local thermodynamic equilibrium) radiation model. Limb-viewing radiance profiles at 4.3 μm and typical radiance spectra were estimated for five different thundercloud charge distributions and ambient ionic conductivities. Limb-view broadband 4.3 μm enhancements of up to a factor of two above ambient nighttime levels were predicted for tangent heights between 77 km and 120 km, with the largest enhancements at 80 km. Picard et al. (1997) pointed out the importance of having a spatially extensive mesoscale convective systems (MCS) with areas $\sim 10^4$ km^2 able to generate electric fields sufficient to excite N_2 ($X^1\Sigma_g^+$, v) as was later demonstrated by U2 aircraft electric field measurements of 1–7 kV/m at about 20 km altitude over large active storms (Blakeslee et al., 1989).

The model of Milikh et al. (1998) discussed possible 4.26 μm CO_2 transient infrared emissions caused by sprites. This study also discussed the importance of electron-impact vibrationally excited N_2 in producing the electronically excited state 001 of CO_2 radiating at 4.26 μm. Milikh et al. (1998) predicted that the ratio of sprite 4.26 μm intensities to the background IR emissions had a minimum at 85 km and changed between 15% and 45% (at 90 km).

The early studies by Armstrong and Lyons (2000) and Armstrong et al. (2001) provided suggestive evidence for possible regional-scale chemical effects of TLEs in observations made by the Halogen Occultation Experiment (HALOE) instrument aboard the Upper Atmosphere Research Satellite (UARS). A plume of stratospheric NO was observed to extend westward from regions of summer thunderstorms in the American Midwestern plains states. It was speculated that this plume may have had its origins in the effects of lightning-induced chemical perturbations in the middle atmosphere. Armstrong and Lyons (2000) and Armstrong et al. (2001) also reported the results of preliminary kinetic modeling of the chemistry of sprites and similar calculations were independently undertaken by Sentman et al. (2000).

Sentman et al. (2003) reported evidence of weak brightening of optical emissions in the nocturnal OH* skyglow layer directly above an active, sprite producing thunderstorm. In that study two dozen bright sprites generated by the underlying thunderstorm were recorded near the center of the outwardly radiating gravity wave pattern. However no distinctive OH* brightness signatures uniquely associated with the sprites were detected at the level of 2% of the ambient background brightness.

Hiraki et al. (2004) calculated the amount of metastable oxygen O (^{1}D) and ground-based oxygen O(^{3}P) produced in sprite halos in the altitude range of 50–90 km during daytime and nighttime. Following the quasi-electrostatic model proposed by Pasko et al. (1997), Hiraki et al. (2004) solved coupled differential equations for the spatial-temporal evolution of the electric field, the space charge density generated by the thundercloud charge and discharge and the rate equation for electrons. Hence the electric field and the electron density were solved self-consistently (coupling of electrodynamics and basic kinetics was considered). Once the electron density was obtained, they integrated in time (during 1 ms) the rate equations for O(^{1}D) and O(^{3}P) whose rate coefficients were previously obtained with an electron energy distribution function calculated with Monte Carlo methods. Hiraki et al. (2004) showed that density enhancements of 10^3–10^4 cm^{-3} (O(^{1}D)) and 10^3–10^5 cm^{-3} (O(^{3}P)) were predicted to occur during 1 ms within sprite halos and with both densities (O(^{1}D) and O(^{3}P)) having a sharp peak at an altitude of 73 km in the nighttime and at 67 km during daytime after a lightning discharge with a CMC of 1000 C km.

Hiraki et al. (2004) evaluated the generation of metastable O(^{1}D) in sprites halos produced by lightning with charge moment changes between 500 C km and 2000 C km during nighttime and between 1000–2000 C km during daytime, respectively. The O(^{1}D) and O(^{3}P) kinetics considered by them were restricted to only one source of O(^{1}D) by electron-impact dissociative excitation ($e + O_2 \rightarrow O(^1D) + O(^3P) + e$) and one sink of O(^{1}D) by collisional deactivation (quenching) by N_2 and/or O_2 ($O(^1D) + N_2/O_2 \rightarrow O(^3P) + N_2/O_2$). They concluded that sprite halos could be a significant local mesospheric source of O(^{1}D) metastable atoms but its nighttime global O(^{1}D) production was found to be four orders of magnitude smaller than that due to daytime solar UV radiation (photolysis of O_3 leading to O(^{1}D)). Still, sprite halos and/or halos alone could be considered a significant nighttime local and global source of metastable O(^{1}D). This theoretical prediction remains unconfirmed due to the lack of observational proofs.

In 2005 Enell et al. (2005) presented preliminary results of a study of NO_x production from TLEs using a coupled ion-neutral chemical model. Later in 2007, Gordillo-Vázquez (2007) independently presented preliminary results on the detailed air plasma chemistry at different altitudes due to nighttime sprite streamers. These calculations incorporated for the first time the self-consistent coupling of the air kinetics (through rate equations of the different chemical species) and the time dependent Boltzmann equation to evaluate the transient electron energy distribution function needed to evaluate rate coefficients for many important non-equilibrium chemical processes driven by streamer electrons. The sprite streamer kinetics investigated included electron-impact excitation, dissociation, ionization, attachment and detachment reactions (Gordillo-Vázquez, 2007). This model also analysed how the presence of sprite streamers influence on the populations of the nine lower vibrational levels of N_2 ($X^1\Sigma_g^+$, v = 0, …, 8).

3.1.5. Sprite chemistry modeling: year 2008

The year 2008 could be considered a sort of a moment of coalescence for the research in sprite chemistry. This special year could be somehow explained by the fact that some other related and needed observational and modeling research fields had reached by that time certain degree of maturity in their respective evolutions. The impulse to sprite chemistry research was then possible thanks to the new high-speed camera technology and computational advances needed for key observations and modeling, respectively.

On the observational side high-speed (10,000 fps) imagery was starting to show very fine details of the sprite streamer time dynamics. Time and spatial development of a single sprite streamer was now possible (see Fig. 3). These newly available high-speed images clearly showed for the first time a descending sprite streamer head and its trailing afterglow (Cummer et al., 2006; McHarg et al., 2007; Stenbaek-

Nielsen and McHarg, 2007). These unprecedented detailed observational investigations of sprite streamers facilitated the development of models dealing with the non-equilibrium kinetics of a single sprite streamer. Though this was a clear step forward, sprites are formed by tens or hundreds of interacting and non-interacting upward and downward propagating streamers.

On the streamer modeling side, between 1997 and 2008 a comparative analysis of the role played by photoionization (originally introduced to study positive streamer propagation) in the propagation dynamics of positive and negative streamers had only been investigated by a few groups. Babaeva and Naidis (1997) had compared the emergence of positive and negative streamers from pointed electrodes. Liu and Pasko (2004) and Pasko (2007) were the first to investigate the effect of photoionization on the propagation and branching of positive and negative streamers in sprites. Luque et al. (2007, 2008b) also investigated the role of photoionization on the propagation and interaction of streamers of both polarities (Luque et al., 2008a). Photoionization of oxygen molecules by UV photons from excited N_2 in air atmospheres is an important and crucial source of free electrons ahead of positive (but also negative) streamers and it plays a key role in our full understanding of streamer propagation dynamics (Zhelezniak et al., 1982).

The use of more complete and realistic plasma-chemical models (Kossyi et al., 1992; Borisov et al., 1993), better modelling of the electrode geometry (Babaeva and Naidis, 1996; Abdel-Salam et al., 2007) and an efficient calculation of the non-local photoionization source (Bourdon et al., 2007; Luque et al., 2007) had finally allowed by 2008 that simulation and experimental results of intrinsic streamer features (such as propagation speeds and diameter of streamer channel) converge within a relatively narrow range (Pancheshnyi and Starikovskii, 2003; Pancheshnyi et al., 2005; Luque et al., 2008b).

Therefore, by 2008, considerable improvements had been achieved in the modeling and comparison with experiments of key intrinsic streamer features. However, these new generation of self-consistent 2D or 3D (with cylindrical symmetry) streamer models with photoionization only incorporated (mainly due to computational limitations) a few number of electron impact processes usually limited to ionization of N_2 and O_2, and two and/or three-body attachment of O_2, some collisional (quenching) de-activation of excited species, and/or some radiative de-excitations processes responsible of optical emitting species (Liu and Pasko, 2004; Pancheshnyi et al., 2005; Luque et al., 2008b).

With the new generation of 2D fluid streamer models of 2008 it was unfeasible to self-consistently couple the full electrodynamics of streamers with complex state-to-state kinetic schemes. These extensive kinetic schemes usually need to include hundreds of different types of reactions controlled by energetic electrons (with electric field dependent rate coefficients), ground and excited neutrals and ions, vibrationally and electronically excited species that usually require very small time steps to guarantee numerical stability and model convergence. Therefore, the kinetic validation and verification (comparison of model predicted streamer head and channel chemical reactivities against chemical measurements) was still far from being achieved and remain an open challenge nowadays.

By 2008 four kinetic models treating the nighttime atmospheric chemistry of sprites were independently developed and published in different journals (Enell et al., 2008; Hiraki et al., 2008; Sentman et al., 2008b; Gordillo-Váquez, 2008).

The study by Enell et al. (2008) extended a preexisting model, the Sodankyla coupled Ion-neutral Chemistry (SIC) model originally developed as a steady-state model for ion-ion reactions (Turunen et al., 1996). The updated SIC version used in Enell et al. (2008) was time-dependent and modeled 36 positive ions, 29 negative ions and 15 neutral components with 17 other neutral background species kept fixed. Electric field dependent rate coefficients of critical kinetic processes like electron-impact excitation, ionization and dissociation of 17 excited neutral species (the molecular major constituents excited during sprites) were calculated by external models. Additionally the mixing ratio of water vapour was fixed to 5 ppmv below 80 km and CO_2 was fixed to 335 ppmv. This model only evaluated the chemical impact of sprites on NO_x and O_3. No other chemical species were investigated.

The approach taken by Enell et al. (2008) did not explicitly model sprite streamers. Instead, to estimate the production of NO_x and its impact on O_3 they limited their sprite parameterisation to a first order estimate and assumed that the region affected by a sprite is on average $\sim 50\ km^2$ wide (sprite area), and extends from 40 to 90 km (leading to a cubic sprite volume). Sprites (or clusters of simultaneous sprites) were assumed to be contained within such a volume. The NO_x change within the volume depended on the fraction of it that is filled with sprite streamers using a filling factor α_f that was assumed to change between 0 and 1. After some considerations, the filling factor was assumed to vary between 5×10^{-5} and 5×10^{-3} in the lower filamentary region of sprites and between 10^{-3} and 10^{-2} in their upper diffuse region.

The model was fed with excited rate coefficients calculated with the time dependent reduced electric fields obtained from typical and extreme ISUAL observations of sprites (Adachi et al., 2006). The maximum electric fields derived from the typical sprite ISUAL observations (between 53 km and 83 km) ranged between 60 Td (83 km), 80 Td (73 km), 120 Td (63 km) and 150 Td (53 km). For the extreme ISUAL observations used by Enell et al. (2008) the maximum electric fields ranged between 250 Td (63 km) and 100 Td (73 km).

Enell et al. (2008) concluded that the NO_x enhancements due to sprites are at most one order of magnitude in the lower (filamentary) sprite region, which means a production of at most 10 mol per event, or (given a global rate of occurrence of three events per minute (Ignaccolo et al., 2006)) some 150–1500 kg per day. Therefore, the study by Enell et al. (2008) indicated that sprites are insignificant as a global source of NO_x. Local effects on ozone were also found negligible, but the local enhancement of NO_x was classified as significant, up to 5 times the minimum background at 70 km in extraordinary cases.

The three other models by Hiraki et al. (2008); Sentman et al. (2008b); Gordillo-Váquez (2008) investigated the nighttime chemical effects of single sprite streamers. The three of them considered different simple parameterizations for the impulsive electric field in a sprite streamer without considering photoionization (Liu and Pasko, 2004).

The model by Hiraki et al. (2008) considered the chemical species were produced predominantly at the streamer tip. They assumed roughly that the tip had an impulsive electric field E_s with a uniform amplitude and a width of r_s of the same order as the streamer radius (Raizer, 1991) and a uniform electron density Ne_s.

Hiraki et al. (2008) considered that the lightning-induced electric field above thunderclouds is directed almost vertically, and the streamer propagates along its direction with a constant velocity of v_s. Therefore, the timescale of electron acceleration, i.e. particle production, at a certain altitude was given by $t_s = r_s/v_s$. For simplicity and maximum estimation they set $E_s = 150$ kV/cm (corresponding to 600 Td at ground pressure), $Ne_s = 10^{14}\ cm^{-3}$, $r_s = 10^{-1}$ cm, and $v_s = 10^7\ cm\ s^{-1}$ taken from Kulikovsky (1997). These parameters were assumed to be scaled as $\sim N$, $\sim N^2$, $\sim N^{-1}$, and 1, respectively, where N stands for the atmospheric gas density. For example, $r_s = 10^{-1}\ (N_0/N)$ cm, N_0 and N being the gas densities at ground level, and at 70 km, $r_s = 10$ m, $t_s = 100$ μs. As mentioned above they neglected the effect of photoionization although it is an important process for local streamer dynamics and makes these parameters slightly shifted from the above N-scaling values (Liu and Pasko, 2004).

The model by Hiraki et al. (2008) used Monte Carlo numerical techniques to compute offline the electron energy distribution function (EEDF) needed to calculate the electron driven rate coefficients. They studied the sprite streamer chemistry triggered by non-thermal electrons by using an ion-neutral model built from the combination of the chemical model of a neutral atmosphere by Iwagami et al. (1998) (with 40 neutral ground and excited species), thermal electrons and 34 ionic atomic and molecular species. The chemical impact of a single sprite

streamer was then obtained by solving gain-loss rate equations for NO_x, O_x (O, O_3) and HO_x (H, OH, HO_2, H_2O_2) chemical species between 40 km and 90 km for different times (0 s, 1 s and 1 h).

The results by Hiraki et al. (2008) showed that the densities of NO, O_3, OH, and H rapidly increase by many orders of magnitude (up to 8) for NO and H and up to several orders of magnitude (between 1 and 3) for O_3 and OH. These important density enhancements were due to reactions triggered by sprite first chemical products such as O, N, and electrons in the timescale of 1–10 s during nighttime. They showed that the sprite streamer chemical impact is sustained over one hour, especially for NO whose concentration remained (after 1 h) 6 orders of magnitude above ambient levels at around 60 km altitude. At 50 km and 70 km (1 h after the inception of one sprite streamer) the density of NO was predicted to remain 2 and 4 orders of magnitude above ambient values, respectively. The final sinks are considered to be NO_2, O_3, HO_2, and H_2O_2 for each species with concentration enhancements of several orders of magnitude. These long lifetime responses are related with source-sink balances of NO-NO_2 and of HO_2-H_2O_2 newly generated in the atmosphere by sprite products. According to Hiraki et al. (2008) the sprite impact on these minor species would be detectable with highly qualified satellite observations, even though it has (they claimed) an uncertainty of one order of magnitude due to initial conditions and uncertainties in cross sections and rate coefficients used for the production of the different chemical species.

According to Hiraki et al. (2008), the significant differences between their model and the sprite chemical model by Enell et al. (2008) were mainly due to the difference in the evaluation of sprite first products due to different input parameters. The model of Hiraki et al. (2008) calculated an altitude dependent production rate on the basis of scaling laws of streamer dynamics and included all possible chemical species produced through electron-impact N_2, O_2 inelastic collisions. However, Enell et al. (2008) considered only some N_2 excited states and N_2^+ identified from ISUAL optical measurements (Adachi et al., 2006), and not included N and O atoms, which are of great importance in the kinetic calculation. Furthermore, the magnitude itself of particle production in Enell et al. (2008) model is considerably smaller with respect to the model of Hiraki et al. (2008). Among other reasons, a key difference between the models by Enell et al. (2008) and Hiraki et al. (2008) was their very different initial (input) values for the chemical species. For example, at 60 km the initial value of the density of NO is $\sim 10^2$ cm^{-3} in the model of Hiraki et al. (2008), while it is $\sim 10^6$ cm^{-3} in the model of Enell et al. (2008). The very final reason for the significant different chemical impact predicted by both models is probably a combination of factors including, model structure, the use of different initial conditions and data sets for reaction rate coefficients.

The nighttime sprite chemical model by Sentman et al. (2008b) is closely inspired in detailed high-speed (10,000 fps) sprite streamer observations distinguishing sprite streamer heads and trailing glows (McHarg et al., 2007; Stenbaek-Nielsen and McHarg, 2008) (see Fig. 3). They modeled the chemical processes triggered by positive sprite streamer heads propagating in the direction of the electric field. Following high-speed observations Sentman et al. (2008b) divided the spatial structure of sprite streamer in three regions: region 1 exhibiting bright optical emissions that were assumed to be caused by strong electric fields localized to within the small volume of the streamer tip and regions 2 and 3 behind the streamer head where no electric field was assumed. The darkness seen in observations behind the streamer head was associated to an electric field free region (region 2) which was also consistent with previous numerical simulations of positive streamers (Kulikovsky, 1998). Finally, after the dark region, observations indicated the presence of a streamer afterglow region (region 3) exhibiting faint optical emissions that Sentman et al. (2008b) assumed that were caused by some sort of chemiluminescence or afterglow processes so that this region 3 was also assumed to be field free.

Sentman et al. (2008b) considered an impulsive electric field within the streamer head modeled as a gaussian profile with a maximum field of $E_0 = 600$ Td during $\Delta t = 6$ μs. The maximum electric field E_0 in the streamer head was estimated on the basis of self-consistent modeling of streamers in an undervoltage environment at 70 km (Liu and Pasko, 2005), which was in turn consistent with modeling based on emission line ratios obtained with the ISUAL experiment aboard the FORMOSAT-2 satellite (Kuo et al., 2005). The sprite chemical model of Sentman et al. (2008b) solved a number of coupled continuity equations (with prescribed electric field) for all the chemical species investigated including electrons, ground and excited neutrals (atoms and molecules) and ions involved in a large set of chemical reactions (87 species and about 800 chemical reactions). The kinetics of vibrational excited molecular states was not considered. The model results were computed at the fixed altitude of 70 km, which was a standard altitude adopted in many sprite modeling studies by that time (Pasko et al., 1997; Liu and Pasko, 2004, 2005). Electric field driven rate coefficients for electron-impact ionization, dissociation, attachment or excitation of electronic states were taken from Kossyi et al. (1992). The sprite chemical model of Sentman et al. (2008b) paid special attention to the kinetics of (1) nitric oxide (NO) since it can have effects on ozone (Crutzen, 1970), (2) optical emitting states species of N_2 (responsible of the characteristic red and blue sprite optical emissions) and (3) O_2 metastables and $OH(X^2\prod, v = 6–9)$ responsable of atmospheric Meinel emissions.

Energetic electrons produced in the sprite streamer head primarily produce metastable nitrogen atoms $N(^2D)$ through electron-impact N_2 dissociative excitation ($N_2 + e \rightarrow N + N(^2D)$). These freshly produced N (^2D) react with ambient O_2 and produce nitric oxide (NO) through $N(^2D) + O_2 \rightarrow NO + O(^1D)$ and $N(^2D) + O_2 \rightarrow NO + O(^3P)$. The densities of $N(^2D)$ are large enough that a significant perturbation is produced in the background density of NO, producing an enhancement of $\sim 10^7$ cm^{-3}, which is ~75% above the predischarge background of 10^7 cm^{-3}. After a few ms the atom interchange reaction $N + NO \rightarrow N_2 + O(^3P)$ begins the slow reconversion of NO to N_2 and $O(^3P)$. This effectively freezes out the NO produced in the streamer, leaving a net positive residue. Based on 2007 high speed observations (McHarg et al., 2007; Stenbaek-Nielsen and McHarg, 2008) Sentman et al. (2008b) considered a nominal sprite streamer diameter of 25 m and a sprite streamer length of 10 km which led to a total excess NO produced by the streamer in their model of $\sim 5 \times 10^{19}$ molecules, that is, the NO density in the streamer trail is enhanced by ~75% above the ambient background at 70 km.

Apart from NO, the model by Sentman et al. (2008b) also found interesting and significant changes in the concentration of electrons, metastable species such as N_2 ($A\ ^3\Sigma_u^+$), $O(^1D)$, $O_2(a\ ^1\Delta_g)$, ground state oxygen atoms $O(^3P)$, excited oxygen atoms $O(^1S)$, excited OH and a variety of positive and negative ions.

Electron densities up to 10^6 cm^{-3} are produced (from a background electron density of 1 cm^{-3}) due to energetic electron-impact ionization of N_2 and O_2 in the streamer head. The main loss mechanisms of electrons in the streamer head is dissociative attachment to O_2 ($e + O_2 \rightarrow O(^3P) + O^-$). The main electron losses in the trailing streamer column are dissociative attachment to O_3 ($e + O_3 \rightarrow O + O_2^-$) and dissociative recombination with the positive ion cluster $N_2O_2^+$ chemically generated within the streamer channel. The lifetime of electrons was found to be ~1 s. According to the model of Sentman et al. (2008b) it is the persistence of cold electrons within the ionized streamer column that appears to be responsible for the observed reignition of sprites from remnants of old sprites. This persistent ionization is partially evidenced by the existence of the so-called early very low frequency (VLF) events, which are abrupt perturbations in amplitude and phase of narrowband VLF signal receptions. They occur within ~20 ms of a causative lightning discharge having either a fast (<20 ms) or slow (~1 or 2 s) onset duration and typical recoveries in the range from ~50 to 180 s (Inan et al., 1996a; Marshall et al., 2006; Inan et al., 2010; Haldoupis et al., 2010; Pasko, 2010).

The metastable N_2 ($A\ ^3\Sigma_u^+$) is produced by direct electron impact, but principally by radiative cascade from N_2 ($B\ ^3\prod_g$) and other N_2 triplet states. It reaches a maximum density of $\sim 2 \times 10^7$ cm^{-3}, and has a

lifetime of ~1 ms. The main sinks of N_2 ($A\ ^3\Sigma_u^+$) are deactivation reactions with O_2.

The dominant source of $O(^1D)$ is electron impact dissociative excitation with losses occurring primarily via collisional deactivation processes with N_2 and O_2. The lifetime of $O(^1D)$ is less than 100 μs.

The long-lived (≥1000 s) metastable species O_2 ($a\ ^1\Delta_g$) is produced with densities of $\sim 10^7$ cm^{-3}, principally by collisional cascade from O_2 ($b\ ^1\Sigma_g^+$), which in turn derives from collisional deactivation of N_2 ($A\ ^3\Sigma_u^+$).

The ground state oxygen $O(^3P)$ is the species created in the largest abundance in a sprite streamer, with densities of $\sim 5 \times 10^7$ cm^{-3}. A large number of processes contribute to its creation, principally dissociation of ground state molecular oxygen O_2 ($X\ ^3\Sigma_g^-$) driven by the singlet N_2 ($a'\ ^1\Sigma_u^-$) created by electron impact excitation in the streamer head and dissociative quenching of N_2 ($B\ ^3\prod_g$). The dominant loss mechanism of O (^3P) is via the slow three-body reaction involving O_2 and N_2 that produces O_3. According to the model of Sentman et al. (2008b) the $O(^3P)$ produced in a sprite streamer has a lifetime of ~1 h.

The chemical model of Sentman et al. (2008b) also discussed possible sprite induced enhancements in the optical emissions from excited OH (Meinel emissions) and $O(^1S)$ (green emissions). Overpopulations of vibrationally active OH were created in the streamer channel by interaction of $O(^3P)$, HO_2 and H through $H + HO_2 \rightarrow OH(v = 0,..,3) + O_2$ and $H + O_3 \rightarrow OH(v = 6–9) + O_2$. Since the model did not consider explicit vibrational kinetics they merged the vibrational excited species OH(v = 0–3) and OH(v = 6–9) into the single species OH*. Thus, according to their predictions, sprite-induced $O(^3P)$ and H perturbations to hydroxyl catalysis could yield a weak (~1 R) enhancement to OH Meinel emissions. To put this predicted sprite enhanced OH brightness into context, the nighttime airglow, or nightglow, generated by these reactions produce natural bright emissions of hundreds of kR from the short-wave infrared (SWIR) $OH(X^2\prod, \Delta v = 2)$ first–overtone Meinel sequences at wavelengths 1.4–2.2 μm. The OH* emission intensities are also significant (several tens kR) in the shorter wavelength 700–900 nm near-infrared (NIR) $OH(X^2\prod, \Delta v = 3, 4, 5)$ Meinel sequences (Sentman et al., 2003). In any case, the predicted sprite enhanced OH* emissions would be very hard to detect even in the NIR optical (700–900 nm) range where the natural Meinel nightglow is smaller.

Similarly, the production of $O(^1S)$ by electron impact dissociation of O_2 and, to a lesser degree, by collisional deactivation of the N_2 ($C\ ^3\prod_u$), could result in a short (10–100 ms) burst of OI 557.7 nm optical emissions with a brightness of ~1 kR (assuming a streamer diameter of 25 m) at 70 km. The detection of any of these airglow emissions from sprite streamers would provide an important tool for studying the chemistry of sprite processes. Sentman et al. (2003) had already reported evidence of weak brightening of optical emissions in the nocturnal OH* skyglow layer directly above an active sprite producing thunderstorm. In that study two dozen bright sprites generated by the underlying thunderstorm were recorded near the center of the outwardly radiating gravity wave pattern. However no distinctive OH* brightness signatures uniquely associated with sprites were detected at the level of 2% of the ambient background brightness (Sentman et al., 2003).

Finally, the positive ions produced in greatest abundance are O_2^+ and O_4^+, with densities of $\sim 10^6$ cm^{-3} and $\sim 4 \times 10^4$ cm^{-3}, respectively. The negative oxygen ion O^- is created via dissociative attachment ($e + O_2 \rightarrow O(^3P) + O^-$) during the ionization impulse, with a density of $\sim 10^5$ cm^{-3}. O^- is destroyed via associative detachment and three-body attachment with O_2, and by charge transfer with O_3. O_2^- is created by dissociative attachment with O_3 and threebody attachment with O_2, with a maximum density of $\sim 2 \times 10^5$ cm^{-3}. The lifetime of oxygen negative ions was found to vary between 1 s and 10 s.

To conclude this section we comment the sprite chemical model of Gordillo-Váquez (2008). The kinetic formalism adopted in this study included the coupling of the rate equations of each of the different 77 species considered (electrons, ions, atoms and molecules) and about 500 chemical reactions with the Boltzmann equation so that, in this way, all the kinetics was self-consistently treated, although, in this model (as in the previous ones already reviewed above), the electrodynamics (neither photoionization nor Poisson equation were considered) was not self-consistently solved with the plasma kinetics. This model assumed that the reduced electric field (E/N) within the streamer head plasma was an external (prescribed) parameter with a step-like shape, that is, $E/N = 400$ Td (~ 3.3 E_k/N) during a short time interval of $\tau_p = 5$ μs while, afterwards, $E/N = 1$ Td.

The assumed value of 400 Td in the sprite streamer head was based on contemporary observations by the ISUAL instrument of the reduced electric fields between 243 Td and 443 Td (2.1–3.7 E_k/N) (Kuo et al., 2005) underlying the brightest sprite optical emissions of several sprites observed between altitudes of 40 and 70 km. The upper limit of E/N reported in Kuo et al. (2005) was in agreement with the electric field magnitudes (≥ 3 E*k*/N) predicted in models of sprite streamers previously published (Liu et al., 2006).

The basic equations controlling the non-equilibrium air plasma chemistry of sprite streamers in the model of Gordillo-Váquez (2008) were a set of differential rate equations for each of the chemical species of type *i* in the streamer plasma where N_i standed for the concentration of the atomic and molecular neutrals, ions (positive and negative) and free electrons that can change as a consequence of gain (G) and loss (L) kinetic processes taking place during and after the short time pulse of the electric field within the streamer head.

The microscopic processes considered in G and L included the chemistry of neutral and ions together with the electron-driven kinetics. The rate coefficients of each of the electron-driven reactions considered were calculated by using appropriate sets of cross sections and the corresponding electron energy distribution function (EEDF) in each time step. In order to do these calculations as accurately as possible, the rate equations for each chemical species was coupled to a time-dependent and spatially uniform Boltzmann transport equation through the collision term on the right-hand side of the Boltzmann equation. These collision terms represent the rate of change in the EEDF due to the different kinds of collisions considered and includes the densities of neutrals (atom and molecules) and ions in the plasma. In this study, the considered electron collisions were elastic, inelastic and superelastic ones. Finally, an equation to account for the condition of macroscopic electrical neutrality was imposed so that the net charge balance in the plasma is satisfied (quasi-neutral plasma) in each time step.

The kinetic calculations of the sprite chemistry model of Gordillo-Váquez (2008) were carried for three different altitudes (63 km, 68 km and 78 km) for which the same $E/N = 400$ Td in the sprite streamer head was assumed as first approach. In addition, all the calculations were conducted for midnight conditions in mid-latitude regions (+38°N) and 0° longitude, using as initial values for the neutral species those provided by the version 3 of the Whole Atmosphere Community Climate Model (WACCM) based on the National Center for Atmospheric Research's (NCAR) Community Atmospheric Model (CAM version 3). This model explicitly considered a constant amount of 4 ppm (ppm) of H_2O in the region investigated (63–78 km) based on water vapour observations from the HALogen Occultation Experiment (HALOE) on board the Upper Atmosphere Research Satellite (UARS).

The model of Gordillo-Váquez (2008) was the first sprite chemical model in quantifying the nighttime change of the atmosphere electrical conductivity due to the presence of sprite streamers. It concluded that the passage of the sprite streamer head produces a sudden increase of the electrical conductivity that ranged between 6 (at 63 km) and 2 orders of magnitude (at 78) with respect to the ambient nighttime values at those altitudes. The measured ambient value of the nighttime electrical conductivity of 10^{-11} mho cm^{-1} (Hale, 1994) at 70 km was used as a reference. This model also found that the perturbations of the ambient electrical conductivity lasted longer (up to 100 s) at higher altitudes (78 km) than at lower altitudes (10–100 ms at 63 km).

The analysis of the time-dependent EEDF showed that the EEDF

transient was quite fast, usually below 100 ns. The latter was the time needed by the EEDF to reach its steady values while the electric field pulse was on. In addition, the deviation of the calculated EEDF from a Maxwellian was evident in the higher electron energy range ($\geq$ 40 eV). It was concluded that, in order to study the electron kinetics in sprite streamers, it was not really crucial to follow in time the EEDF since its timescale (relaxation times) was much shorter (nanoseconds) than that of the streamer head lifetimes (microseconds). Thus, it would be enough to consider the steady state EEDF during the pulse. This was in agreement with previous Monte Carlo time-dependent calculations of the EEDF under sprite streamer conditions (Hiraki et al., 2004).

The model of Gordillo-Váquez (2008) treated a comprehensive variety of important aspects of the non-equilibrium air plasma chemistry triggered by sprite streamer heads. The kinetic mechanisms investigated dealt with the optical emitting species in the UV, NUV, visible and NIR, electrons, excited atomic and molecular species (including key metastables such as N_2 ($A\ ^3\Sigma_u^+$) and $N(^2D)$), nightglow-enhancing radiative species like $O(^1S)$ and OH), impact on nitric oxides like NO, NO_2 and NO_3 as well as the influence of sprites on the chemistry of important positive ions like O_2^+, N_2^+ or the long-lasting $N_2O_2^+$, and negative ions such as O_2^- or O^-. The model of Gordillo-Váquez (2008) also explored the activation by sprite streamers of vibrationally excited ambient CO_2 that could re-emit IR radiation detectable from space.

The analysis of the enhanced electron concentrations over ambient values of ~30, 50 and 70 cm^{-3} at 63, 68 and 78 km, respectively, indicated that, depending on the altitude, the electron density can reach values of up to 10^6 cm^{-3} (63 km), 4×10^4 cm^{-3} (68 km) or remain relatively low with values hardly above 10^2 cm^{-3} (78 km) after the sprite streamer pulse. After the pulse the electron density exhibited relatively high values ($\geq 10^3$ cm^{-3}) at 63 and 68 km for almost 1 s. In contrast, the chemical model by Sentman et al. (2008b) (using a peak reduced electric field of 600 Td during 6 μs) predicted an enhanced electron density of ~10^6 cm^{-3} during 1 s at 70 km.

According to the model of Gordillo-Váquez (2008), the main kinetic mechanisms controlling the production of O^- before and after the streamer pulse were electron dissociative attachment of O_2 ($e + O_2 \rightarrow O(^3P) + O^-$) and O_3 ($e + O_3 \rightarrow O_2 + O^-$), respectively. However the main loss of O^- both before and after the pulse was associate detachment by N_2 ($O^- + N_2 \rightarrow N_2O + e$). This was the first time that associate detachment of O^- by N_2 was included, quantified and discussed in the context of the atmospheric chemistry of sprites. Associate detachment of O^- by N_2 is a relevant process due to two reasons: First, it can contribute to the production of nitrous oxide (N_2O) which is an important greenhouse gas, and second it releases free electrons that, as we will discuss later, can have key consequences in the electrodynamics of sprite streamers (Gordillo-Vázquez, 2010; Luque and Gordillo-Vázquez, 2011a). The detachment of O^- by N_2 has also contributed to explain, due to its characteristic time, the appearance of delayed sprites ocurring tens to hundreds of milliseconds after their parent lightning (Cummer and Füllekrug, 2001).

The trend followed by O_2^- was the same for the three altitudes investigated by Gordillo-Váquez (2008) and its highest value was reached at 63 km. In general, the peak values of the O_2^- concentration were found quite after the end of the igniting pulse producing the weakly ionized (but highly excited) non-equilibrium mesospheric air plasma. The trend predicted was that the higher the altitude the lower the O_2^- concentration and the more delayed (with respect to the pulse end) its peaked value in time. The main kinetic mechanism controlling the production of O_2^- before the end of the electric pulse ($\leq$ 5 μs) was found to depend on the altitude. At 63 km, the three-body electron attachment dominates ($e + O_2 + O_2 \rightarrow O_2^- + O_2$), however charge transfer ($NO^- + O_2 \rightarrow O_2^- + NO$) was the dominant production mechanism of O_2^- at 68 km and 78 km. The losses of O_2^- before the end of the sprite streamer pulse at 63 and 68 km was fundamentally the charge transfer between O_2^- and ozone ($O_2^- + O_3 \rightarrow O_2 + O_3^-$). At 78 km O_2^- is mainly lost through charge transfer with oxygen atoms ($O_2^- + O(^3P) \rightarrow O^- + O_2$).

During the sprite streamer electric pulse, the number density of $N_2O_2^+$ predicted by the model of Gordillo-Váquez (2008) exhibited the sharpest increase at the lowest altitude (63 km) while its growth became smoother at higher altitudes (78 km). An interesting feature of $N_2O_2^+$ in this model is the fact that it kept relatively high values at 63 km (10^4 cm^{-3}) and 68 km (10^3 cm^{-3}) up to 500 s and even longer times after the pulse was over. Before the end of the pulse, the main kinetic channel responsible for the production of $N_2O_2^+$ was $O_2^+ + N_2 + N_2 \rightarrow N_2O_2^+ + N_2$, while, for later times after the pulse, the main losses of $N_2O_2^+$ ions were due to electron dissociative recombination mechanisms leading to NO ($e + N_2O_2^+ \rightarrow NO + NO$) and N_2 and O_2 ($e + N_2O_2^+ \rightarrow N_2 + O_2$).

The sprite chemistry model of Gordillo-Váquez (2008) investigated the processes triggered by sprite streamers that produced enhancements in the populations of nitride oxides such as NO, NO_2 and NO_3. We will only comment here the nighttime sprite kinetics of NO (see Fig. 4). NO at 63 and 68 km exhibited a growth in the time domain after the pulse of a bit less than two orders of magnitude (63 km) and a factor of 8 (68 km) above ambient values after ~200 s. At 78 km its concentration remains constant or exhibits a slight increase or decrease, both less than a factor of 2, depending on whether humid air or dry air was considered. Gordillo-Váquez (2008) considered 64 production mechanisms and 44 removal channels of NO. Right before the end of the electric pulse, the main reactions (in order of importance) contributing to the formation of NO at 63 km and 68 km were $N(^2D) + O_2 \rightarrow NO + O(^3P)$ and $e + N_2O_2^+ \rightarrow NO + NO$. At 78 km, electron recombination with $N_2O_2^+$ was replaced by a charge transfer process ($NO^- + O_2 \rightarrow O_2^- + NO$) as the second largest source of NO. The metastable $N(^2D)$ is produced in the sprite streamer head by electron impact dissociative excitation ($e + N_2 \rightarrow N(^2D) + N + e$).

The two principal losses of NO before the end of the electric pulse at 63 km were predicted to be due to $O(^3P) + NO \rightarrow NO_2$, $N_2(A\ ^3\Sigma_u^+) + NO \rightarrow NO(A) + N_2$, while, at 68 km and 78 km, the second mechanism was replaced by $HO_2 + NO \rightarrow OH + NO_2$. At 10 ms the first and second production channels of NO at 63 and 68 km are the same as before the end of the pulse. The loss of NO at about 10 ms at all altitudes studied was mainly due to $O(^3P) + NO \rightarrow NO_2$, $N + NO \rightarrow N_2 + O(^3P)$ and $HO_2 + NO \rightarrow OH + NO_2$ (at 78 km). Finally, at ~100 s, the production of NO at 63 km is mainly due to $N + O_2 \rightarrow NO + O(^3P)$ and $O(^3P) + NO_2 \rightarrow O_2 + NO$ with the process $N(^2D) + O_2 \rightarrow NO + O(^3P)$ being much less important. However at 68 km and 78 km, at ~100 s, the process $N(^2D)$

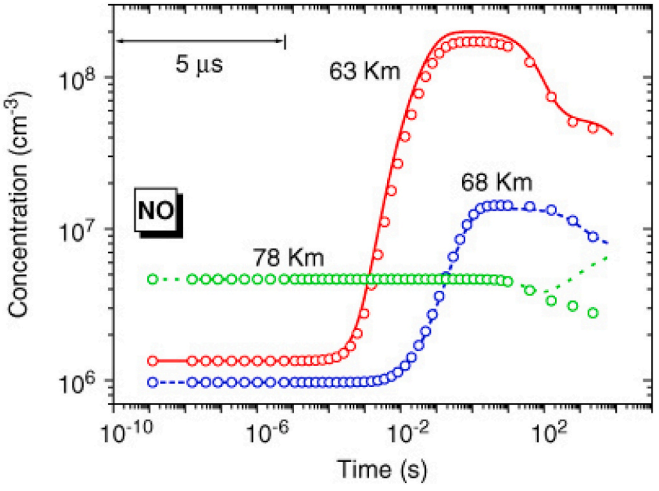

Fig. 4. Predicted time-dependent behaviour of the concentration of nitrogen oxide (NO) produced by a sudden electric pulse of 400 Td lasting 5 μs associated to the strength and duration of the electric field in the head of a sprite streamer for three different altitudes in humid air (with 4 ppm of water vapor; lines) and in the case of a dry mesosphere (open circles). Image reproduced from Gordillo-Váquez (2008).

+ O_2 → NO + $O(^3P)$ (dominant during the streamer pulse) becomes again the second (68 km) and first (78 km) most important mechanism producing NO.

The sprite kinetics of the molecular metastable N_2 ($A\ ^3\Sigma_u^+$) is also of great interest since, once produced, it can contribute to the formation of the greenhouse gas N_2O.

A visible feature in the trend followed by $N_2(A\ ^3\Sigma_u^+)$ in the model of Gordillo-Váquez (2008) was that although the difference between its initial values at 63 and 78 km was less than one order of magnitude, the impact of a single sprite event created a considerable difference between them right after the pulse. This meant that, after a sharp increase during the pulse duration, the concentration of $N_2(A\ ^3\Sigma_u^+)$ at 63 km was almost four orders of magnitude higher than at 78 km.

After a relatively long plateau region that lasts up to one millisecond (for 63 and 68 km) and almost 0.01 s for 78 km, the number density of $N_2(A\ ^3\Sigma_u^+)$ was predicted to decrease abruptly. So, before the end of the electric pulse, the main pumping reactions of $N_2(A\ ^3\Sigma_u^+)$ at 63 and 68 km were electron-impact excitation closely followed by radiative and collisional de-excitation from $N_2(B\ ^3\prod_g)$: $N_2 + e \rightarrow N_2(A\ ^3\Sigma_u^+) + e$, $N_2(B\ ^3\prod_g) \rightarrow N_2(A\ ^3\Sigma_u^+) + h\nu$ and $N_2(B\ ^3\prod_g) + N_2 \rightarrow N_2(A\ ^3\Sigma_u^+) + N_2$, while at 78 km, $N_2\ (B\ ^3\prod_g) \rightarrow N_2\ (A\ ^3\Sigma_u^+) + h\nu$ was followed by $N_2 + e \rightarrow N_2\ (A\ ^3\Sigma_u^+) + e$ and $N_2(B\ ^3\prod_g) + N_2 \rightarrow N_2(A\ ^3\Sigma_u^+) + N_2$.

The loss mechanisms of $N_2(A\ ^3\Sigma_u^+)$ before the end of the streamer pulse were, for all the altitudes analysed, three different collisional de-excitation channels that (in order of importance) were: $N_2(A\ ^3\Sigma_u^+) + O_2 \rightarrow N_2 + 2\ O(^3P)$, $N_2(A\ ^3\Sigma_u^+) + O_2 \rightarrow N_2O + O(^3P)$, followed by a third process (with a much weaker rate than the two previous ones) $N_2(A\ ^3\Sigma_u^+) + N_2 \rightarrow 2\ N_2$. After the streamer pulse, the source terms of $N_2(A\ ^3\Sigma_u^+)$ were radiative and collisional de-activation (quenching) of $N_2(B\ ^3\prod_g)$ while the loss reactions are the same as during the pulse.

In addition to molecular optical emitting species like $N_2(B\ ^3\prod_g)$, $N_2(C\ ^3\prod_g)$ and $N_2(a\ ^1\prod_g)$ responsible of the first (red) and second (blue) positive systems of N_2 and of the N_2 Lyman Birge Hopfield (ultraviolet) optical emissions, the model of Gordillo-Váquez (2008) also discussed possible sprite triggered green (557.7 nm) and red (630 nm) optical emissions due to excited atomic oxygen like $O(^1S)$ and $O(^1D)$, respectively. The sprite induced $O(^1S)$ green optical (see Fig. 5) emissions can contribute to enhance the natural nightglow that could be imaged and/or spectroscopically detected by appropriate sensors since the 557.7 nm optical emissions lies on a spectral region with weak N_2 optical emissions due to sprite streamers. However the 630 nm optical pulse due to sprite excited $O(^1D)$ could be more challenging to detect since it is predicted to last much less (70–80 μs) than the green flash (several tens of ms) and, in addition, it would be easily mistaken for the red optical emissions of the first positive system of N_2.

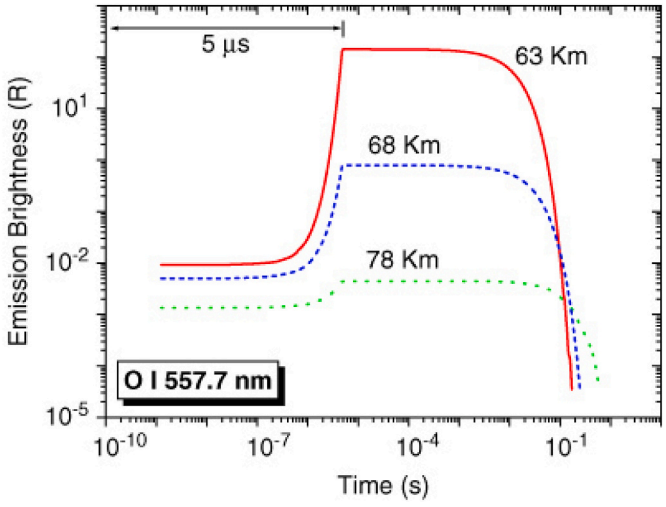

Fig. 5. Predicted time-dependent behaviour of the emission brightness of the green (557.7 nm) line of the metastable atomic oxygen electronic state $O(^1S)$ produced by a single sprite streamer. Note that the green brightness increases at lower altitudes where the ambient density is larger. Image reproduced from Gordillo-Váquez (2008).

According to the nighttime sprite chemistry model of Gordillo-Váquez (2008), the most important microscopic mechanism producing the excited state $O(^1S)$ during the streamer pulse is $N_2(C\ ^3\prod_g) + O_2 \rightarrow N_2 + O(^3P) + O(^1S)$ and the losses of $O(^1S)$ at 63 and 68 km are mainly caused by $O(^1S) + O_2 \rightarrow O_2 + O(^3P)$, $O(^1S) + H_2O \rightarrow OH + OH$, $O(^1S) + H_2O \rightarrow H_2 + O_2$, and $O(^1S) \rightarrow O(^1D) + 557.7$ nm while, at 78 km, $O(^1S) \rightarrow O(^1D) + 557.7$ nm becomes the second most important removal reaction of $O(^1S)$ after $O(^1S) + O_2 \rightarrow O_2 + O(^3P)$. It should be however noted that Gordillo-Váquez (2008) did not consider the dissociation excitation ($e + O_2 \rightarrow O(^3P) + O(^1S) + e$) as a source of $O(^1S)$. This process was considered in the model of Sentman et al. (2008b) and it is most probably as important (or a bit more) as $N_2(C\ ^3\prod_g) + O_2 \rightarrow N_2 + O(^3P) + O(^1S)$ to produce $O(^1S)$.

When the electric pulse is off, the dominant production process leading to $O(^1S)$ at 63 km is $N_2(A\ ^3\Sigma_u^+) + O(^3P) \rightarrow N_2 + O(^1S)$. At 68 km, the most important production channels of $O(^1S)$ are first $N_2(C\ ^3\prod_g) + O_2 \rightarrow N_2 + O(^3P) + O(^1S)$ followed by $N_2\ (A\ ^3\Sigma_u^+) + O(^3P) \rightarrow N_2 + O(^1S)$ but, at 78 km, these two processes are reversed becoming $N_2(A\ ^3\Sigma_u^+) + O(^3P) \rightarrow N_2 + O(^1S)$ the dominant process. The losses of $O(^1S)$ after the pulse are predicted to be same as the ones operating during the streamer pulse.

The detection of oxygen metastable $O(^1D)$ could be of relevance in the plasma chemistry of sprites because it could be a significant by-product accompanying the formation of NO in the reaction $N(^2D) + O_2 \rightarrow NO + O(^1D)$ considered by the model of Sentman et al. (2008b). Instead, $N(^2D) + O_2 \rightarrow NO + O(^3P)$ was considered by Gordillo-Váquez (2008) as the main source of NO. After the formation of $O(^1D)$ by electron-impact dissociative excitation of O_2 during the sprite streamer pulse, the model of Sentman et al. (2008b) predicted that $O(^1D)$ can also be formed by $N(^2D) + O_2 \rightarrow NO + O(^1D)$ in the streamer afterglow. However, $O(^1D)$ is quickly quenched by collisions with N_2 and O_2 so that, at the end, $O(^1D)$ results in a short (70–80 μs) living species (Gordillo-Váquez, 2008; Sentman et al., 2008b).

Sprites could also activate ambient CO_2 molecules and produce transient infrared (IR) glows that can be potentially detectable from space. In 2008 there were only two early studies about the modelling of IR emission from the upper atmosphere caused by (1) heating of sub ionospheric electrons due to thundercloud electric fields (Picard et al., 1997) leading to excited CO_2 by reactions with vibrationally excited N_2 previously activated by electron collisions, and (2) CO_2 IR transient emissions caused by sprites (Milikh et al., 1998). These two previous investigations dealt with the kinetic mechanisms responsible for the 4.26 μm IR radiation from excited CO_2. In this context, the sprite chemistry model by Gordillo-Váquez (2008) contributed to widen the discussion on the possible kinetic mechanisms underlying not only the transient 4.26 μm caused by sprite but also other possible IR glows detectable at 9.4 μm, 13.9 μm and 14.9 μm also originated from sprite excited CO_2. The brightnesses of these sprite induced IR glows were analysed at 63 km, 68 and 78 km. It was found that the role of N_2 ($X\ ^1\Sigma_g^+$, v = 1) was critical in producing sufficiently concentration of CO_2* radiating in 4.26 μm. The strongest sprite induced CO_2 glows at 78 km were found to emit, in order importance, at 4.26 μm, 14.9 μm, 13.9 μm and 9.4 μm reaching their maxima about 100, 1, 1 and 10 s after the sprite streamer pulse, respectively.

3.1.6. Early non conclusive sprite chemistry observations: 2008–2010

Possible TLE enhancement of odd nitrogen (NO_x) and odd hydrogen (HO_x) might influence the ozone balance of the middle atmosphere. Also, the chemical balance of other important greenhouse gases like N_2O might be affected by streamers of some TLEs like sprites in the

mesosphere and/or blue jets and, blue starters and cloud corona discharges in the stratosphere and upper troposphere. The atmospheric sources of nitrous oxide (N_2O) are not yet completely understood (Sheese et al., 2016; Kelly et al., 2018).

In 2008 two independent studies were published about the use of two satellite instruments (MIPAS and GOMOS) aboard the European Space Agency (ESA) ENVIronmental Satellite (ENVISAT) in an attempt to investigate sprite chemistry by observing lower mesospheric NO_2 trends with tropospheric lightning activity (Arnone et al., 2008; Rodger et al., 2008). None of these investigations reached conclusive observational evidence. Arnone et al. (2008) showed a statistical difference between the amount of NO_2 observed by the Michelson Interferometer for Passive Atmospheric Sounding (MIPAS) mid-infrared emission spectrometer and thunderstorms activity within a field of view (FOV) of 500 × 30 km regions recorded by the World Wide Lightning Location Network (WWLLN) (see Fig. 6). Their statistical analysis suggested NO_2 enhancements of about 10% at 52 km height and tens of percent at 60 km height immediately after thunderstorm activity (see Fig. 7). The work by Rodger et al. (2008) compared regional variations of column amounts of NO_2 observed by the Global Ozone Monitoring by Occultation of Stars (GOMOS) UV–visible spectrometer with respect to the lightning activity obtained from observations with the Optical Transient Detector (Christian et al., 2003) in the tropical and northern land and oceanic mid-latitude regions (Rodger et al., 2008). The area between land and oceanic regions was compared, because ~85–90% of lightning activity occurs above land (Christian et al., 2003). They reported no evidence of any correlation within the detection levels of the GOMOS measurements.

The study by Lee and Shepherd (2010) reported observations of supersonic neutral velocities, called supersonic bursts (for over 8 s) of enhanced $O(^1S)$ emission rates (detected at wavelength 557.7 nm) for tangent altitudes of 73–80 km during summer daytime by the Wind Imaging Interferometer (WINDII) on board the Upper Atmosphere Research Satellite (UARS) in northern latitudes. Coincidences in space and time between supersonic velocity profiles and space-based lightning detection observed by the Orbital Transient Detector (OTD) at a wavelength of 777.4 nm were found in a limited number of cases in the high-latitude summer of July 1996. Theory suggests that an electric field of 173 V/m is required to generate a typical supersonic velocity of 750 m/s forced by ion-neutral collisions at 73 km. The electric field must have sufficient energy to generate excited oxygen $O(^1S)$ atoms by different possible direct and/or indirect mechanisms such as: $e + O_2 \rightarrow O(^3P) + O(^1S) + e$ (direct electron-impact dissociative excitation), $e + O(^3P) \rightarrow O(^1S) + e$ (direct electron-impact excitation), or $N_2\ (A\ ^3\Sigma_u^+) + O(^3P) \rightarrow N_2 + O(^1S)$ (indirect excitation by energy transfer from $N_2(A\ ^3\Sigma_u^+)$) or $N_2(C\ ^3\prod_g) + O_2 \rightarrow N_2 + O(^3P) + O(^1S)$ (indirect dissociative excitation of

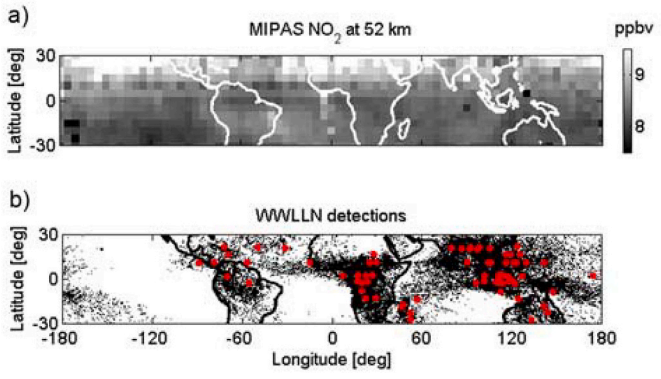

Fig. 6. Panel (a) Mean nighttime NO_2 at 52 km height by MIPAS. Panel (b) WWLLN lightning activity (black, detections between 21 and 22 local hour; red, WWLLN-MIPAS coincidences) for the period August to December 2003. Image reproduced from Arnone et al. (2008).

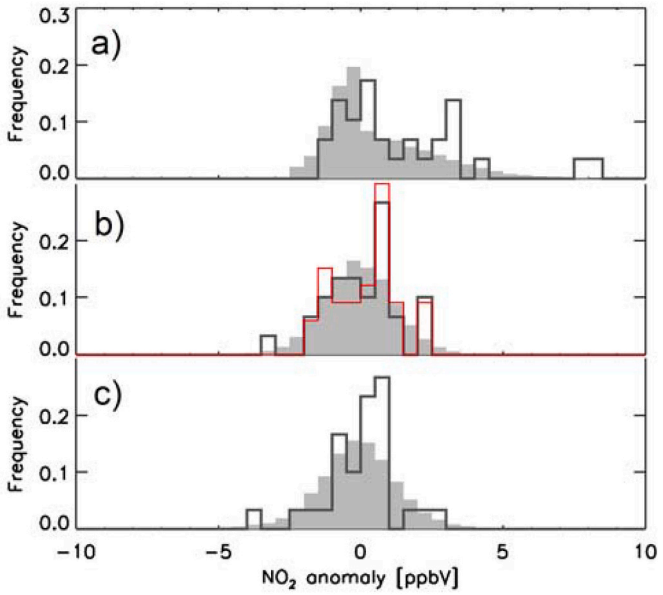

Fig. 7. Global distribution of NO_2 anomalies over the region 30°S to 20°N (shaded, NO_2, gray line, WWLLN-NO_2), with static coincidence window of 20 min and 30 km × 500 km. Measurements of MIPAS are for heights (a) 60 km, (b) 52 km, and (c) 47 km. At 52 km height the dynamical correlation case is superimposed (red). In this image WWLLN-NO_2 were obtained integrating over a time window of 20 min prior to the MIPAS observation and using a threshold of 5 lightning strokes. At 52 km altitude (see panel (b)), the overal static WWLLN-NO_2 distribution (gray line) shows an asymmetry compared to the background NO_2 (shaded). According to Arnone et al. (2008) these results suggest that a significant fraction of all WWLLN-NO_2 coincidences (possibly 15%–20%) show an enhancement of about +1 ppbV compared to background NO_2, i.e. a + 10% change. This fraction is roughly compatible with the expected number of coincidences deduced from the sprite to lightning occurrence ratio discussed above. Image reproduced from Arnone et al. (2008).

by energy transfer from $N_2(C\ ^3\prod_g)$). Both $N_2(A\ ^3\Sigma_u^+)$ and $N_2(C\ ^3\prod_g)$ would have been previoulsy excited by electron-impact collisions. Daytime sprites were suggested by Lee and Shepherd (2010) as a possible source of the transient detected bursts of $O(^1S)$.

During the day, the ionospheric conductivity is significantly higher than at night and conventional breakdown is prevented at mesospheric altitudes. Therefore, daytime sprites (and/or halos) have to be initiated at lower altitudes. Due to the higher atmospheric density, larger electric fields are required to cause air breakdown originated by lightning. This results in that only exceptionally large lightning events with extremely large CMCs (6000–8000 C km) can trigger daytime sprites (Stanley et al., 2000). Typical daytime altitudes of 50–60 km (Stanley et al., 2000) for lightning driven electric breakdown leading to daytime sprites are clearly below the 73 km where bursts of $O(^1S)$ were reported by Lee and Shepherd (2010) but still $O(^1S)$ produced by daytime sprites can not be completely disregarded due to the many uncertainties about the maximum altitudes and kinetics of (the very little studied) daytime sprites.

A recent daytime zero dimensional (0D) non–selfconsistent modeling of a single sprite streamer predicts transient (1 ms) enhancements of up to 10^{-3} ppm for the $O(^1S)$ concentrations at 42 km altitude (Winkler and Notholt, 2014). This is clearly not sufficient to account for the detected 8 s burst of $O(^1S)$. However, it is also necessary to add that (1) sprites can have many streamers with extremely complex combined or sequential chemistries (sprite streamers can appear in the same or different times with the ambient air already being chemically pre–treated), and that (2) sprite chemistry modeling is still in its infancy (especially during daytime).

3.1.7. Sprite optical (380–900 nm) spectroscopy: 1995–2020

Remote optical spectroscopy in the near–ultraviolet (NUV), visible (VIS) and near–infrared (NIR) is a key primary diagnostic technique to identify some chemical species excited by TLEs. Spectroscopic investigations can help in understanding pieces of the complex non–equilibrium air plasma kinetics triggered by TLEs. What is the true extend of the chemical impact caused by many local transient non-equilibrium chemical sources occurring between the upper troposphere and the upper mesosphere of the atmosphere?

Unfortunately, only the most abundant chemical species are significantly affected by TLEs and, consequently, emit enough light within the NUV–VIS–NIR optical ranges to be detected. There can be relatively dark (metastable) excited species such as, for example, $N_2(A\ ^3\Sigma_u^+)$ that, once excited, can play a key role in the production of certain atmospheric species like nitrous oxide (N_2O), a major greenhouse gas that has recently overtaken chlorofluorocarbons (CFCs) as the dominant anthropogenic cause of ozone depletion. Also, there could be some other chemical species like O_3, H_2O_2, or key radicals like HO_2, OH and other polar diatomic molecules whose atmospheric abundances could be influenced by the presence of TLEs. Microwave/submilliter and/or far infrared spectroscopy techniques would then be needed to identify changes in the relative concentrations of those species. Absorption spectroscopy could also be useful (Langford et al., 2004).

To date only ground and aircraft–based NUV–VIS–NIR spectroscopy has been used to characterize optical emissions by TLEs. We comment below the advances in TLE–related NUV–VIS–NIR spectroscopic investigations.

Soon after the publication of the first TLE images (of a sprite) recorded during the night of 22 to 23 September 1989 (Franz et al., 1990), the interest of the international community in spectroscopic features of TLEs started. Spectra of TLE can inform about the type of atoms and/or molecules that produce optical emissions, their degree of vibrational and electronic excitation, and if TLEs are able (or not) to produce a possible and measurable heating of the surrounding atmosphere. Early observational works (Mende et al., 1995; Hampton et al., 1996) reported the first spectroscopic studies of the N_2 first positive system (FPS, $B\ ^3\prod_g \rightarrow A\ ^3\Sigma_u^+$) from the "body of sprites occurring between 70 km and 90 km of altitude. These early spectral investigations of TLEs used regular (30 fps) video recording in the visible and near-infrared spectral range (550 nm to 840 nm) and low (between 6 and 10 nm) spectral resolutions.

The first theoretical analysis of sprite spectra was published by Green et al. (1996). Using spectra fitting they derived preliminary vibrational populations of $N_2(B\ ^3\prod_g)$ and $N_2(A\ ^2\prod_u)^+$ involved in sprite induced optical emissions of the N_2 FPS and N_2^+ first negative system (FNS). The results of Green et al. (1996) were the first to discuss the possible nature of the different molecular excitation mechanisms present in sprites and to provide some quantitative analysis on the relative populations of $N_2(B\ ^3\prod_g)$ vibrational levels up to $v = 10$ derived from the data reported by Mende et al. (1995) and Hampton et al. (1996). However, the results concerning the emission from the N_2 first positive system presented by Mende et al. (1995) and Hampton et al. (1996) mostly covered $\Delta v = 2$, 3 and 4, and only a few transitions from the $\Delta v = 1$ bands that allowed little experimental information on the $v = 0$ and $v = 1$ relative populations. It is also worth mentioning that Green et al. (1996) modeled the expected radiance levels and vibrational distributions (of $N_2(B\ ^3\prod_g)$ and $N_2(A\ ^3\Sigma_u^+)$ at 70 km as a function of electron energy. The latter allowed Green et al. (1996) to publish the first estimate of electron energies in sprites in a range between 0.4 eV to 2 eV. The $N_2(B\ ^3\prod_g)$ state vibrational distribution was best matched using a 1 eV Boltzmann electron distribution function. The 1 eV energy estimate of Green et al. (1996) led Heavner (2000) to an overestimate of the total energy in a sprite of 1.2 GJ. This was largely because of the significant enhancement in vibrational excitation over electronic excitation at the lower (1 eV) energy with respect to the case at higher energies (2 eV and above).

Later Milikh et al. (1997) published a model of sprite spectra using a steady state approach for the underlying electron energy distribution function and a very simplified kinetic scheme only considering electron impact vibrational excitation of $N_2(B\ ^3\prod_g)$, $N_2(C\ ^3\prod_g)$ and $N_2(A\ ^2\prod_u)^+$, radiative decay and quenching. This model did not consider processes like intersystem collisional transfer (ICT), vibrational redistribution, energy pooling and other vibrational mechanisms that can significantly influence sprite spectra.

Unfortunately, the number of spectroscopic campaigns of TLEs since the mid–1990s has been scarce. Later results (Morrill et al., 1998; Bucsela et al., 2003) reported spectroscopic investigations of the low-altitude "tendrils" (blurred motion of rapidly moving point-like structures (Liu and Pasko, 2005; Stenbaek-Nielsen et al., 2007) of sprites at 53 km and 57 km covering from 600 nm up to 900 nm with low spectral resolutions of 7 nm and 11 nm, respectively. More recently, altitude-resolved sprite spectra of the N_2 FPS have been reported with an imaging (vertical) slit spectrograph covering between 640 nm and 820 nm and using 3 ms (300 fps) and ~ 3 nm temporal and spectral resolutions, respectively (Kanmae et al., 2007).

Regarding near-ultraviolet (below 400 nm) spectra of sprites, the only measurements available to date (without correction for instrument response function) are those focusing on optical emissions of the N_2 s positive system (SPS, $C\ ^3\prod_g \rightarrow B\ ^3\prod_g$) from the "body" of sprites at 65 km altitude (Heavner et al., 2010). This near-ultraviolet sprite spectrum was recorded during the EXL98 observation campaign from an aircraft at 14 km altitude with ~4 nm spectral resolution and a recording rate of 60 fps.

High–speed (10,000 fps) slitless spectroscopy of sprite streamer heads and column-shaped glows were reported for the first time in 2010 from aircraft observations including blue spectral features Kanmae et al. (2010a) and from ground-based facilities Kanmae et al. (2010b) with the spectra consisting only of the N_2 FPS due to the atmospheric absorption of the blue component through the long line of sight.

Gordillo-Vázquez (2010) presented the first full kinetic model to include detailed vibrational kinetics of sprites. The prediction of this model at 78 km agreed with the vibrational distribution function (VDF) of $N_2(B\ ^3\prod_g)$ in the 84.4–86.4 km range measured by Kanmae et al. (2007) and more recently by Kuo et al. (2019). Besides, the model of Gordillo-Vázquez (2010) predicted the shape and trend of the VDF of $N_2(C\ ^3\prod_g)$ at 78 km for different temporal resolutions. The results of the model of Gordillo-Vázquez (2010) exhibited a very good agreement with available VDF of $N_2(B\ ^3\prod_g)$ for the observed vibrational levels (from $v = 2$ to $v = 6$) and predicted no enhancement of $v = 2$ contrary to controversial observations at 57 km (due to possible errors in the instrument sensitivity calibration above 850 nm) (Bucsela et al., 2003) but in agreement with more certain results at 53 km (Bucsela et al., 2003). In addition, this model provided the detailed kinetic mechanisms underlying the behavior of $N_2(B\ ^3\prod_g, v = 2)$ together with further predictions about the shape of the VDFs of $N_2(B\ ^3\prod_g)$ and $N_2(C\ ^3\prod_g)$ as they should eventually appear when sprite spectra were recorded by high–speed video cameras at 1000 frames per second (fps) and 10,000 fps.

Later in 2011 Luque and Gordillo-Vázquez (2011b) found that the VDFs of $N_2(B\ ^3\prod_g)$ and $N_2(C\ ^3\prod_g)$ depend very weakly on the driving electric field. Also in 2011, Gordillo-Vázquez et al. (2011) used a full vibrational kinetic model to derive the synthetic spectra of halos in the spectral ranges 200–500 nm and 640–1065 nm for different spectral resolutions (between 2 nm and 10 nm), rotational temperatures (220 K and 1000 K) and observation altitudes corresponding to mountain (3 km and 4.3 km), airplane (14 km), balloon (35 km) and space observation platforms. They calculated the non-equilibrium vibrational distribution functions (VDF) of different excited electronic states of molecular nitrogen (N_2) associated to halo optical emissions in the ultraviolet (UV), due to the N_2 Lyman-Birge-Hopfield (LBH) and Vegard-Kaplan (VK) band systems, and near UV, visible and near infrared (NIR) due to the first and second positive systems of N_2. Comparison of synthetic halo spectra with the single halo spectrum existing to date showed reasonable agreement after the observed halo spectra was corrected for instrument

sensitivity response.

Gordillo-Vázquez et al. (2012) published a study showing that sprites, beads and halos had similar optical spectra, but measurable differences in the near IR and near UV spectra. In particular, near infrared (NIR) and ultraviolet (UV) spectra of sprites, halos and beads corresponding to the first and second positive systems of N_2 were calculated for different observation altitudes (3.25 km, 14 km, 35 km) and space (nadir) platforms. The calculated non-equilibrium VDFs of the $N_2(B\ ^3\prod_g)$ states in halos and beads showed that the calculated NIR emissions produced strong N_2 FPS transitions that differed from the calculated sprite spectral emission patterns at ~888 nm but particularly pronounced differences were found in the NIR spectral region at ~1046 nm and ~1231 nm corresponding to the N_2 – FPS (0,0) and (0,1) transitions, respectively. The blue – near UV spectra from N_2 SPS transitions in halos and beads also exhibited slightly different spectral features when compared to the blue – near UV spectrum of sprites for bands originating from higher v levels ($v > 0$).

Unfortunately, the spectrographs used in the few TLE spectroscopic campaigns carried out so far were originally designed for aurora spectroscopy (Hallinan et al., 1985) and the best spectral resolution achieved until 2013 was ~3 nm, which was not enough to spectrally resolve the different low–lying vibrational transitions of the N_2 FPS.

The lack of TLE spectroscopic observations with high spectral resolution motivated our group at the IAA–CSIC in Granada (Spain) to build a TLE-dedicated instrument called GRAnada Sprite Spectrograph and Polarimeter (GRASSP). This spectrograph has a mean spectral resolution

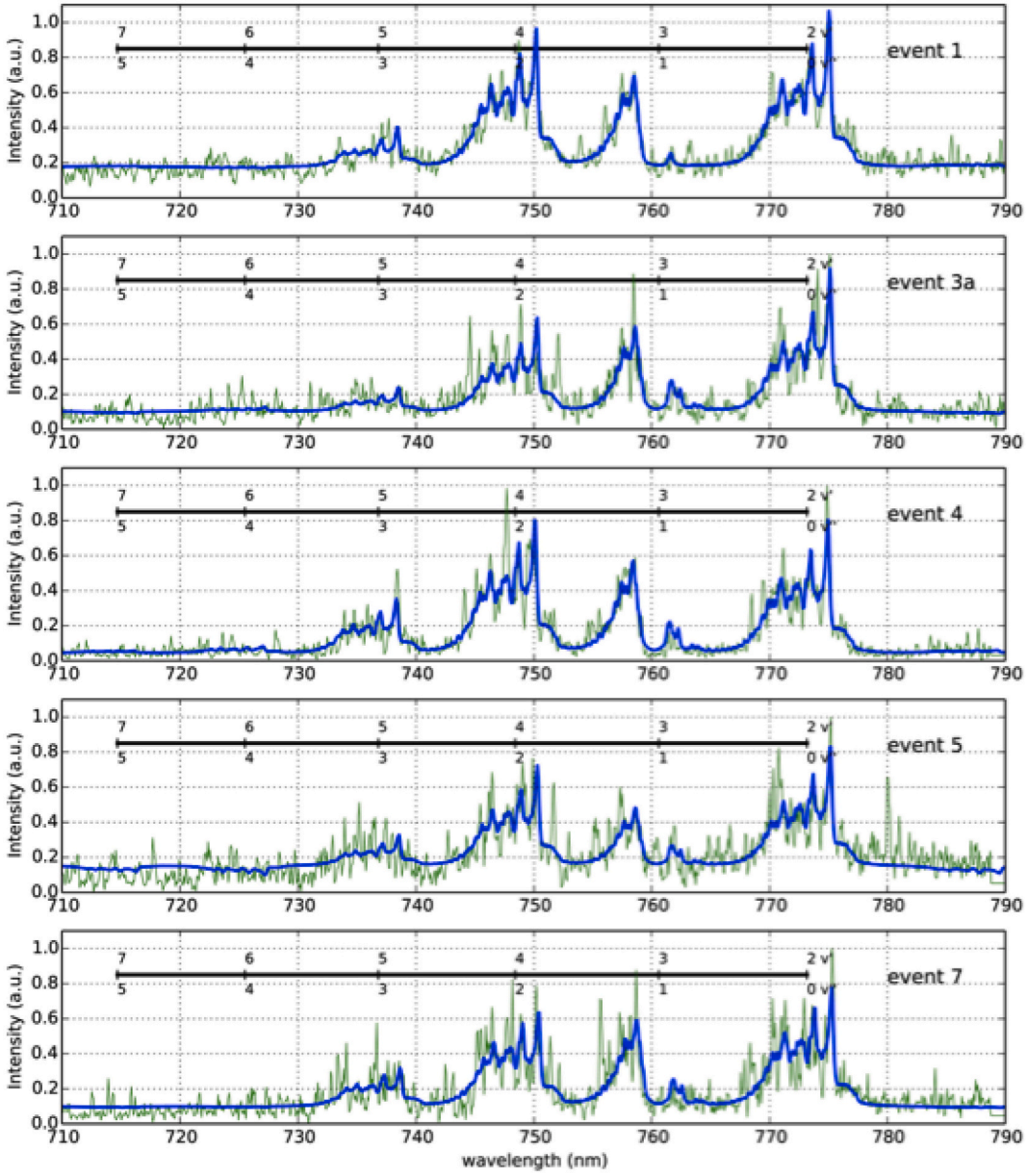

Fig. 8. Spectral fitting (blue line) of recorded (green line) carrot and multicolumn sprite spectra corresponding to the (2, 0) rovibronic transition of the N_2 ($B\ ^3\prod_g \rightarrow A\ 3\Sigma_u^+$) in the recorded and synthetic spectra. The observed spectra were recorded with a mean spectral resolution of 0.24 nm, while the synthetic spectra were calculated using a fixed resolution of 0.24 nm. The sprite spectra were recorded with a ground-based high spectral resolution TLE spectrograph named GRASSP placed in the Ebro Valley (Spain) during the August-September 2015 TLE imaging and spectroscopy campaign. The spectra correspond to carrot sprites (events 1) at 70–73 km, single column sprites (events 3a) at 66–67 km, column carrot sprite (event 4) at 72–74 km and multicolumn sprites (events 5 and 7) at 70–71 km and 69–70 km, respectively. Image reproduced from Gordillo-Vázquez et al. (2018). Note that the sprite spectra do not exhibit the characteristic 777.4 nm atomic oxigen line typical of lightning spectra.

of 0.25 nm (with a linear dispersion of 0.07 nm/pixel) and can cover (by adapting the grating) a movable free spectral range of 100 nm between 450 nm and 900 nm with 40 ms (25 fps) temporal resolution (Passas et al., 2016b). GRASSP is in operation for ground–based systematic imaging and spectroscopic surveys of all sorts of TLEs in Europe since October 2012 when the first GRASSP version (Parra-Rojas et al., 2013b) was deployed in the Calar Alto Astronomical Observatory (CAHA) (37° 13′ 23″ N 2° 32′ 45″ W) 2168 m above sea level in southeast Spain. GRASSP recorded from CAHA many images of distant TLEs (Passas et al., 2014) and could also carried out meteor spectroscopy (Passas et al., 2016a) during TLE spectroscopy field campaigns.

An upgraded version of GRASSP is now available and relocated (since May 2015) in Castellgali (Barcelona, 41°40′ 36″ N, 1° 50′ 24″ E) 266 m above sea level and close to the Ebro valley, a hot spot lightning location in Europe where TLE activity is usually occurring. From there GRASSP recorded high-resolution spectra of carrot and column–like sprites in the 700–800 nm range (see Fig. 8). Although a limited number of sprite spectra were recorded, this study revealed that (1) the 777.4 nm line (typical of regular lightning) is not present in the recorded spectra of sprites, and that (2) sprite streamer heating is not important at 66–74 km altitudes in the mesosphere (Gordillo-Vázquez et al., 2018).

Although no TLE spectroscopic measurements strictly speaking have been made so far from space, some important results have been achieved by space borne high speed photometers using different spectral filters. For instance, ISUAL confirmed that vacuum ultraviolet optical emissions in the N_2 Lyman Birge Hopfield band is an optical marker of TLEs (Chang et al., 2008). From the International Space Station, the high–speed narrow-band photometers of JEM-GLIMS operating at 337 nm and at 391 nm detected emissions from sprites (Sato et al., 2015). Finally, the very high–speed 337 nm photometer of ASIM has shown the frequent occurrence of streamer formed electrical discharges in thunderclouds that, contrarily to lightning, do not emit 777.4 nm light and that could open an entire new avenue of research in the field of atmospheric electricity (Soler et al., 2020).

3.1.8. *Sprite chemistry modeling: 2009–2020*

The four sprite chemistry models published in 2008 already commented above were devoted to investigate the local chemical impact of sprite streamer heads which are the most visible optical feature of sprites. However, high–speed optical recording of sprite streamers had recently showed that after the dark region behind the streamer head there was a persisting (milliseconds) optical trailing glow extending 2–10 km (McHarg et al., 2007). In addition, coordinated imaging of sprites and associated Extreme Low Frequency (ELF) detections (Cummer et al., 1998; Hu et al., 2007; Li et al., 2008) had already suggested that there could be an electrical current associated with sprites that might be related with the existence of an undervoltage electric field in the sprite streamer trailing afterglow.

Sentman and Stenbaek-Nielsen (2009) published a study where they explored the possible local chemical effects of the sprite streamer trailing afterglows at 70 km altitude. **A model** was considered for the electric field in the trailing column behind the streamer head where the electric field varied in magnitude over undervoltage values within the range $E/E_k = 0.25–1$ ($E/N \sim 30–120$ Td) and with a duration of one millisecond (Sentman and Stenbaek-Nielsen, 2009). One interesting result of this non–selfconsistent sprite chemistry model was that it set a preliminar upper limit $E < 0.5E_k$ for the electric field in the streamer trailing glow. This upper limit was derived from the fact that the brightness of the weak streamer optical tail was well below the saturation level of the imaging camera. From calibrations against stellar brightnesses (McHarg et al., 2007), the imager saturation was estimated to be a factor of ~2.2 below the peak brightness of the streamer heads, and the optical signal in the tail was at least an order of magnitude below saturation in the available high-speed sprite imagery (McHarg et al., 2007) (see Fig. 3). By referring to the calculated $N_2(B\ ^3\prod_g)$ they estimated that the electric field in weak sprite streamer tails did not exceed $0.5E_k$ for the trailing field, thus establishing an upper limit $E < 0.5E_k$. This limit was used to determine enhancements of chemical species in the trailing afterglows of sprite streamers.

The results obtained with this model indicated that the electron density was slightly decreased (with respect to streamer head values) on account of enhanced dissociative attachment in the undervoltage environment with electron densities being relatively more insensitive to the trailing electric field values than were the O^- densities. After assuming $E = 0.5E_k$ in the streamer trailing afterglow the densities of $O(^3P)$ and the metastable species $O(^1D)$ and $N_2(A\ ^3\Sigma_u^+)$ were enhanced by a modest factor of 2 or less compared with a field-free tail. O_2 (a $^1\Delta_g$) exhibited slightly greater enhancements, by up to a factor of 3, and O^- showed enhancements by up to a factor of 5 (Sentman and Stenbaek-Nielsen, 2009).

The numerical structure of this sprite streamer afterglow model was essentially the same as the previous sprite streamer head chemical model (Sentman et al., 2008b).

In spite of its limitations the nighttime sprite streamer trailing afterglow chemical model of Sentman and Stenbaek-Nielsen (2009) was an important step forward contributing to our understanding of the local chemical impact of a full sprite streamer (head and trailing glow).

Another important step forward that contributed to indirectly shed light on the atmospheric chemistry triggered by sprites came from the side of very detailed modeling of sprite streamer propagation dynamics in a varying density environment like the atmosphere of the Earth (Luque and Ebert, 2010). According to this model the densities of charged particles increase like the gas density N so an exponentially increasing number of electrons is liberated around the head. These electrons drift upwards, where the ion density is basically frozen (neglecting small variations due to attachment). Hence at some point the electron density surpasses the ion density and creates a net negative charge that is responsible for the increase in the electric field; then a second wave of electron impact ionization and excitation of N_2 with electric field $E \sim E_k$ sets in (Luque and Ebert, 2010). This was in agreement with observations by Morrill et al. (2002) and explained the variety of accumulated sprite observations showing an increase of luminosity in the sprite streamer channel after about 1 ms (Cummer et al., 2006; McHarg et al., 2007; Stenbaek-Nielsen and McHarg, 2008; Li and Cummer, 2009) (see Fig. 3). The predicted brightness for the sprite streamer trail optical emissions (first positive system of N_2) was an order or magnitude lower than the streamer head brightness of 2×10^8 R (Luque and Ebert, 2010).

Therefore (Luque and Ebert, 2010) explained the glowing trail by an increase of the reduced electric field up to values of E_k (and not only to 0.5 E_k as previously considered by Sentman and Stenbaek-Nielsen (2009). The mechanism of light emission was the same as in the streamer head: excitation of nitrogen by electron impact. This was also independently proposed by Liu (2010). Morrill et al. (2002) measured the intensity ratio between the second positive band of N_2 and the first negative band of N_2^+ integrated during the complete sprite evolution (about 10 ms), suggesting that the emitting states were excited under $E \simeq E_k$. On the other hand, Liu et al. (2009) analyzed data from the ISUAL instrument on board the FORMOSAT–2 satellite and concluded that in the early stages a sprite emits light mostly from regions where $E \simeq 4E_k$. The simulations of Luque and Ebert (2010) successfully explained both observations: initially most light is emitted from the streamer head where $E \simeq 4E_k$ but as it propagates a larger proportion of light is emitted from the trail, where $E \simeq E_k$. The ultimate kinetics leading to this relatively high electric field value in sprite streamer trailing regions is not yet completely clear though attachment instability seems to play a key role in the yet incomplete kinetic mechanism able to fully explain sprite streamer trailing glows (Luque et al., 2016). The role of attachment instability (that reduces the electron density allowing higher glow electric fields) in sprite streamer models is prevented by the action of electron associative detachment from O^- ($O^- + N_2 \rightarrow N_2O + e$), charge transfer from O^- to O_2^- ($O^- + O_2 \rightarrow O_2^- + O(^3P)$) and the subsequent

detachment from O_2^- ($O_2^- + M \rightarrow e + O_2 + M$). All this combined with the low pressure environment of the dry mesosphere (with just an average water concentration of a few ppm) makes that sprite streamer models with detachment and charge transfer predict short (at most 5 milliseconds) trailing glow optical emissions, which is contrary to observations of sprite streamer glows lasting up to 100 milliseconds (Luque et al., 2016). According to Luque et al. (2016), the rate of charge transfer between O^- and O_2^- could be higher (than the one available in the literature) due to, for example, the low temperature of the mesosphere, which would lead to a fast conversion between O^- and O_2^-. In that case detachment would proceed via $O_2^- + M \rightarrow O_2 + M + e$. Being an endothermic reaction in contrast to associate detachment ($O^- + N_2 \rightarrow N_2O + e$), which is exothermic, the detachment from O_2^- requires a higher field to be relevant. By assuming a fast conversion between O^- and O_2^-, the sprite streamer models would predict that the decay of a sprite streamer glow will vary from a characteristic time of a few milliseconds to a much longer one of tens of milliseconds (Luque et al., 2016). Finally, an important point to consider is that the available rates usually comes from experiments done under conditions (pressure, temperature) that are usually far from the ones in the mesosphere and that, consequently, might not be optimum for modeling the kinetics of upper atmospheric (low pressure) electrical discharges such as sprites. New basic experiments to measure rate coefficients (for detachment and charge transfer reactions) recreating upper atmospheric conditions are then necessary.

In contrast to the dry air of the mesosphere, in humid air at atmospheric pressure (or in the humid troposphere at higher pressure than in the mesosphere) electron detachment from O^- is very much inactivated by the efficient formation of the more stable O_3^- ion through the three-body reaction $O^- + O_2 + M \rightarrow O_3^- + M$. Since O_3^- is a stable ion (Pancheshnyi, 2013), further detachment processes are negligible (Luque et al., 2017). Moreover, O^- ions are also lost at high pressure through charge transfer $O^- + O_2 \rightarrow O_2^- + O(^3P)$, but in humid air, the resulting O_2^- ions quickly form water clusters and are thus stabilized (Luque et al., 2017). This explains why in humid air at atmospheric pressure the attachment instability can fully operate leading to incomplete screening of the electric field able to produce long (~100 ns)–lived glows (also called secondary streamers) and also the formation of a small glow close to the electrode (Luque et al., 2017). It was found in (Luque et al., 2017) that screening is weaker for streamers with a low leading ionization (10^{13} cm^{-3}) and small radius (0.5 mm). This low leading ionization is typical of negative streamers, which explains why in the experiments of Kochkin et al. (2012, 2014, 2016) glows appear preferentially in negative discharges. Higher values of the leading ionization are usually associated to positive streamers propagating in virgin air, which seem to prevent the formation of long-lived glows in channel of positive streamers (Luque et al., 2017). There are, however, cases in which glows form in positive streamers. That is, for example, the case in sprite streamers, which are generally positive streamers in the dry mesosphere that are shown in observations (Stenbaek-Nielsen and McHarg, 2008; Stenbaek-Nielsen et al., 2013) and predicted by microscopic simulations without considering electron detatchment (Luque and Ebert, 2010; Liu, 2010; Luque and Gordillo-Vázquez, 2011c; Luque et al., 2016). However, as mentioned above, when detachment is included in models of sprite streamers developing in the low pressure and dry ambient of the mesosphere they only predict short (some few milliseconds) glows. This is contrary to observations so that the kinetic explanation of the long–lasting glows of sprite streamers remains unclear.

Experimental studies under controlled conditions of the formation of different types of water clusters are important and needed to obtain accurate rate coefficients of positive (Brasseur and Solomon, 2005) and negative (de Urquijo et al., 2013) water clusters that could be of interest for streamer kinetics in humid air under different pressure scenarios (from the upper troposphere to the mesosphere).

The investigations of Gordillo-Vázquez and Luque (2010) found the key role played by associate detachment of O^- ion in the atmospheric electrical conductivity variations caused by sprites. This study investigated the electrical conductivity of a sprite streamer channel at three different altitudes (63 km, 70 km and 80 km). The authors discussed the hypothesis that the electrical conductivity stays constant along the full length of a streamer channel, contrary to expectations based on scaling laws. Then they applied this hypothesis and extrapolations from a numerical electrodynamical simulation to study the air plasma kinetics after the passage of a streamer. They tested two possible scenarios for the physical origin of trailing sprite optical emissions: a single pulse and a single pulse with a delayed re–enhancement of the electric field up to the reduced breakdown value E_k/N in a long–lasting pulse in the range 2 ms (80 km), 10 ms (70 km) and 15 ms (63 km) after the initial one. The simulations of Gordillo-Vázquez and Luque (2010) showed that the narrowband VLF observations of Dowden et al. (2001) agreed with persistent electric fields in the sprite lasting for several milliseconds and that associative detachment of O^- ions by N_2 ($O^- + N_2 \rightarrow N_2O + e$) could significantly affect the atmospheric conductivity in the presence of sprites. This investigation was the first to show that associative detachment of O^- is an important source of delayed (few milliseconds) electrons in undervoltage environments typically found in sprite streamer trailing glows (Gordillo-Vázquez and Luque, 2010).

The process of associative detachment $O^- + N_2 \rightarrow N_2O + e$ was earlier discussed by Gordillo-Váquez (2008) as the main mechanism responsible for the loss of O^- ions in sprite streamers. The kinetic model of Sentman et al. (2008a) did not include O^- detachment in its kinetic scheme while some other associative dettachment processes (also included in the kinetic model of Gordillo-Váquez (2008) were considered.

The large increase in conductivity induced by associative detachment of O^- by N_2 would significantly affect the dynamics of a self-consistent streamer model in relatively long time-scales. By 2010 no self-consistent, electrodynamic sprite streamer models had yet included the production of O^- in the streamer head and the subsequent detachment of electrons in the streamer channel. The model of Gordillo-Vázquez and Luque (2010) in combination with the increase in the sprite channel electric field predicted by Luque and Ebert (2010) and Liu (2010) showed that associative detachment is important to understand the sprite streamer dynamics (and induced kinetics) over the time scale from milliseconds to hundreds of milliseconds.

In 2011, Evtushenko and Mareev (2011) published a model to investigate the disturbances of the mesospheric ion composition during lightning-triggered nighttime and daytime sprites at altitudes of 75 km and 85 km. The focus of this work was to explore electron, positive and negative ions (NO^+, O_2^+, N_2^+, O^-) and water cluster ion perturbations taking place in the mesosphere in response to a lightning produced quasi-electrostatic electric field also responsible for the glowing diffuse upper region of sprites. However, their selected 75 km and 85 km altitudes for the occurrence of daytime sprites were not in agreement with previous reports suggesting that typical daytime sprite altitudes are in the range 50–60 km (Stanley et al., 2000). For nighttime conditions, these authors carried out a parametric study to analyse the impact of changing the lightning flash impulse time and the amplitude of the resulting lightning induced mesospheric quasi–electrostatic electric field. No analysis was intended of the sprite streamer atmospheric chemistry. However these authors checked their model against that of Sentman et al. (2008b) at 70 km and found similar enhanced values for O^- concentrations but its predicted lifetime was strongly shorter (<0.1 ms) than the relatively long (1–2 second) O^- lifetime calculated in the sprite streamer chemistry model of Sentman et al. (2008b). This discrepancy was probably due to the different kinetics and model structure.

The key role of O^- detachment by N_2 ($O^- + N_2 \rightarrow N_2O + e$) in electric breakdown under low pressure conditions and, particularly, in explaining delayed sprite inception was illustrated in a paper by Luque and Gordillo-Vázquez (2011a). Ten years ago models typically assumed that the net change in the density of free electrons in sprites or halos was

determined by the competition between electron impact ionization and electron dissociative attachment to oxygen molecules (Pasko, 2010; Liu and Pasko, 2004; Luque and Ebert, 2009; Hu et al., 2007), and that the balance between them is achieved with an electric field termed the conventional breakdown field (~120 Td). According to those models, free electrons were removed in an electric field whose strength was below the breakdown field, but they were multiplied in a field that is stronger than the breakdown field. The work of Luque and Gordillo-Vázquez (2011a) used a simple model of the electric response in the mesosphere at timescales of tens of milliseconds to show that in the upper atmosphere, electrons multiply also under field strengths significantly below that of the conventional breakdown field because, at low pressure, electron associative detachment form atomic oxygen negative ions O^- (Moruzzi and Price, 1974; Rayment and Moruzzi, 1978) that counteracts the effect of dissociative attachment.

The conventional breakdown assumption consisting in that electrons are inert after they form O^- is valid only at high pressures, close to 1 atm, where three-body stabilization of O^- dominates (Luque and Gordillo-Vázquez, 2011a). The relevance of associative detachment was known in the low-pressure plasma community already in the 1970s, when studies of low-pressure electric discharges (Moruzzi and Price, 1974; Rayment and Moruzzi, 1978) showed that there is no apparent electron attachment in air below ~0.1 atm (corresponding to altitudes above ~15 km in the atmosphere), but it had apparently escaped the attention of researchers working on atmospheric electricity. Only very recently, the relevance of associative detachment for sprite streamers was pointed out using a full chemical kinetic model (Gordillo-Váquez, 2008; Gordillo-Vázquez and Luque, 2010).

The model used by Luque and Gordillo-Vázquez (2011a) coupled chemical kinetics to dielectric relaxation, and the simulations indicated that associative detachment could explain measurements of the time and altitude of the inception of delayed sprites (Gamerota et al., 2011). Therefore, the authors concluded that associative detachment is a fundamental process in upper atmospheric electrodynamics with potential influence on other atmospheric electrical phenomena like blue jets and giant blue jets (Pasko et al., 2012) and the long-standing problem of the initiation of lightning inside thunderclouds, where measured electric fields are lower than the conventional breakdown threshold (Williams, 2006).

Winkler and Notholt (2014) published a daytime sprite streamer chemistry model in 2014. This model used a prescribed streamer electric field employing a streamer parametrisation as previoulsy considered in earlier sprite streamer chemistry models (Sentman et al., 2008b; Gordillo-Váquez, 2008; Hiraki et al., 2008). It implemented the associate detachment of O^- by N_2 leading to N_2O and free electrons (Luque and Gordillo-Vázquez, 2011a) using steady–state electron rate coefficients for a given reduced electric field since the typical pulse duration of a sprite streamer head is much longer that electron energy distribution function relaxation times at low mesospheric altitudes (Hiraki et al., 2004; Gordillo-Váquez, 2008).

They considered 91 chemical species and tested their model for daytime sprite streamer heads occurring at 31 km, 42 km and 54 km, which are consistent with expected daytime sprite altitudes (Stanley et al., 2000). However, for comparison, they also showed results of their model for nighttime sprites at 42 km altitude (probably the lowest limit altitude – or very close to it – of nighttime sprites). The focus of the chemical analysis was placed on nitrogen, hydrogen and oxygen, and in particular on ozone perturbations. Their simulations were restricted to 15 min after the passage of the sprite streamer head so that transport processes could be consistently disregarded.

According to Winkler and Notholt (2014) the initial effects of the breakdown electric fields at the tip of sprite streamers included a short-term loss of ozone (O_3) due to ion–chemical reactions, production of nitrogen radicals, and liberation of atomic oxygen (see below). The latter led to the formation of ozone. In terms of relative ozone change, this effect was predicted to decrease with altitude.

The model results of Winkler and Notholt (2014) indicated that the subsequent ozone perturbations due to daytime sprites streamers differ considerably from the ones of night-time events. For night-time conditions, reactive nitrogen produced at the streamer heads was rapidly converted (through $NO + O_3 \rightarrow NO_2 + O_2$) into significantly less reactive NO_2, and there is basically no ozone depletion. The situation was different for daytime conditions where NO_x causes catalytic ozone destruction by mainly electron impact O_3 dissociation ($e + O_3 \rightarrow O(^3P) + O_2 + e$) right after the pulse streamer is over followed by charge transfer ($O_2^- + O_3 \rightarrow O_3^- + O_2$), $NO + O_3 \rightarrow NO_2 + O_2$ and $OH + O_3 \rightarrow HO_2 + O_2$ that becomes the dominant O_3 sink after a few seconds. After a few minutes O_3 is mainly destroyed by $NO + O_3 \rightarrow NO_2 + O_2$. As a consequence, the model of Winkler and Notholt (2014) predicted significant ozone loss due to sprite streamers in the daytime atmosphere, in particular at higher altitudes. At an altitude of 54 km, ozone in the streamer column has decreased by about 15% fifteen minutes after the sprite event. Interestingly ozone enhancements of 5% and 7% were also predicted at 42 km for daytime and nighttime sprite streamers, respectively.

Parra-Rojas et al. (2015) published a one-dimensional self–consistent model to study the chemical and thermal effects of a single sprite streamer in the Earth mesosphere. An interesting new feature of this approach was that they used sprite streamer profiles with three different driving current durations (5 ms, 50 ms, and 100 ms) between 50 and 80 km of altitude. They considered a kinetic scheme of air with more than 90 chemical species and about 900 chemical reactions. Their model predicted strong increases in practically all the concentrations of the species studied at the moment of the streamer head passage. Moreover, their densities remained high during the streamer afterglow phase. The concentration of electrons reached values of up to 10^8 cm^{-3} in the three cases analyzed. The model of Parra-Rojas et al. (2015) also predicted an important enhancement, of several orders of magnitude above ambient values, of nitrogen oxides and several metastables species.

Therefore Parra-Rojas et al. (2015) investigated the electrical, chemical, and thermal impacts of a single sprite streamer with different driving current durations in the terrestrial mesosphere (50–80 km). In order to quantify the temporal evolution of each chemical species, their model solved a set of differential continuity equations for each of the chemical species considered coupled with the Boltzmann equation, the Ohm law, and an energy conservation equation.

Using as initial conditions the electric current density profiles provided for a set of altitudes by the streamer model of Luque and Ebert (2010), they extended them using different constant driving current durations (5 ms, 50 ms, and 100 ms). For this, they obtained the reduced electric field of a single sprite streamer for each of the altitudes considered so that the maximum current density occurs at the same time as the maximum reduced electric field. The constant driving current generates a high-field phase shorter than the driving current whose duration and value were, respectively, directly proportional to the altitude considered and close to breakdown (~120 Td).

At low altitudes and for the cases of 50 ms and 100 ms driving currents, they found a set of oscillations at the final stage of the E/N afterglow. They suggested that these undervoltage E/N oscillations built upon the opposite trends of electron production by associative detachment of O^- by N_2 and electron loss by dissociative recombination of electrons with O_4^+ during the driving current. At low altitudes, the electric field of the streamer head causes a huge growth in the electron concentration of up to 12 orders of magnitude (10^8 cm^{-3}) above ambient values. The tremendous increase in the electron concentration is driven by direct electron impact ionization of N_2 and O_2. In a similar way, the density of O^- exhibits a sharp enhancement past the streamer head due to dissociative attachment of O_2.

Their model also predicted quite significant enhancements in the concentration of metastable species (N_2 ($A\ ^3\Sigma_u^+$), O_2($a\ ^1\Delta_g$), O_2($b\ ^1\Sigma_g^+$), $O(^1D)$, and $O(^1S)$) capable of storing energy for a relatively long time. The production of metastables is mainly caused by electron impact

processes fueled by the high electron concentration caused by the streamer head electric field. They found an important (more than 2 orders of magnitude above ambient values at 50 km of altitude) and long–lasting (1–1000 s) enhancement of the concentration of mesospheric N_2O, which is both a strong greenhouse gas and a O_3 depleting one (see Fig. 9). The presence of significant N_2O concentrations in the atmosphere for long times could substantially affect the ozone concentration. Thus, sprites could be a low mesospheric and/or high stratospheric source of N_2O with potential effects on the delicate chemical equilibrium of the atmosphere.

At 65 km altitude the sprite chemistry model of Parra-Rojas et al. (2015) indicates that the concentration of N_2O due to a single sprite streamer and 10 ms after its onset can be about 1 order of magnitude above its ambient value. This sprite produced N_2O could be transported by winds to the upper mesosphere lower thermosphere (MLT) region so that it could contribute to the enhanced N_2O layer recently observed by ACE-FTS in the MLT (Sheese et al., 2016) that disagrees with available global simulations in mid and low latitudes of the MLT between 60 km and 80 km where sprites usually occur (Kelly et al., 2018). Future more detailed self–consistent sprite streamer microphysical simulations starting at different altitudes and for longer times (tens of milliseconds) would be needed to better constrain the local chemical impact of sprites in the MLT region.

Parra-Rojas et al. (2015) also evaluated the source emission apparent brightness of the first (FPS) and second (SPS) positive systems of N_2 associated with key visible optical emissions of sprites, the CO_2 infrared emission at 4.26 μm and 14.9 μm, and the Meinel band of N_2^+ associated with red and near-infrared emissions. As expected, at low altitudes (< 65 km) the reddish and bluish emission brightness of FPS and SPS exceed 1 MR by 4 orders of magnitude both at the streamer head and during the afterglow. In the same range of altitudes but at the final stages of the E/N afterglow, the 4.26 μm IR emission brightness can exceed 100 GR due to the high $CO_2(00^01)$ density production by electron impact collision and by VV processes involving N_2 ($X\,^1\Sigma_g^+$, v) for the cases of intermediate (50 ms) and long (100 ms) driving currents. These results suggested the possibility of detecting sprite IR emissions from space with the appropriate space or balloon detectors pointing towards the limb.

Moreover, Parra-Rojas et al. (2015) found that the Meinel band emission brightness grows with decreasing altitudes but does not reach 1 MR (or barely reaches it) at 50 km of altitude.

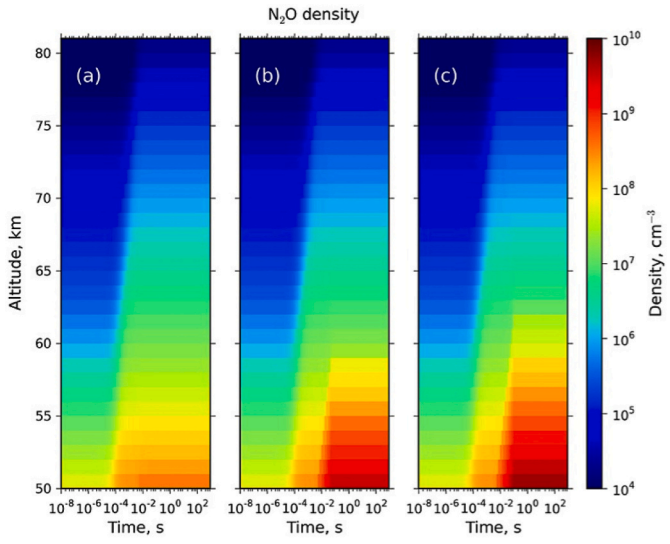

Fig. 9. Altitude-time evolution of the N_2O density due to a single sprite streamer with (a) 5 ms, (b) 50 ms, and (c) 100 ms driving current originitaing sprite streamer trailing glows of the same duration in agreement with high-speed sprite streamer observations (Stenbaek-Nielsen and McHarg, 2008) and with glow electric fields of ~120 Td (conventional breakdown field) (Luque and Ebert, 2010). Image reproduced from Parra-Rojas et al. (2015).

Finally, the nighttime sprite streamer chemistry model of Parra-Rojas et al. (2015) predicted a relatively important increase in the temperature of the low altitude (< 65 km) atmosphere surrounding a single sprite streamer within relatively long (5–50 s) time scales. This gas temperature enhancement was predicted to increase at lower altitudes and in direct connection with the duration of the sprite streamer driving current. According to Parra-Rojas et al. (2015) a gas temperature increase ($\Delta T/T$) of up to ~6.1% could be reached at 50 km for the intermediate case considered (50 ms driving current). This could produce maximum variations of approximately 30 K (in the extreme case of a 100 ms driving current) at low altitudes (< 55 km) and at about 5–10 s after the passage of the streamer head.

The above result is consistent with the no measurable sprite heating reported by a recent spectroscopic and imaging investigation of sprites occurring between 66 km and 76 km Parra-Rojas et al. (2015) are also consistent with previous sprite streamer heating estimations of Pasko et al. (1998) indicating that the heating of the neutrals within 10 ms would be in the range $\Delta T/T = 2$–0.2% (or 0.5–5 K). However, the significant sprite streamer heating predicted by the model of Parra-Rojas et al. (2015) is expected to take place on a delayed time scale of about 5–10 s and in the scenario corresponding to sprite streamer driving currents lasting 50 ms and 100 ms.

Parra-Rojas et al. (2015) carried out a detailed investigation of the different kinetic mechanisms underlying the predicted delayed sprite streamer heating. This gas temperature enhancement was predicted to be mainly caused by the collisional quenching of the vibrationally excited $CO_2(v_1, v_2^{l_2}, v_3)$ (previously excited through VV collisions with $N_2(X\,^1\Sigma_g^+, v)$ and, also, by the radiative decays of $CO_2(00^01)$ underlying the 4.26 μm IR emission). Therefore the role played by vibrationally excited CO_2 is crucial in the predicted delayed sprite streamer heating and it would be important to keep investigating their role in the physics and chemistry of other TLEs like blue starters, blue jets or giant blue jets occurring in the upper troposphere and stratosphere.

A further investigation of thermal IR CO_2 emissions due to sprite streamers was carried out by Romand et al. (2018). They developed a nighttime sprite streamer chemical model accompanied with radiative transfer computations. This radiative modeling is of great interest and came to complement previous nonlocal thermodynamic equilibrium (non–LTE) radiative transfer studies performed by Picard et al. (1997) for 4.3 μm CO_2 optical emissions caused by thundercloud electric fields at mesospheric altitudes.

In particular, Romand et al. (2018) computed the ground state vibrational kinetics of CO_2 and N_2 induced by a sprite streamer in the 40 to 70 km altitude range until several tens of seconds after the visible flash was over. Then, as mentioned above, they calculated the consecutive time-dependent thermal infrared spectra that could be observed from the stratosphere (from a balloon platform), high troposphere (from an aircraft), and low troposphere (from an aircraft or a high altitude observatory) using a non–LTE radiative transfer model. Their simulations predicted a strong production of CO_2 in the (001) vibrational level which lasts at least 40 s before falling to background concentrations. According to the model of Romand et al. (2018) this led to enhanced emissions in the long-wavelength infrared (LWIR), around 1000 cm^{-1} (9.4 μm), and midwavelength infrared (MWIR), around 2300 cm^{-1} (4.6 μm). The maximum sprite infrared signatures (sprite spectra minus background spectra) reached several 10^{-7} $W/sr/cm^2/cm^{-1}$ after propagation through the mesosphere and stratosphere, to an observer located at 20–40 km of altitude. This maximum signal was predicted to be about 1 order of magnitude lower if propagated down to the troposphere. From the two spectral bands, the 1000 cm^{-1} (9.4 μm) signal was predicted to be detected more easily than the 2300 cm^{-1} one (4.6 μm), which is more affected by atmospheric absorption (CO_2 self–trapping at all altitudes and H_2O mostly in the troposphere). With a sufficiently sensitive instrumentation, mounted in an open stratospheric balloon

platform for example, the 1000 cm^{-1} (9.4 μm) band could be detected from altitudes in the 20–40 km range (Romand et al., 2018). The disturbance obtained in the concentration of CO_2 (001) was consistent with that previously found by Gordillo-Váquez (2008) and Parra-Rojas et al. (2015).

In 2020 Pérez-Invernón et al. (2020) calculated the chemical influence and optical emissions of a sprite streamer at altitudes between ~67 km and ~ 74 km and during 0.85 ms. They used a self-consistent 2D model coupled with a kinetic scheme of 131 species interacting through 952 chemical reactions (see Fig. 10). Their results suggest that the injection of N_2O by sprites in the mesosphere lower thermosphere (MLT) over midlatitudes and low latitudes is not enough to account for the disagreement between satellite observations and global simulations (Kelly et al., 2018). Future improvements in computational capabilities will allow more extensive spatiotemporal microscopic simulations to confirm (or not) this preliminary conclusion. The obtained injection of NO and N and O(^{3}P) species is in agreement with previous results based on 0D and 1D models. They also estimated the contribution of the optical emissions of a simulated sprite streamer to the photometers of ASIM and TARANIS, concluding that the altitude of the streamer head can not be estimated from space-based optical measurements operating at nadir because the Lyman Birge Hopfield vacuum ultraviolet band optical emissions from the sprite glow and the transient $N_2(a\ ^1\prod_g, v)$ VDF are influenced by the radiative decay of $N_2(w\ ^1\Delta_u, v)$ to $N_2(a\ ^1\prod_g, v = 0)$ preventing the estimation of the sprite streamer head altitude from space–based and nadir–pointing photometric recordings. Ihaddadene and Celestin (2017) had previoulsy published a method to trace back the altitude at which a sprite streamer is propagating using the ratio of optical signals at different wavelengths. Their method was based on streamer simulations at different altitudes but using a single (lumped) pair of Einstein and quenching coefficients for each electronic excited state of N_2 with no distintion among vibrational levels. However, as the simulations of Pérez-Invernón et al. (2020) have shown, light emissions from the sprite streamer channel are very important when compared to those of the sprite streamer head. Therefore, there is not a unique or distinct "sprite altitude" to determine. This was not considered by Ihaddadene and Celestin (2017) because they did not simulate a streamer that travels several kilometers. Instead, they simulated a small streamer at different altitudes that was not allowed to evolve long enough so that important optical emissions could emerge from the sprite streamer channel. In addition, as mentioned above, they only considered a single (lumped) pair of Einstein and quenching coefficients for each excited electronic state of N_2 with no distintion among vibrational levels for the Lyman Birge Hopfield band emissions.

The main conclusions from the work of Pérez-Invernón et al. (2020) are (1) that single non-bifurcated sprite streamers can inject 9.7×10^{20} atoms of N, 5.9×10^{19} molecules of NO and 1.2×10^{18} molecules of N_2O between the altitudes 67 km and ~ 74 km during 0.85 ms after its onset, (2) the radial dependence of the production of NO and N_2O by a single sprite streamer is calculated for the first time and (3) the contribution of the sprite streamer optical signature to the ratio between optical signals recorded by different photometric recordings of ASIM and TARANIS was estimated.

3.1.9. The first conclusive sprite chemistry observations: 2020

The first conclusive observational evidence showing the influence of sprites in the upper atmosphere chemistry was published early in 2020 although the supportive observations were carried out between October 2009 and April 2010.

In particular the study of Yamada et al. (2020) presented the first observational evidence of the HO_2 radical production (see Fig. 11) above sprite-producing thunderstorms from the coincidence of temporal-spatial observations of HO_2 spectra, sprite events, and thunderstorms tracked by two space instruments (a submillimeter-wave limb spectrometer and an ultraviolet/visible Imager) and a ground-based very low frequency (VLF) radiation lightning detection network. A total of

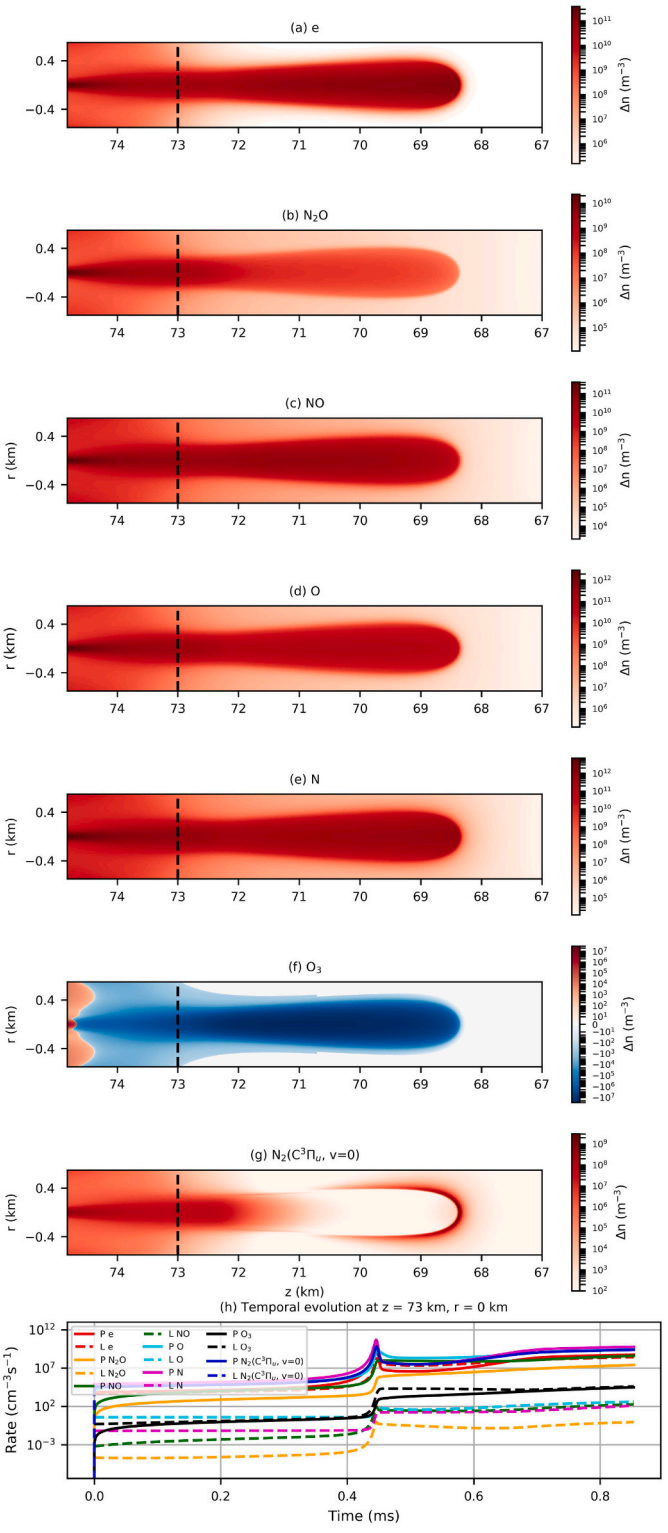

Fig. 10. (a-g) Density enhancement with respect to background of different chemical species produced by a simulated sprite streamer 0.85 ms after its onset between altitudes 68 km and 74.82 km. (h) Temporal evolution of the rates of production (P) and losses (L) of the species plotted in panels (a-f) at the position z = 73 km, r = 0 km. Image reproduced from Pérez-Invernón et al. (2020).

three low–latitude (4° S–28° N) areas were identified with enhanced HO_2 levels of approximately 10^{25} molecules. Accompanying chemical sprite model calculations indicated an increase in HO_2 in the considered altitude region but the predicted production due to a single sprite event

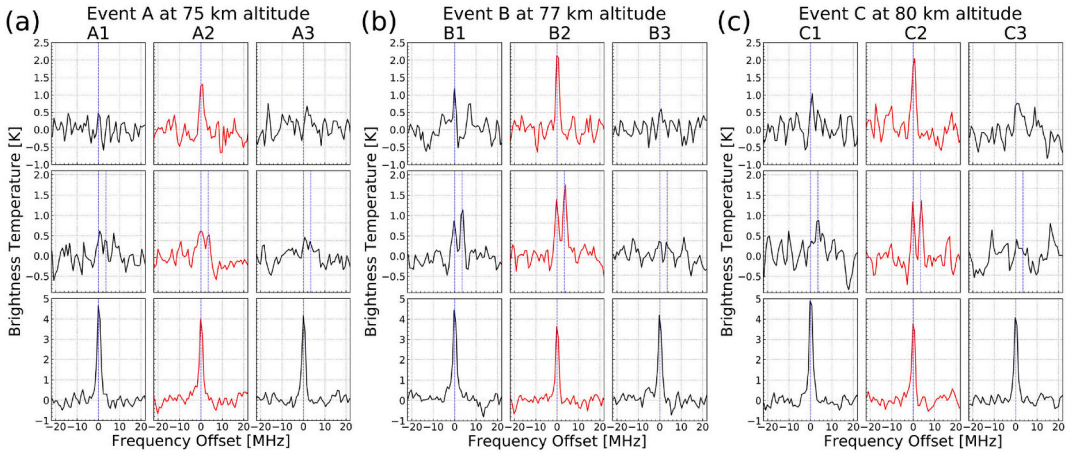

Fig. 11. Panels (a)-(c) show SMILES submillimiter spectra at anterior, coincidence, and posterior positions of each sprite event (labelled A, B and C). The first and third columns for each event show the observation spectra at anterior and posterior positions, respectively, and the second column shows the SMILES observation spectra at the event area (red lines). The first, second, third rows for each event show the SMILES observation spectra for the HO_2 transition at 649.701 GHz, HO_2 transitions at 625.660 and 625.664 GHz, and O_3 transition at 625.371 GHz, respectively. The blue vertical lines represent the frequency of the molecular transitions. The horizontal axes show frequency offset from the transition frequency. The tangent heights of SMILES observation spectra are 75, 77, and 80 km for events A, B and C, respectively. Image and caption reproduced from Yamada et al. (2020).

was smaller than the observed enhancement. The observations of Yamada et al. (2020) suggested that sprites can potentially contribute with 1% of the nighttime background HO_2 generation at altitudes of 75–80 km globally.

According to Yamada et al. (2020) slight decreases in O_3 spectral intensities at each event were also observed by the Submillimeter–Wave Limb–Emission Sounder (SMILES), although it was difficult to separate these perturbations from spectral noises and latitude and altitude variations of O_3 abundance.

SMILES was successfully launched and attached to the Japanese Experiment Module (JEM) on the International Space Station (ISS) on 25 September 2009. It was making atmospheric observations since 12 October 2009 with the aid of a 4 K mechanical cooler and superconducting mixers for submillimeter limb–emission sounding in the frequency bands of 624.32–626.32 GHz and 649.12–650.32 GHz. SMILES was of great value for retrieving very high-resolution vertical profiles of atmospheric minor constituents in the middle atmosphere, such as O_3 with isotopes, HCl, ClO, HO_2, BrO, and HNO_3. Unfortunately, SMILES observations were suspended since 21 April 2010 owing to the failure of a critical component (Kikuchi Ki et al., 2010).

SMILES observation spectra ranging from 649.12 GHz to 650.32 GHz was used to detect the HO_2 transition at 649.701 GHz (see Fig. 11). Another SMILES frequency window ranging from 625.1 GHz to 626.3 GHz was also used to detect the 625.371 GHz O_3 transition and weaker HO_2 transitions (625.660 and 625.664 GHz) than the HO_2 transition at 649.701 GHz. The SMILES frequency resolution was 1.2 MHz. The integration time for a single spectrum was 0.47 s, with a vertical sampling interval of approximately 2 km in limb observations and an approximately 6 km (horizontal) × 3 km (vertical) FOV at the tangent point. The observation geometry of SMILES was the limb in the northward and eastward directions.

Yamada et al. (2020) estimated that the global production of HO_2 molecules by nighttime sprite events at altitudes of 75–80 km was approximately 10^{28} molecules (with 10^{25} molecules of HO_2 produced by a sprite event). For that they assumed a sprite global occurrence frequency between one and three sprites per minute, while the total amount of background HO_2 was considered 10^{30} molecules if the background concentration of HO_2 was assumed to be 0.9×10^6 molecules/cm^3 at the altitude range (as determined from high resolution HO_2 vertical profiles from SMILES soundings, see below).

Thus, a global production of 10^{28} molecules of HO_2 by nighttime sprite events was considered to potentially account for 1% of the global amount of nighttime HO_2 at 75–80 km. The background concentration of HO_2 was derived from the average of SMILES L2r product data in nighttime at 75–80 km during the SMILES observation period. The authors claimed that the retrieved production was not necessarily showing the production of HO_2 from single sprites but rather the accumulation of production by the entire sprite-producing thunderstorm. The authors of this study disregarded other possible sources of HO_2 as solar proton and energetic electron precipitation events since these processes take place at high-latitude regions and their activity was quite small at the low-latitude region where observations by SMILES took place from 12 October 2009 to 21 April 2010 (Andersson et al., 2014). Horizontal transportation by zonal winds with HO_2 produced by photolysis in daytime regions was also disregarded due to the low zonal winds at 75–80 km (Baron et al., 2012) so that the distances the air masses could have been moved away from the line of sight of SMILES were considered smaller than 200–300 km that were of the same order of magnitude that the area of the parent thunderstorms.

Finally, according to Yamada et al. (2020) the impact of sprite chemistry on the Earth atmosphere may increase in the future because the source of HO_2 production and the triggering of sprite occurrence are mesospheric water vapor and tropospheric lightning, respectively. These two factors might be increasingly important in the near future due to greenhouse gas emissions and global warming, respectively.

3.2. *Mesosphere: Elves*

Elves were predicted in the early 1990s by Inan et al. (1991), later on filmed from the space shuttle (Boeck et al., 1992) and finally detected from ground-based observatories (Fukunishi et al., 1996). The observed dynamic features of elves were soon shown to be consistent with a two–dimensional model of the interaction with the lower ionosphere of intense electromagnetic pulses (EMPs) from lightning discharges (Inan et al., 1996b). This model indicated that optical luminosities (produced at 85–95 km altitudes) as observed from a distance would appear to expand laterally at speeds faster than the speed of light. The optical output of elves is produced as a result of the heating of ionospheric electrons by the EMP of a lightning discharge. The heating of electrons by the EMP of lightning was recorded by Farges et al. (2007) through the measurement of ultra–short blackouts of narrowband radio emissions in the medium (500–1500 kHz) frequency range. Data acquired by an array of horizontally spaced photometers named Fly's Eye (sensitive in the range 185 nm to 800 nm) developed by the STAR Lab group at Stanford

University in the mid 1990s and boresighted with a low-light level image intensified camera provided the first measurement of the rapid lateral expansion of the optical luminosity of elves, occurring over time scales substantially less than 1 ms (Inan et al., 1997). A few years before, Taranenko et al. (1992) and Taranenko et al. (1993) predicted that the optical emission spectra of elves had contributions from the first and second positive systems of N_2 and estimated that their maximum brightness would be ~40 MR and ~ 6 MR, respectively, lasting for about 50 μs.

The launch in 2004 of the ISUAL instruments on board the FORMOSAT–2 satellite was a new opportunity to investigate elves from space. Many elve optical recordings were carried out by ISUAL including the confirmation that elves cause ionization in the lower ionosphere and that they are sources of Lyman Birge Hopfield vacuum ultraviolet optical emissions (Kuo et al., 2007).

The paper of Kuo et al. (2007) presented numerical simulation of elves based on an electromagnetic finite difference time domain (FDTD) model of the optical emissions between 185–800 nm and of their spatial-temporal evolution. To account for the effect of atmospheric attenuation, three major attenuation mechanisms: O_2, O_3, and molecular Rayleigh scattering were considered. Validations of the electromagnetic FDTD model were conducted in three ways: by comparing the calculated and observed photon fluxes in the ISUAL spectrophotometric channels, by directly comparing the simulated and observed morphologies of elves, and by comparing the computed photon counts of the ISUAL Imager based on the derived peak currents for two elve-associated NLDN (National Lightning Detection Network) CG discharges with those recorded by the ISUAL Imager. In all three ways, very good agreement was achieved.

The paper of Kuo et al. (2012) adopted the chemical reaction set (90 species and about 300 reactions) of Sentman et al. (2008b) into a previously developed elve model (Kuo et al., 2007) to investigate the full chemical processes triggered by elves. After the passage of electric field pulses, the resulting molecular and atomic metastable species $N_2(A\ ^3\Sigma_u^+)$, $O(^1D)$, $O(^1S)$ $O_2(b\ ^1\Sigma_g^+)$, $O_2(a\ ^1\Delta_g)$ may initiate another series of chemical reactions and can produce dim chemiluminescence, for example the 762 nm emission from the O_2 atmospheric 0–0 band ($b\ ^1\Sigma_g \rightarrow X\ ^3\Sigma_g$), 557.7 nm emission from $O(^1S \rightarrow {}^1D)$ or the 630 nm emission from $O(^1D \rightarrow {}^3P)$. These optical emissions due to chemiluminescence offered the unique opportunity to study the post-impulse chemical processes in elves.

The elve kinetic model of Kuo et al. (2012) computed the relative intensity ratios of the major and minor optical emissions in elves with the time spanning from several microseconds to 10 s. From this model, the brightness of N_2 FPS, SPS, LBH, N_2 FNS, O_2 atmospheric band, O_2^+ 1 N, O I ($^1S \rightarrow {}^1D$) at 557.7 nm and O I ($^1D \rightarrow {}^3P$) at 630 nm were computed to be 4.2 MR, 0.67 MR, 0.82 MR, 11.6 kR, 4 kR, 2.4 kR, 10 kR and 6 R, respectively, for a lightning peak current of 280 kA. Other peak currents (140 kA and 360 kA) were also investigated. The inferred relative intensities and the modeled elve spectrum were used to constrain the involved radiative states and to infer their percentages that fall within the ISUAL Imager filter passbands (N_2 FPS, 762, 630, 557.7, 427.8 nm filters) through comparing the modeling results to the ISUAL observed values.

The model of Kuo et al. (2012) neither include vibrational kinetics nor an evaluation of the possible influence of elves on local and/or global concentration of nitrogen oxides (NO_x). In this respect, Pérez-Invernón et al. (2018a) developed a fully coupled kinetic (including vibrational kinetics) and electromagnetic model for elves produced by CG lightning, compact intra–cloud discharges (CIDs) and Energetic In–cloud Pulses (EIP). This model was used to quantify the possible local chemical impact and optical signatures produced by electromagnetic pulses (EMP) in the lower ionosphere.

For the case of elves produced by CGs their local chemical impact was evaluated by estimating the production of NO molecules. They analyzed the elves triggered by CG lightning discharges whose current peaks were 90, 154, and 220 kA. The weakest of these discharges produced an elve slightly above the ISUAL detection threshold, estimated in parent lightning discharges with peak currents of about 80 kA (Kuo et al., 2007; Chern et al., 2014; Blaes et al., 2016; Pérez-Invernón et al., 2018b), while the strongest discharge corresponds to a typical CG with a risetime between 2 and 3 μs (Rakov and Uman, 2003). The simulated elves triggered by CG lightning discharges with current peaks of 90, 110, and 220 kA generated about 5×10^{17}, 6×10^{19}, and 4×10^{20} molecules of NO, respectively.

Pérez-Invernón et al. (2018a) also computed the total amount of energy locally deposited in the mesosphere by these three elves, obtaining 2×10^5, 7×10^5, and 10^6 J, respectively. According to these quantities, the production rate of NO by elves in terms of energy was predicted to be in the range between 2.5×10^{12} and 4×10^{14} molecules of NO/J, that is, between 4 and 2 orders of magnitude below the NO production rate of halos (see next section). According to ISUAL observations, elves are 74% of all detected TLEs (Chen et al., 2008; Chen et al., 2019). The results of their elve simulations together with the observation of elves by ISUAL led them to estimate that the total global amount of NO created by elves ranges between 10^{-10} and 10^{-7} teragrams of nitrogen per year (Tg N/year). This quantity is between 10 and 7 orders of magnitude lower than the estimated global annual production of NO by lightning discharges (between 5 and 9 Tg N/year; Nault et al. (2017); Schumann and Huntrieser (2007). The global chemical influence of elves with regard to NO production was then concluded to be negligible or extremely small.

In the case of elves triggered by CIDs located at 18 km of altitude, Pérez-Invernón et al. (2018b) set lightning currents modeled by Watson and Marshall (2007) as sources of EMP. They used the Modified Transmission Line Exponential Increasing model proposed by Watson and Marshall (2007) for downward positive discharges, with a peak current of ~400 kA (Cummer et al., 2014; Liu et al., 2017; Lyu et al., 2015). The EIP negative current source located at 13 km of altitude was taken from Liu et al. (2017), who simulated an EIP–driven elve produced by a current with a peak value of ~542 kA.

As discovered by Newsome and Inan (2010) and modeled by Marshall et al. (2015), Liu et al. (2017) and Pérez-Invernón et al. (2018a), the EMPs produced by CIDs and EIPs trigger a succession of two elves or elve doublet as a consequence of the primary wave ground-reflexion. The delay between the consecutive elves at a given distance from the center is different in the case of CIDs and EIPs due to the different altitudes of the current sources. According to the model of Pérez-Invernón et al. (2018b) for elves produced by CIDs and EIPs, the total number of NO molecules produced by their simulated CID–and EIP–driven elves is of about 10^{21} molecules.

Therefore observations and electromagnetic and kinetic simulations of elves suggest that they have a negligible chemical impact in the atmosphere in terms of their NO production. Elves can, however, produce nonnegligible amounts of metastable species like $N_2(A\ ^3\Sigma_u^+)$, $O(^1D)$, O (^1S) $O_2(b\ ^1\Sigma_g^+)$, $O_2(a\ ^1\Delta_g)$. The role of $N_2(A\ ^3\Sigma_u^+)$ produced by an enhanced concentration of mesospheric electrons heated by elves could be specially important as a precursor of N_2O in the mesosphere lower thermosphere (MLT) region where recent observations by the Atmospheric Chemical Experiment – Fourier Transform Spectrometer (ACE-FTS) have detected an enhanced layer of N_2O that disagrees with present global scale simulations between 60 km and 80 km in the mid and low latitudes of the MLT (Sheese et al., 2016; Kelly et al., 2018) where upper atmospheric electrical activity occurs.

Recent estimates by Blaes et al. (2016) of the global production rate of elves resulting from ground-based observations (see Fig. 12) suggest that 4.658.579 elves were produced in 2013, representing 0.82% of all GLD360-recorded lightning events that year (488.608.023 lightning or ~ 15 lightning flashes per second, that is, one third of the consensus ~45 lightning flashes per second of LIS (Christian et al., 2003)). This means

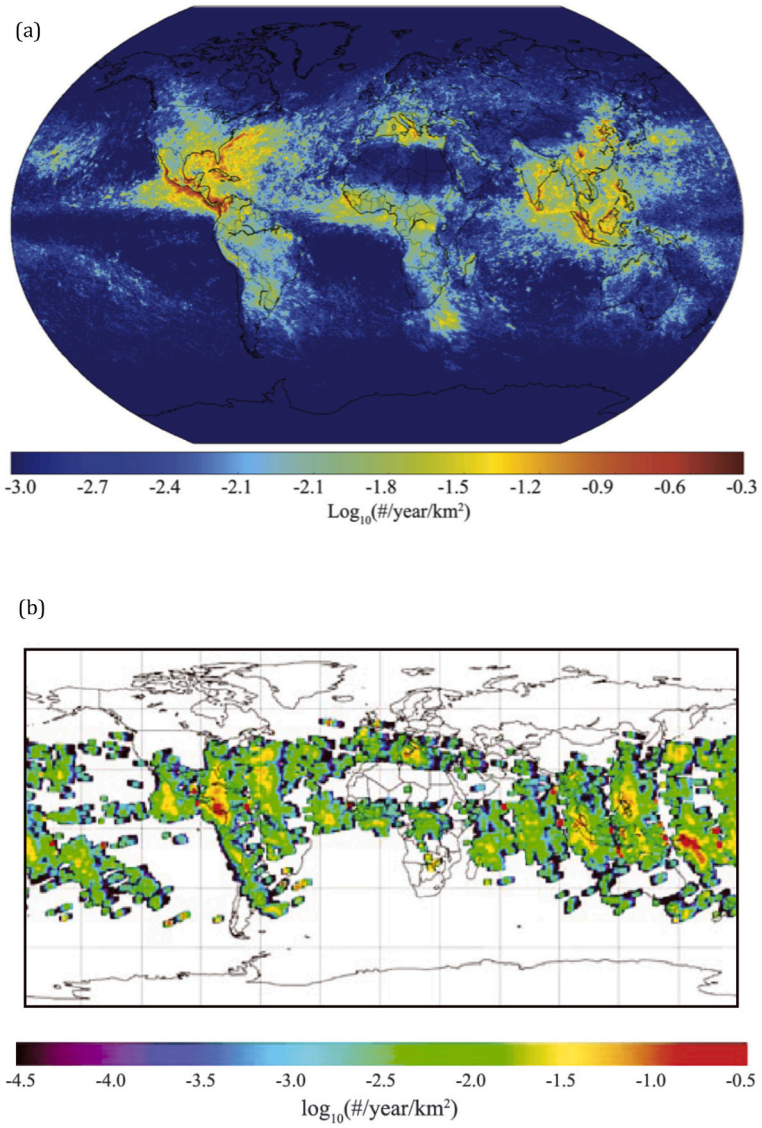

Fig. 12. (a) The estimated global distribution of elve production estimated using GLD360 peak currents (note that GLD360 performs continuous ground-based observations). According to According to Blaes et al. (2016) the production probability of elves as a function of peak current fits a linear regression, with a 50% elve probability for peak currents of 88 kA. This finding along with global data from the GLD360 lightning geolocation network was used to extrapolate the global elve production rate. The result was that ~0.8% of all cloud-to-ground lightning discharges produce elves. This global distribution of elves exhibits remarkable similarities with the (b) elve distribution from ISUAL observations but without the ISUAL polar orbit gaps in coverage Chen et al. (2008). Images reproduced from Blaes et al. (2016) and Chen et al. (2008).

that the elve global rate is of about 7.4 elves per minute (15 times more than that of halos and sprites). According to the elve electrodynamic and kinetic simulations of Pérez-Invernón et al. (2018a) elves produced by CGs with peak currents of 154 kA and 220 kA would produce ~2.5 × 10^{17} and ~ 1.3 × 10^{18} molecules of N_2O, respectively, between 80 km and 90 km and once the halo contribution is removed. Since the global rate of elves is about 15 times that of sprites we find that the number of N_2O molecules produced by elves in a year between 80 km and 90 km can vary between 2.9 × 10^{24} and 1.5 × 10^{25}, which is a bit more than the contribution due to sprites according to recent self-consistent sprite streamer simulations up to 0.85 ms (Pérez-Invernón et al., 2020). Considering the N_2O background concentration (1 ppbv –4 ppbv) between 80 km and 90 km, it seems that elves might not be the main cause of the enhanced N_2O layer recently observed in the MLT (Sheese et al., 2016; Kelly et al., 2018). In the scenario that the global production rate of elves is ~20 elves per minute (assuming 0.82% of 45 lightning flashes per second), the numbers above would change by a factor three that still remains insufficient by itself to explain the mesospheric N_2O source between 60 km and 80 km at mid and low latitudes (Kelly et al., 2018).

Finally, elves can cause ionization at the base of the ionosphere. Chen et al. (2008) showed that in very active regions, a 5% increase in the local electron density (ionization) in the region could appear with possible implications in the local chemical composition (Gordillo-Vázquez et al., 2016). The local ionization enhancements caused in hot elve regions, as well as the dynamics of their return to normal, was measured by studying LOng Recovery Early VLF events (LOREs). LOREs represent a small subclass of early VLF events which associate with direct tropospheric lightning effects on the mesosphere and lower ionosphere caused by induced quasi–electrostatic (QE) and electromagnetic pulsed (EMP) field that may lead to ionospheric conductivity modifications. While LOREs have abrupt onsets and onset duration similar to those of typical early VLF events, they differ from early VLF events by their long recoveries, which range from several minutes up to ~20 to 30 min, or even longer. The origin of LOREs was experimentally identified in the studies of Haldoupis et al. (2012, 2013) and Salut et al. (2012, 2013) to be associated with unusually large peak currents of CG lightning discharges capable of producing elves. In order to study the underlying chemistry of LORE events Gordillo-Vázquez et al. (2016) considered two relaxation model scenarios. They first considered a weak enhancement in electron density and then a much stronger one caused by an intense lightning EMP acting as an impulsive ionization source. The full nonequilibrium kinetic modeling of the perturbed mesosphere in the 76 to 92 km range during LORE–occurring conditions predicted that the electron density relaxation time is controlled by electron attachment at lower altitudes, whereas above 79 km attachment is balanced totally by associative electron detachment so that electron loss

at these higher altitudes is controlled mainly by electron recombination with hydrated positive clusters $H^+ (H_2O)_n$ and secondarily by dissociative recombination with NO^+ ions, a process which gradually dominates at altitudes >88 km. The calculated recovery times agreed fairly well with LORE observations.

3.3. Mesosphere: Halos

As mentioned above sprite halos, a distinctive type of TLE, are diffuse optical emission (see Fig. 13) associated with lightning discharges that initially looked like elves but upon close examination were revealed to be a separate lower altitude phenomenon ocurring at 70–80 km (when the reduced electric field created by lightning reaches the air breakdown value of ~120 Td) with typical diameters of 100 km and durations between 1 and 3 ms (Barrington-Leigh and Inan, 1999; Barrington-Leigh et al., 2001).

Halos are usually seen accompanying sprites but are also seen to appear alone (Wescott et al., 2001b; Marshall and Inan, 2006; Kuo et al., 2013). Halos are associated with negative or positive CG lightning discharges (Bering et al., 2002, 2004b; Bering et al., 2004a; Frey et al., 2007), since the return stroke stage of CG lightning can transfer more total charge than intracloud or cloud–to–cloud lightning discharges (Maggio et al., 2009; Rakov and Uman, 2003).

Newsome and Inan (2010) reported similar occurrence rate for halos generated by positive CGs and negative CGs but results from (Bering et al., 2004a; Frey et al., 2007; Williams et al., 2012) have shown that negative halos (produced by negative CGs) may be more common than positive halos (produced by positive CGs).

Halos alone can be produced by CMCs from about 300 C km up to 1300 C km for negative halos and up to about 500 C km for positive ones, respectively (Williams et al., 2012; Lu et al., 2018). However, it seems that the threshold of lightning strength for halo alone production does not considerably depend on the polarity of parent strokes Lu et al. (2018). Also, negative halos seem to last less (~0.5 ms) than positive halos (~1.5–2 ms). Kuo et al. (2013) detected a halo without sprite streamers caused by a negative CG with a CMC = −1250 C km. The absence of sprite streamers could be due to the fact that the causative lightning was extremely impulsive (< 0.1 ms) producing high electric field (2 or 3 times E_k) at 75–90 km altitudes that also relax more quickly due to the extra ionization created by the high fields that would prevent the formation of sprite streamers (Li et al., 2012).

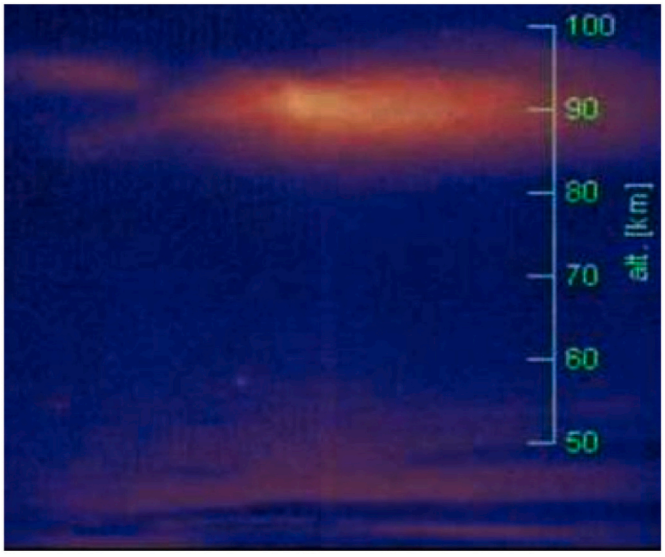

Fig. 13. False color image of a halo without sprite recorded at 1000 frames per second in 1999 by the University of Alaska from the Wyoming Infrared Observatory.

Recent surveys by ISUAL (aboard the FORMOSAT–2 satellite between 2004 and 2016) indicate that halos are about 6% (almost as frequent as sprites) of all TLEs detected by ISUAL during its 12–year lifetime (Chen et al., 2019). With a halo proportion of ~6% of all the ISUAL observed TLEs (Chern et al., 2014; Chen et al., 2019), the computed total amount of NO created by halos is estimated to be $\sim 2 \times 10^{-7}$ teragrams of nitrogen per year (Tg N/year) (Pérez-Invernón et al., 2018a). This value is strongly lower than the estimated production of NO by lightning discharges, in the range 5 and 9 Tg N/year (Nault et al., 2017; Schumann and Huntrieser, 2007). According to these numbers, the global chemical influence of halos with regard to NO production might be very small or negligible. ISUAL observations scanned 45 degree south to 25 degree north latitude during the northern summer and 25 degree south to 45 degree north latitude during the northern winter. It is therefore important to clarify whether halos could play (or not) some possible impact on the upper mesosphere chemistry. Several authors have contributed to explore the sprite halo / halo alone chemistry since the year 2004.

Hiraki et al. (2004) evaluated the generation of metastable $O(^1D)$ in sprites halos produced by lightning with charge moment changes between 500 C km and 2000 C km during nighttime and between 1000–2000 C km during daytime, respectively. The $O(^1D)$ and $O(^3P)$ kinetics considered by Hiraki et al. (2004) were restricted to only one source of $O(^1D)$ by electron-impact dissociative excitation ($e + O_2 \rightarrow O(^1D) + O(^3P) + e$) and one sink of $O(^1D)$ by collsional deactivation (quenching) by N_2 and/or O_2 ($O(^1D) + N_2/O_2 \rightarrow O(^3P) + N_2/O_2$). Hiraki et al. (2004) concluded that sprite halos could be a significant local mesospheric source of $O(^1D)$ metastable atoms but its nighttime global $O(^1D)$ production was found to be four orders of magnitude smaller than that due to daytime solar UV radiation (photolysis of O_3 leading to $O(^1D)$). Still, sprite halos and/or halos alone can be considered a significant nighttime global source of metastable $O(^1D)$. However, no observations to date have verified this prediction.

Eight years after the Hiraki et al. (2004) paper on sprite halos $O(^1D)$ metastables Liu (2012) developed a multiple ion 2D fluid self–consistent model of sprite halos to investigate the ionospheric response to the lightning quasi-electrostatic field using a realistic ambient electron density profile. The model took into account four symbolic ion species and O^- ions that were considered separately. In particular the model investigated the role of electron detachment of O^- in the dynamics of sprite halos. It should be noted that the effect of electron associative detachment (AD) of O^- by N_2 ($O^- + N_2 \rightarrow N_2O + e$) on mesospheric electrical conductivity perturbations due to sprite streamers and on the delayed (non conventional or AD mediated) electrical breakdown and sprite streamer dynamics was previously investigated by Gordillo-Váquez (2008); Gordillo-Vázquez (2010); Luque and Gordillo-Vázquez (2011a), respectively.

The modeling results of Liu (2012) for a sprite halo caused by a positive CG stroke with 600 C km charge moment change showed that the front of the halo can descend to ~70 km altitude and that the electron density behind the halo can be elevated to a value close to the one at 85 km altitude. Measurements of early/fast VLF events produced by electron density changes associated to sprite halos allowed the characterization of their spatial extension (Moore et al., 2003). The halo brings down the lower ionosphere boundary by about 15 km that is much larger than the lowering of the ionosphere boundary by a halo without the O^- detachment process. Liu (2012) stated that the large descending extent of the sprite halo enabled by the detachment process may be critical for initiation of sprites at ~70 km altitude. This had already been discussed by Luque and Gordillo-Vázquez (2011a) (main paper and supplementary material with 2D fluid simulations) when describing sprite inception mediated by O^- associative detachment.

Liu (2012) also showed that the electron density below the halo front was not significantly reduced from the ambient value, i.e., there was no pronounced attachment “hole” forming below the halo front. To have a small electron density about 10^3 m^{-3} at sprite initiation altitude for

formation of individual streamers (Qin et al., 2011), the ambient electron density at this altitude must be close to this value.

Finally, Liu (2012) concluded that the electron density can increase even in subbreakdown condition ($E < E_k$) sprite/sprite halo altitudes as was previously found by Luque and Gordillo-Vázquez (2011a).

By the year 2013 two models were published to investigate different aspects of sprite halo/halo atmospheric chemistry (Evtushenko et al., 2013; Parra-Rojas et al., 2013a).

The halo chemistry investigations of Evtushenko et al. (2013) used two approaches. One approach was based on what they called a point (zero dimensional) model. The second approach used a self–consistent one dimensional model based on previous studies (Evtushenko and Mareev, 2011; Luque and Gordillo-Vázquez, 2011a). These two models (approaches) implemented a kinetic scheme of more than 260 reactions and about 60 chemical species with half of them being positive and negative ions where the focus was mainly placed. These authors found that sprite halos at 75 km could lead to significant enhancements in the concentrations of water cluster ions such as $H_5O_2^+$, H_3O^+, $H_7O_3^+$ or $H_9O_4^+$, atomic and molecular metastables like O_2 ($b\ ^1\Sigma_g^+$), O_2 ($a\ ^1\Delta_g$)), N_2 ($A\ ^3\Sigma_u^+$), $N(^2D)$ and $O(^1D)$. Evtushenko et al. (2013) found that the halo induced concentration of $O(^1D)$ was of the order of 10^4 cm^{-3} in agreement with previous results reported by Hiraki et al. (2004). The work of Evtushenko et al. (2013) did not evaluate optical emissions due to halos.

Also in 2013, weeks after the paper of Evtushenko et al. (2013), another study by Parra-Rojas et al. (2013a) was published to detailed investigate non-equilibrium halo kinetics. Parra-Rojas et al. (2013a) developed a one-dimensional electrochemical model considering 20 chemical species to self-consistently describe the response of the Earth mesosphere to different types of lightning discharges between 50 and 87 km of altitude. The model solved the statistical equilibrium equations of each species coupled with the Boltzmann transport equation and with the quasi-electrostatic electric field equation.

This model predicted an increase of up to 70 cm^{-3} in the electron density in the range 55 km–81 km for positive CG lightning and a negligible mesospheric electron density perturbation in the case of negative CG lightning. For all the positive CG and some negative CG, with current moment higher than 200 kA km, considered, the model of Parra-Rojas et al. (2013a) also showed an enhancement of several orders of magnitude in the concentration of ground–state negative (O^-, O_2^-, NO_2^-) and positive (O_2^+, O_4^+) ions and in electronically excited positive ions such as N_2^+ ($A\ ^2\prod_u$) responsible for the N_2^+ Meinel emissions and N_2^+ ($B\ ^2\Sigma_u^+$).

The predicted N_2 first and second positive systems emission brightnesses were predicted to exceed 1 MR and 500 kR, respectively, for a 100 km diameter halo at 77 km. The calculated concentration of metastables such as N_2^+ ($A\ ^2\prod_u$) and $O(^1D)$ were predicetd to reach values of up to 10^2 cm^{-3}, which for the case of $O(^1D)$ was about two orders of magnitude lower than Hiraki et al. (2004) $O(^1D)$ predictions for nighttime halos.

Finally, as for the perturbation of neutrals Parra-Rojas et al. (2013a) found that only atomic oxygen and nitrogen out of the 13 ground-state neutral species considered exhibited substantial variation within the halo. Neither nitrogen oxides (NO_x and N_2O) nor CO_2 was predicted to change their density.

Pérez-Invernón et al. (2018a) published a self-consistent 2D fluid model coupling the electrodynamics of halos with a extensive kinetic scheme considering more than 130 chemical species and about 1000 chemical reactions including complex vibrational kinetics of electronic states of molecular nitrogen underlying halo optical emissions such as the first and second positive systems of N_2 and the Lyman Birge Hopfield (LBH) vacuum ultraviolet optical emissions. This is the most ambitious model to date aiming to investigate both the local and possible global chemical impact of halos on the atmospheric chemistry.

The halo chemistry model of Pérez-Invernón et al. (2018b) allowed them to predict the spectra of a single halo and its chemical impact in the mesosphere within short (few milliseconds) and long (one second) time scales after being triggered. To perform this long-time simulation with this 2D electro-kinetic model of a single halo, they avoided the sprite inception problem simulating a second discharge that removed the electric field produced by the first one several milliseconds later. The calculated spectra agreed with previous model results (Gordillo-Vázquez et al., 2011, 2012) and with the spectra of the first positive system of N_2 of sprite halos (Wescott et al., 2001b), sprites detected by Kanmae et al. (2007) and more recently with the high-resolution sprite spectra reported by Gordillo-Vázquez et al. (2018).

Pérez-Invernón et al. (2018a) considered three charge moment change (CMC) scenarios, namely, 140 C km, 350 C km and 560 C km. The main local chemical effect of halos was predicted to be at altitudes around 75 km. Furthermore, the horizontal chemical influence was predicted to extend up to 20 km from the center of the halo.

According to the chemistry of halos predicted by Pérez-Invernón et al. (2018b) the density of some initial ground state neutrals suffers an enhancement in the center of the halo 3 ms after its onset. The atomic nitrogen N, whose background concentration was negligible, increases by about 8.8×10^{21} molecules. The increase of N was followed by other species like O, N_2O, NO_2 and NO, with increases with respect to their ambient values of ~0.7%, ~ 0.2%, ~ 0.1%, and ~ 0.01%, respectively. The concentration of NO_x would also increase after the extinction of the halo, as the produced N atoms will rapidly be converted into NO and NO_2 after interacting with O_2. In particular, 3 ms after the halo inception in the 560 C km scenario, the most perturbed atomic and molecular ground state and metastable species were N, O, and $N(^2D)$, $O(^1D)$ and N_2 ($A\ ^2\Sigma_u^+$), O_2($b\ ^1\Sigma_g^+$), O_2($a\ ^1\Delta_g$), O_2($A\ ^3\Sigma_u^+$), which concentrations were increased by between ~4×10^2 cm^{-3} and ~ 10^4 cm^{-3}, respectively. The most affected negative and positive ions after 3 ms were predicted to be O^-, O_2^- and N_2^+ and O_2^+ with density variations above background values in the range 80–100 cm^{-3} (O^-), 5–10 cm^{-3} (O_2^-), 10–20 cm^{-3} (N_2^+) and 40–200 cm^{-3} (O_2^+).

The main processes that contribute to enhance the densities of N and O according to this model are the collisions of electrons with N_2 and O_2, respectively. The enhancement in the density of N_2O is due to the associative detachment of O^- by N_2, while the increase of NO is influenced by processes that involve $N(^2D)$ and O_2. Finally, NO interacts with molecules containing O atoms to create NO_2.

The relative increase of the N_2O and NO species densities with respect to background in the center of the halo 1 s after its onset was predicted to be ~0.2% and ~ 0.1%, respectively. Despite the high relative enhancement of atomic nitrogen, its absolute increase is of 10^{22} atoms (of the same order that NO). The "long-time" (1 s) halo chemistry simulations of Pérez-Invernón et al. (2018a) found a larger ratio of NO_x to N, as N was converted into NO_x. These results suggest that halos have a nonnegligible local and regional NO_x chemical influence in the upper atmosphere near thunderstorms.

Arnone et al. (2008) found a local enhancement of NO_x produced by sprites streamers of ~10% at 52 km of altitude, increasing up to 60 km. Therefore, we can conclude that the chemical influence of a halo regarding to the production of NO_x is between 1 and 2 orders of magnitude below the influence of a sprite.

Pérez-Invernón et al. (2018b) also estimated the energy deposited in the mesosphere by a halo. Their model calculated the total flux of electrons produced by the lightning-generated electric field. Given both the temporal evolution of the flux of electrons and the electric field, the power deposited in the mesosphere was calculated as the product of these two quantities and the total volume of the halo. Finally, the total deposited energy was estimated knowing the duration of the event. This calculation led them to estimate that the total amount of energy deposited in the mesosphere by a halo was about 10^6 J. Therefore, the production rate of NO by a halo could be approximated in terms of energy as 10^{16} molecules of NO/J, one order of magnitude lower than the production rate of NO by lightning, estimated in 10^{17} molecules of NO/J (Price et al., 1997).

Finally, Pérez-Invernón et al. (2018a) also analised the temporal evolution of electrons in halos up to 1 s. Their halo chemistry model predicted that O^- ions were transformed into electrons between 15 ms and 1 s. The main chemical process that contributed to this transformation was the associative detachment reaction $O^- + CO \rightarrow e + CO_2$ that exceeded other associative detachment processes when the applied electric field was zero. However, at the very initial moment when the halo develops and the electric field is high, the rate of this reaction does not increase, since it does not depend on the electric field (Moruzzi et al., 1968).

Future longer–time (some seconds) microphysical simulations and remote chemical observations would be needed to better constrain the local chemical impact of halos in the mesosphere lower thermosphere (MLT) region especially regarding their possible contribution to the enhanced N_2O layer recently observed by ACE-FTS in the MLT (Sheese et al., 2016) that disagrees with available global simulations in mid and low latitudes between 60 km and 80 km near where halos usually occur (Kelly et al., 2018). According to the 1 s long simulations of halos by Pérez-Invernón et al. (2018b), halos produced by CG lightning with a charge moment change (CMC) of 560 C km would inject 1.7×10^{20} molecules of N_2O (about 10 times more than a full sprite with all its streamers as simulated up to 0.85 ms between ~74 km and ~ 69 km (Pérez-Invernón et al., 2020)). Since the global occurrence rate of halos is similar (1 event every two minutes) to that of sprites they found that the global contribution of halos would be $\sim 1.7 \times 10^{26}$ molecules of N_2O in the mid and low latitudes of the mesosphere lower thermosphere (MLT) region in one year. Considering the ambient concentration of N_2O at 80 km altitude, halos would contribute with ~0.03% per year to the total N_2O in the mid and low latitudes of the MLT. This contribution is small and by itself could not yet explain the enhanced layer of N_2O in the MLT (Kelly et al., 2018).

3.4. Mesosphere: Giant blue jets

Giant Blue Jets were discovered in 2001 during observations from Arecibo Observatory in Puerto Rico (Pasko et al., 2002). This first giant blue jet was observed starting at 03:25:0.782 UTC on 15 September 2001, lasted a total of 24 video frames (~ 33 ms each), and concluded with an intense lightning flash in the underlying thundercloud in frame 25. The event propagated upwards from a thundercloud to an altitude of about 82 km (da Silva and Pasko, 2012) and looked bluish and reddish in color in the lower (below 40 km) and upper parts, respectively.

The apparent diameter of the breakdown filaments in the original recorded images of giant blue jets provided conclusive evidence pointing to the presence of filamentary branching structures as an essential component of the observed new phenomenon (Pasko et al., 2002) in agreement with the streamer structure also found in blue jets (Wescott et al., 2001b).

According to (Pasko et al., 2002), the transition (apparent in frame 10) between the upper region dominated by hot spots and the lower region dominated by relatively smooth filamentary structure was estimated to be at an altitude of 42 km. This transition height was similar to the normal upper terminal altitude of blue jets and the lower terminal altitude of sprites. Also, Pasko et al. (2002) found that the upward branches of the reported phenomenon exhibited a diffuse termination at an altitude of approximately 82 km in frame 8. The 82 km termination closely coincides with the steep ledge of the lower ionospheric conductivity profile typically recorded during night-time rocket measurements in equatorial regions (Hale et al., 1981).

Five years after the discovery of giant blue jets a study by Lehtinen and Inan (2007) investigated the possible persistent ionization caused by giant blue jets. The results of this study indicated the possibility of substantial ionization at altitudes below 50 km, which exhibited an initially rapid (few seconds) recovery due to electron attachment, followed by a long enduring recovery (> 10 min) determined by the time scale of mutual neutralization of negative and positive ions. Such recovery signatures may be observable in subionospheric VLF data in the form of early/fast events with long lasting recoveries (Gordillo-Vázquez et al., 2016). Analysis also indicates that electrons may sometimes be quickly ($\leq$ 1 ms) removed by the dissociative attachment mechanism in the presence of a high electric field, while the negative and positive ions remain and persist for extended periods of time. In such cases, the initial rapid recovery may not be observable in VLF data due to its typical time resolution of ~10 to 20 ms (Lehtinen and Inan, 2007).

The model of Lehtinen and Inan (2007) was based on a previous four-constituent model proposed by Glukhov et al. (1992). Lehtinen and Inan (2007)slightly modified the model of Glukhov et al. (1992). The changes consisted in adding a fifth component (separating all negative ions into light and heavy negative ions) and in considering the detachment from heavy negative ions and the rate of conversion from light to heavy negative ions.

The presence of streamers in giant blue jets and their ability to produce high electric fields in their heads can generate electrons with sufficiently high energies (8–10 eV) that would be able to trigger a cascade of non-equilibrium chemical reactions in the surrounding giant blue jet atmosphere that could eventually lead to local chemical perturbations. Due to the dramatic reduction in the air pressure at high altitudes above thunderstorms, the same streamers, which develop on time scales of several nanoseconds and exhibit diameters of a fraction of millimeter at ground level, appear as many kilometer long channels with diameters of the order of hundred meters and formation time of several milliseconds, easily observable above thunderclouds by low-light imaging systems deployed hundreds of kilometers away (Pasko et al., 2002; Su et al., 2003). These streamers preserve their ability to produce highly active chemical species (Enell et al., 2008; Arnone et al., 2008; Sentman et al., 2008b; Gordillo-Váquez, 2008) and can effectively treat thousands of cubic kilometers of atmosphere in a single event (Pasko, 2008).

The work by da Silva and Pasko (2013) theoretically investigated the streamer-to-leader transition dynamics in giant blue jets using a one dimensional radial model assuming a constant electric current. They calculated and compared the temporal dynamics at the discharge axis of gas temperature and electron density at ground level, 20 km and 40 km and were able to determine that the maximum altitudes where a leader could be formed ranged between 24 km and 58 km for constant electric currents of 1 A and 100 A, respectively (see Fig. 14). Recently, van der Velde et al. (2019) recorded four giant blue jets with a high speed camera at a temporal resolution of 0.2 to 1 ms. These authors demonstrated that some giant blue jets evolve stepwise through the middle atmosphere (up to 40 km) during the rising stage. However, their optical observations suggest that the stepwise propagation above 22–23 km is not produced by an advancing leader.

During its 12-year operation ISUAL registered very few (127) giant blue jets (Chen et al., 2019). This may suggests that giant blue jets have a chemical impact that, though possible locally, would be negligible at global scale. However, future more detailed global space observations would be needed to firmly determine their occurrence rate.

More recently, Boggs et al. (2019) accomplished the first observations of giant blue jets from geostationary orbit. They reported the occurrence of fourteen giant blue jets produced in the same thunderstorm using optical measurements provided by the Geostationary Lightning Mapper (GLM) on board the Geostationary Operational Environmental Satellite-R series (Rudlosky et al., 2019). These observations suggest that giant blue jets could have a non-negligible influence in the chemical composition of the mesosphere over some thunderstorms at a local scale. GLM detections of giant blue jets recorded optical emissions through a 1-nm bandwidth around the 777.4-nm neutral oxygen emission line (OI) with temporal resolution of 2 ms and spatial resolutions ranging from 8 km (nadir) to 14 km (at the edge of its field of view). The visibility of giant blue jets with GLM comes from features like that the majority of them produce long continuous light (777.4 nm) emissions, large (and sustained) peak flash optical energies over a single location and small lateral propagation distances in comparison with

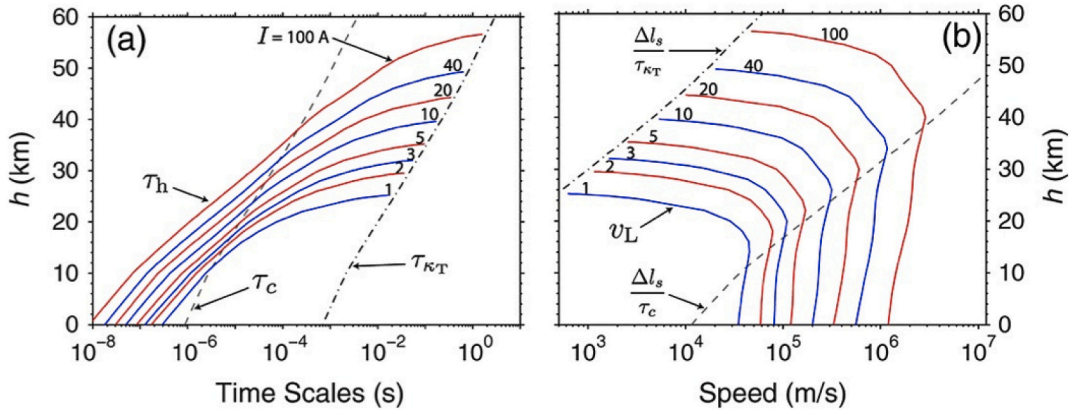

Fig. 14. Panel (a) streamer-to-leader transition time (τ_h) and panel (b) leader speed with altitude, for several different currents from 1 A to 100 A flowing through the leader head. Panel (a) displays τ_h, as well as, the ambient values of τ_c and τ_{K_T}, where τ_{K_T} is the time scale for heat conduction and τ_c is a time characterizing the gas dynamic expansion of the leader channel (for $t \ll \tau_c$, air heating is isochoric, while for $t \gg \tau_c$, heating is isobaric). The maximum altitude (end of solid line) where a leader can be formed as a function of the current in the leader stem requires $\tau_h < \tau_{K_T}$. Panel (b) displays the calculated leader speed with $v_L = \Delta l_s/\tau_h$ and τ_c and τ_{K_T} plotted in units of speed (i.e. $\Delta l_s/\tau_c$ and $\Delta l_s/\tau_{K_T}$). Note that τ_h (the streamer-to-leader transition time) is the time scale on which the leader increases in length by an amount Δl_s or the time needed to heat the channel up to 2000 K according to da Silva and Pasko (2013). Image reproduced from da Silva and Pasko (2013).

typical GLM lightning flashes that radiate discrete optical pulses (Boggs et al., 2019). Considering that giant blue jets are composed of upward moving vertically oriented channels, localized GLM detection is expected and integration of the emission source along the vertical channel will also contribute to increasing the contrast between central and surrounding pixels (Boggs et al., 2019). From the video images in Fig. 1 of Boggs et al. (2019), the bright channel segment reaching 26 km altitude in frames 11–14 resembles a bright return stroke channel. If GLM indeed observes the giant blue jet above the cloud, this would indicate that at least some portion of the giant blue jet channel emits at the 777.4 nm band. ISUAL–detected giant blue jets also showed some emissions at the 777.4-nm band (Chou et al., 2010; Kuo et al., 2009), but it was difficult to tell if these emissions were from the giant blue jets or the lightning inside the cloud. Considering streamers do not emit at 777.4 nm in the upper atmosphere (Kanmae et al., 2007, 2010a; Gordillo-Vázquez et al., 2018) the results reported by Boggs et al. (2019) may indicate some portion of the giant blue jet above the cloud is composed of leaders. Therefore, further chemical modeling of giant blue jets is needed considering future detailed surveys of giant blue jets recorded with geostationary instruments.

3.5. Stratosphere and upper troposphere: blue jets and blue starters

Blue jets and blue starters are two types of low altitude TLEs that last a few milliseconds and occur between thundercloud tops and the lower–mid stratosphere up to about 40 km (blue jets) (see Fig. 15) and 20–25 km (blue starters) (Wescott et al., 2001a). Both jets and starters were discovered in 1994 and were first documented in two papers (Wescott et al., 1995, 1996). Soon after blue jet discovery Sentman and Wescott (1995) suggested that upward discharges might create long-lived chemical byproducts and thus could have long term consequences in the atmosphere. This would be of critical importance at the altitude of the ozone layer since it could affect its chemical composition. Blue jets move upward with velocities of the order $\sim 10^5$ m s^{-1} and they typically exhibit diameters of a few hundred meters at their base and increase with altitude (see Fig. 15) (Wescott et al., 2001a). In 2001 Wescott et al. (2001a) published evidences suggesting that blue jets and starters produce ionization in the upper troposphere lower stratosphere. Both blue jets and starters have been recently observed from space (Chanrion et al., 2017; Chou et al., 2018; Liu et al., 2018; Chanrion et al., 2019).

Pasko et al. (1996a) and Sukhorukov et al. (1996a) suggested the first models to explain the formation of blue jets in terms of propagation

Fig. 15. One of the first color images of a blue jet over a large thunderstorm north of Reunion Island in the Indian Ocean taken in March 1997. The base of the blue jet that can be seen above the top of the thunderclouds is ~400 m wide at 18 km altitude, and the tip of the blue jet is at ~35 km altitude. The pink streak across the bottom is due to an aircraft passing during the 2 min exposure time. The blue color come from the second positive system of N_2 and the first negative system of N_2^+. Image reproduced from Wescott et al. (2001a).

of positive and negative streamers initiated due to conventional electric breakdown above charged thunderclouds. Petrov and Petrova (1999) suggested afterwards that blue jets could be similar to the streamer corona around a leader. Some years later Raizer et al. (2007) proposed the bi–leader theory to explain blue jets. This model considers that blue jets are a consequence of the development of two leaders of positive and negative polarity growing in opposite directions. Streamers originated from the upward propagating leader could be sustained by relatively moderate cloud charges as claimed in a number of papers by the same author (Raizer et al., 2006, 2007, 2010). Streamers in blue jets can reach a few tens of kilometers in the vertical direction (Raizer et al., 2006) and the terminal altitude of the upward propagating leader above the thundercloud increases with the electric current carried by the leader da Silva and Pasko (2013).

As commented in Pasko (2008) one key limitation of earlier models (Raizer et al., 2006, 2007; Pasko and George, 2002) to explain blue jets

is that they postulate the presence of a leader near the cloud top without really providing a link to experimentally documented charge distributions and lightning phenomenology in thunderstorms leading to the initiation and upward escape of the leader process from the thundercloud top. There is an experimental evidence that blue jets are initiated as normal polarity intracloud lightning discharges between upper positive and lower negative charge centers (Krehbiel et al., 2008) and the models commented above do not reflect these related scenarios.

As discussed in Pasko (2008), Krehbiel et al. (2008) described the charge imbalances in thunderstorms as a fundamental condition allowing propagation of leaders downward as CG lightning or upward as jet discharges, therefore demonstrating that upward discharges are analogous to cloud–to–ground lightning and providing a unified view on how lightning escapes from a thundercloud. Krehbiel et al. (2008) noted that in accordance with the existing experimental evidence the lightning initiation happens between adjacent charge regions of different polarities where the electric field is maximum. If the negative and positive charge centers are approximately equal in magnitude the bi–directional discharge propagates in the form of positive leaders inside the negative charge region and in the form of negative leaders inside the positive charge region (Riousset et al., 2007). The modeling presented in Krehbiel et al. (2008) indicates that blue jets occur as a result of electrical breakdown between the upper storm charge and the screening charge attracted to the cloud top; they are predicted to occur 5–10 s or less after a cloud–to–ground or intracloud discharge produces a sudden charge imbalance in the storm. Therefore, results presented in Krehbiel et al. (2008) provide experimentally substantiated mechanisms of escape of lightning leaders from cloud tops complementing previous theoretical works (Petrov and Petrova, 1999; Pasko and George, 2002; Raizer et al., 2006, 2007).

Therefore we see that blue jets are formed by hot leaders and by many cold streamers indicating that the triggered atmospheric chemistry involves a thermal (equilibrium) component and a cold (non–equilibrium) component driven by the streamer electric field. A transition from hot leader channels to cold streamers appears in blue jets as they move upward.

The mechanisms underlying the inception of blue starters have not been so widely investigated as those producing blue jets. It was suggested that blue starters could just be immature blue jets only reaching up to 18–20 km altitude (Wescott et al., 1996).

An important element to complete the understanding of both blue jets and starters is their spectral characterization. There are no spectra to date of neither blue jets nor blue starters. There are however a number of photometric and multispectral video observations revealing that most of their optical emissions are blue (as its name indicates) mainly due to optical emissions of the second positive system of N_2 and the first negative system of N_2^+. In the study by Wescott et al. (2001a) the image of a blue jet was digitized on a 24–bit color scanner and separated into its constituent red, green, and blue components. The blue jet was very evident in all three color separations, but red and green only appeared in the very brightest lower one third of the jet. This is most likely due to saturation of the film and not to real red or green emissions from the jet. It was suggested that the red could be due to the first positive system of N_2 though it should be strongly quenched at these low altitudes. Nothing was said about the 777.4 nm line of atomic oxygen. If blue jets contain upward moving hot leaders they should produce near infrared 777.4 nm optical emissions originated by excited atomic oxygen that are typically observed in downward moving lightning leaders (Walker and Christian, 2019). The radiative lifetime of the 777.4 nm line is about 10 ns so that it is hardly affected by quenching.

In the case of blue starters it was found that in the color TV frame there was also (apart from the blue camera response of 1 MR) about 70 kR or 7% of the blue total in both the red and the green channels (Wescott et al., 2001a).

As we have seen above it was not until 2008 when a comprehensive understanding of blue jet structure and formation mechanisms were finally settled. However, the study of the possible chemical influence of streamers in blue jets started soon after their discovery because of its possible impact in the stratospheric chemistry with possible critical influence on the ozone layer.

The analysis of the electron energy distribution function (EEDF) and transport coefficients for air plasmas for the conditions of the Earth troposphere where blue jets, blue starters and giant blue jets have been observed can be important for further electrodynamic and kinetic modeling of these phenomena. Such study was accomplished by Gordillo-Vázquez and Donkó (2009) considering that the relative humidity of the air between 0 and 15 km can change (according to satellite measurements) between 15% and 100% depending on the altitude investigated and the ground temperature. These relative humidity conditions are typical of tropical region where lightning and the associated TLE activity is high. The calculations performed in Gordillo-Vázquez and Donkó (2009) suggest that the relative humidity has a clear impact on the behaviour of the EEDF and on the magnitude of the transport coefficients of air plasmas at ground (0 km) and room temperature conditions (293 K). At higher altitudes (11 and 15 km), the influence of the relative humidity is negligible when the values of the gas temperature are assumed to be the ambient ones corresponding to those altitudes, that is, ~ 215 K (at 11 km) and ~ 200 K (at 15 km). However, it was found that enhancements (of maximum 100 K) in the background gas temperature (that could be reasonably associated with the action of the leader of blue jets and/or giant blue jets) would lead to a remarkable impact of the relative humidity on the EEDF and transport coefficients of air plasmas under the conditions of blue jets, blue starters and giant blue jets at 11 and 15 km. The latter effects are predicted to be noticeable for relatively low reduced electric fields (E/N ~ 25–100 Td) present in streamer glows (Luque and Ebert, 2010) and, consequently, could be controlling the glow kinetics of streamers in blue jets, blue starters and/or giant blue jets. However, for much higher fields such as, for instance, 400 Td (representative of the fields in corona streamer heads), the impact of increasing the relative humidity and gas temperature is only slightly noticeable in the attachment coefficient that can exhibit an increase of up to one order of magnitude at 11 km and 15 km for temperatures of 313 K and 308 K, respectively.

There are five publications to date dealing in some detail with the plasma chemistry of blue jet streamers. One of these studies investigated blue jet streamer analogs in the laboratory at 0.4 Torr (equivalent to about 37 km altitude). In chronological order, the work of Mishin (1997) first evaluated the chemical influence of single blue jet streamer by using a plasma chemistry model with a concise kinetic scheme of nitrogen and oxygen where the discharge (streamer) parameters were taken by contemporary works on blue jet formation (Sukhorukov et al., 1996b).

The model of Mishin (1997) predicted that after 100 s at 30 km altitude nitric oxide (NO) and ozone (O_3) increase in about 10% and 0.5% over background, respectively. At an altitude of 20 km, he predicted enhancements in NO and O_3 due to blue jets of ~1000% and 4% and they will vary with the atmospheric pressure as $\sim p^2$. Six years later, in 2003, the work of Smirnova et al. (2003) (also based on the blue jet formation model of Sukhorukov et al. (1996b)) used a more elaborated chemical model (Borisov et al., 1993) with >30 species and a different set of electron impact and excited neutral rate coefficients (relative to Mishin (1997)) that changed both qualitatively and quantitatively the results of Smirnova et al. (2003) simulations with respect to the previous work of Mishin (1997). The model of Smirnova et al. (2003) predicted a larger increase of NO, and a smaller relative increase of O_3 at 30 km and 20 km compared to the values of Mishin (1997). The production of NO in the study of Smirnova et al. (2003) was critically controlled by reactions with excited species such as $N(^2D)$, $N_2(A\ ^3\Sigma_u^+)$ and $O(^1D)$. Smirnova et al. (2003) also found that the fact of considering chemical processes with $O(^1D)$, $O(^1S)$ and $O_2(A\ ^3\Sigma_u^+)$ increased the NO production by four times as compared with simulations performed without these excited species. Finally, Smirnova et al. (2003) also predicted important

production of molecular metastable species such as $N_2(A\ ^3\Sigma_u^+)$ and $O_2(A\ ^3\Sigma_u^+)$ with the latter having a longer lifetime so that it was suggested that optical emissions from $O_2(A\ ^3\Sigma_u^+)$ in the ultraviolet range (260–380 nm) could be possible.

As mentioned above both the chemical model of Mishin (1997) and the one of Smirnova et al. (2003) were based on the early blue jet physical model of Sukhorukov et al. (1996b). However it was later pointed out by Mishin and Milikh (2008) that the electric field at the streamer head in the model of Sukhorukov et al. (1996b) was unrealistically small. This results in considerable underestimation of electron-driven kinetic processes such as ionization, attachment, dissociation and excitation that critically limit and/or underestimate the possible chemical effects caused by blue jets in the upper troposphere and lower stratosphere region.

In 2015, Winkler and Notholt (2015) published an elaborated model to asses the atmospheric chemical impact of blue jet streamers considering updated electron-impact rate coefficients including associative detachment and other neutral and excited species chemistries. This model prescribes streamer pararemeters such as the streamer pulse duration and the strength of the electric field at the streamer head. This model evaluated the influence of a blue jet streamer on key chemical species such as NO_x and O_3 during daytime and nighttime together with positive and negative ions, excited atomic and molecular species and characteristic optical emissions during nighttime. The model predictions were applicable to altitudes between 18 km and 38 km.

An important different resulting from the chemical model of blue jet of Winkler and Notholt (2015) with respect to previous blue jet chemical models was its ability to provide preliminary quantitative estimations of the hot chemistry by-products due to the blue jet leader (see Fig. 16). The leader parameters were prescribed following da Silva and Pasko (2013). It was assumed that the leader propagates up to 30 km altitude. Accordingly, the leader duration time linearly decreased from about 200 ms at 18 km to zero at 30 km. The electric field in the leader channel had an undervoltage value (60 Td was assumed) corresponding to an electron temperature of about 1.2 eV. After the leader phase, the electric field was put off. The translational (gas) temperature of ions and neutral species was assumed to linearly decrease from 2700 K at 18 km to 1500 K at 30 km. A reduced hot chemistry scheme of 30 reactions was implemented to account for the leader chemistry.

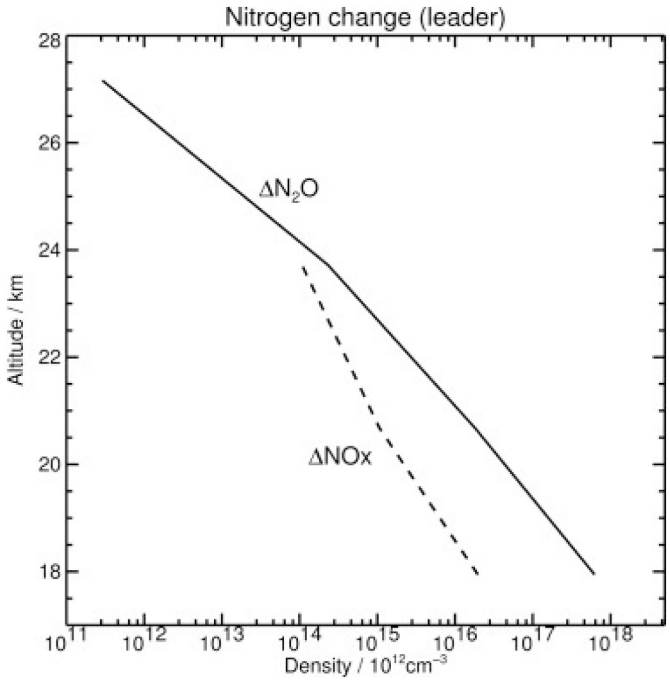

Fig. 16. Predicted altitude change of N_2O and NO_x due to the leader chemistry of Blue Jets according to the blue jet chemical model of Winkler and Notholt (2015). The N_2O excess decreases exponentially with altitude. The predicted enhancement of N_2O is almost 10^{18} molecules per cm^{-3} at 18 km. This corresponds to an increase of more than five orders of magnitude with respect to ambient values. The enhancement at 27 km is of about 50% of the initial concentration. Also note the important predicted NO_x enhancement. At 18 km, it is of the order of 10^{16} cm^{-3}. This is an enormous number compared to the typical NO_x background values at 18 km which is $\sim 10^9$ cm^{-3}. It is also larger that the predicted Blue Jet streamer NO_x production of $\sim 10^{12}$ cm^{-3} at 18 km altitude. Image reproduced from Winkler and Notholt (2015). (For interpretation of the references to colour in this figure legend, the reader is referred to the web version of this article.)

The blue jet streamer chemical model of Winkler and Notholt (2015) had three limitations: the first obvious restriction is that it was not a self–consistent model, that is, electrodynamics and kinetics were not really coupled. The second and third limitations were that it did not consider vibrational kinetics, and that the model (though not self-consistent) only considered the presence of electric field in the streamer head so that chemical species can only be produced and/or activated by the action of high electric fields in the streamer head. There are, however, high temporal resolution observations of sprite streamers (Stanley et al., 1999; Cummer et al., 2006; McHarg et al., 2007; Stenbaek-Nielsen and McHarg, 2008) showing the presence of glowing regions in the streamer tail. Further simulations of sprite streamers by Luque and Ebert (2010) showed that the origin of such luminous streamer glows was due to a secondary wave of impact ionization and excitation of N_2 in electric fields close to the breakdown value (120 Td), in agreement with observations by Morrill et al. (2002). It is therefore expected that blue jet streamers propagating at upper tropospheric and lower stratospheric altitudes also exhibit trailing optical emissions indicating that those streamer tails are also active non–equilibrium chemistry sources producing reactive species due to the action of an electric field in the trailing streamer region. It is also true that those nighttime blue jet streamer tail glows would last much less (between some tens and some hundreds of microseconds at 18 km and 38 km, respectively) than those of sprite streamers (tens of milliseconds) but still their chemical effect could significantly add to that of the streamer head pulse typically lasting between 50 ns (at 18 km) and 1300 ns (at 38 km) at nighttime.

In the following we comment the chemical predictions of the Winkler and Notholt (2015) blue jet streamer and leader model. For a blue jet streamer, it was found that at 27 km altitude the production of NO and NO_2 reaches values of 10^{10} cm^{-3} and 5×10^{10} cm^{-3} during nighttime, respectively. The concentrations of NO and NO_2 increase and decrease by roughly a factor of two during daytime (with respect to nighttime values). This effect was due to reactions in the sunlit atmosphere which convert NO_2 back into nitric oxide (Winkler and Notholt, 2014). The sum of NO_x (odd nitrogen) remains basically the same for daytime and nighttime model simulations so that the NO_x is kept constant until the end of the simulation 100 s after the electric pulse of the blue jet streamer is off (Winkler and Notholt, 2015). The NO produced by blue jet streamers is originated by electron impact dissociative excitation of N_2 leading to the excited $N(^2D)$ and $N(^2P)$ that give rise to a rapid formation of NO which reaches its maximum concentration about 10 ms after the electric field pulse. On longer time–scales, NO is converted to NO_2 through $O_3 + NO \rightarrow NO_2 + O_2$.

The blue jet streamer causes a small (3%) increase of ozone at higher altitudes of ~30 km and a much larger one of 300% at 18 km. These values are considerably larger than the model predictions of Mishin (1997) and Smirnova et al. (2003). The atomic oxygen generated during the streamer electric field pulse leads to a production of ozone through the three-body reaction $O(^3P) + O_2 + O_2 / N_2 \rightarrow O_3 + O_2 / N_2$. As a result there is an increase of ozone between 1 ms and 100 ms after the electric field pulse, until all the atomic oxygen has been consumed. After a few seconds, O_3 starts to slowly decrease again, mainly due to reaction with NO following $O_3 + NO \rightarrow O_2 + NO_2$ (Winkler and Notholt, 2015) ending

in O_3 concentrations that are almost the same for daytime and nighttime after 100 s of simulation.

The relative increase of NO_x with altitude due to a blue jet streamer changes from approximately a factor of two (with respect to background) at 37 km to more than two orders of magnitude (a factor 600) at 18 km. The absolute NO_x increase varies between 3×10^9 cm^{-3} at 37 km and 10^{12} cm^{-3} at 18 km. As discussed in Winkler and Notholt (2015) the increase of NO_x by a blue jet streamer significantly exceeds the atmospheric background values but their relative enhancements depends on the stratospheric background NO nighttime/daytime profiles which are more variable than the ozone profile due to the pronounced diurnal cycle of the odd nitrogen species.

According to the blue jet chemical model of Winkler and Notholt (2015) one streamer of a blue jet has a modest impact on the concentration of N_2O, which was found to increase by 4% at 18 km altitude, ~ 1% at 27 km and ~ 0.5% at 38 km. As shown in Parra-Rojas et al. (2015) for sprite streamers the formation of N_2O is critically controlled by the duration of the streamer trailing glow in which an electric field close to breakdown (~ 120 Td) exists and continuously produces $N_2(A\ ^3\Sigma_u^+, v)$ and O^-. Therefore, the probable underestimation of the N_2O production by blue jet streamers found in Winkler and Notholt (2015) (that used the same reaction coefficient rates used in Parra-Rojas et al. (2015) for reactions involving $N_2(A\ ^3\Sigma_u^+, v)$ and O^- to produce N_2O) might be mainly caused by the fact that no electric field was considered in the streamer trailing glow region. The formation of N_2O in the streamer glow is due to $N_2(A\ ^3\Sigma_u^+, v) + O_2 \rightarrow N_2O + O$ and associative detachment $O^- + N_2 \rightarrow N_2O + e$ which releases electrons that can condition the propagation dynamics of blue jet streamers (Luque and Gordillo-Vázquez, 2011a). The efficiency of O^- associative detachment increases with the availability of O^- which reaches its maximum (~ 10^9 cm^{-3} at 27 km) right after the pulse (Winkler and Notholt, 2015).

As mentioned above a distinct feature of the blue jet chemical model of Winkler and Notholt (2015) is its quantitative evaluation of the high temperature chemistry of a blue jet leader between 18 km and 27 km altitude. The initial conditions for the leader chemistry simulations were the final chemical environment left by the blue jet streamer. However, according to Winkler and Notholt (2015), the precise initial conditions for the leader simulations were found to have a minor importance. The leader chemistry results included effects on the electron density, negative ions (O^-, O_2^-, NO_2^-, NO_3^-), nitrogen species (N, NO, NO_2, N_2O), oxygen species (O, O_3) and optical emissions. The leader chemistry was evaluated for daytime conditions but nighttime conditions were claimed to produce similar results (Winkler and Notholt, 2015).

The blue jet leader mainly releases electrons through the reaction $N + O \rightarrow NO^+ + e$ that produces electron densities of the same order (~ 10^6 cm^{-3}) at 18 km and at 27 km but it is significantly smaller than the electron density produced by a blue jet streamer. The leader produced concentrations of negative ions such as O^- and O_2^- were between five (O^-) and six (O_2^-) orders of magnitude below those produced by a blue jet streamer. The blue and red optical emissions due to the second and first positive systems of N_2 were weaker than those of blue jet streamers but were found to last longer (100 ms and 1 ms for leader and individual streamer optical emissions, respectively).

The blue jet leader was found to produce a significant thermal production of nitrous oxide (a key greenhouse gas and the most important ozone depleting gas nowadays) (see Fig. 16). The main thermal source of N_2O in the blue jet leader channel was found to be $N_2 + O_2 \rightarrow N_2O + O$, which rate coefficient is strongly temperature dependent so that this reaction becomes a very important source of N_2O as the gas temperature rises. It was found that the production of N_2O decreases exponentially with altitude (the gas temperature is 2700 K at 18 K and 1500 K at 27 km). The enhancement of N_2O is almost 10^{18} molecules per cm^{-3} at 18 km (an increase of more than five orders of magnitude with respect to ambient values) while it is about 50% at 27 km.

According to Winkler and Notholt (2015) the blue jet leader also produces an important increase of NO_x. At 18 km the leader produced enhancement of NO_x is of the order of 10^{16} cm^{-3} (100 times less than N_2O), which is about 10^9 cm^{-3} above the NO background value at 18 km (see Fig. 16). This value is much larger than the NO_x production due to a blue jet streamer that is 10^{12} cm^{-3} at 18 km. But what is the thermal source of NO_x? Is it due to a Zeldovich mechanism that can efficiently produce NO above 1500 K? The work of Winkler and Notholt (2015) does not seem to mention it. Apart from a possible blue jet Zeldovich mechanism, the huge amount of thermally produced N_2O could react with available $O(^1D)$ – thermally produced (but not shown by the authors though the concentration of thermally produced ground atomic oxygen increases) – and/or with the $O(^1D)$ left by streamers (although O (^1D) is less than $O(^1S)$ according to Winkler and Notholt (2015)) to produce NO through $N_2O + O(^1D) \rightarrow 2\ NO$. This reaction is considered in the work of Winkler and Notholt (2015) but not discussed in this context (thermal production of NO_x).

Regarding the leader produced ozone it was found that while the effect is small (almost negligible) at 27 km, there was a quite significant loss of ozone at lower altitudes. Ozone is predicted to strongly decrease (more than five orders of magnitude with respect to ambient) at 18 km as a consequence of the blue jet leader chemical activity. Moreover, the ozone decrease is by orders of magnitude stronger than the ozone production due to blue jet streamers (Winkler and Notholt, 2015). The enormous depletion of O_3 at low altitudes (18 km) coincides with the important increase of N_2O at lower altitudes (see Fig. 16). The NO produced by $N_2O + O(^1D) \rightarrow 2\ NO$ can cause a depletion of ozone through the catalytic cycle $NO + O_3 \rightarrow NO_2 + O_2$ and $NO_2 + O \rightarrow NO + O_2$ (which rates coefficients increase exponentially with the increase of the gas temperature) leading to the net loss reaction $O_3 + O \rightarrow 2\ O_2$.

Other catalytic cycles, apart from the NO one, involving hydrogen oxide (HO) and chlorine radicals (Cl) (the three of them considered in the work by Winkler and Notholt (2015)) can also destroy ozone via $XO + O_3 \rightarrow XO + O_2$ and $XO + O \rightarrow X + O_2$ with X = HO and Cl. The recycling of the X molecules allows one X to destroy many (typically 10^3–10^5) ozone molecules before it is converted to a less–reactive molecule. This cycle is representative of the many forms of catalytic cycles that have been found to be important. Bromine is interesting as its most important catalytic cycle is a combined ClO/BrO cycle, and thus increases in chlorine make bromine more potent as an ozone-destroying agent (Portmann et al., 2012). The NO_x cycle is dominant in approximately the middle stratosphere (~ 23 km–44 km), the HO_x cycle prevails in the upper (~ 47 km–50 km) and lower (~ 23–18 km) stratosphere and the ClO_x/BrO_x catalytic cycle dominates in the upper stratosphere at about ~44–47 km (Portmann et al., 2012). The work by Winkler and Notholt (2015) does not comment on how blue jets affect the atmospheric chemistry of HO_x radicals or how HO_x can impact on ozone depletion by the action of blue jet streamers and/or leaders at low altitudes (below approximately 23 km).

The paper of Hoder et al. (2016) presented results of laboratory experiments to study analogs of blue jet streamer heads under conditions close to those of the upper atmosphere (the images in Fig. 17 show the emergence of a blue jet reaching altitudes of 22 km recorded during the Thor mission in 2015 (Chanrion et al., 2017)). Spectrally and highly spatiotemporally resolved optical emissions originating from radiative states $N_2(C\ ^3\prod_u)$ (second positive system of N_2) and N_2^+ $(B\ ^2\Sigma_u^+)$ (first negative system of N_2^+) were recorded from laboratory produced positive streamer discharges. Periodic ionizing events were generated in a barrier discharge arrangement at a pressure of 4 Torr of synthetic (dry) air aimed to simulate the pressure conditions at altitudes of ~37 km.

Abel inversion and a 2D fitting procedure were used in Hoder et al. (2016) to derive the local spectral signatures within the over 10^6 m s^{-1} fast propagating streamers. The reduced electric field strength distribution within the streamer head was determined from the ratio of the N_2^+ $(B\ ^2\Sigma_u^+)$ / $N_2(C\ ^3\prod_u)$ band intensities with peak values up to 500 Td and overall duration of about 10 ns. The 2D (radial dimension as a function of time) profiles of the streamer head electric fields were used as an

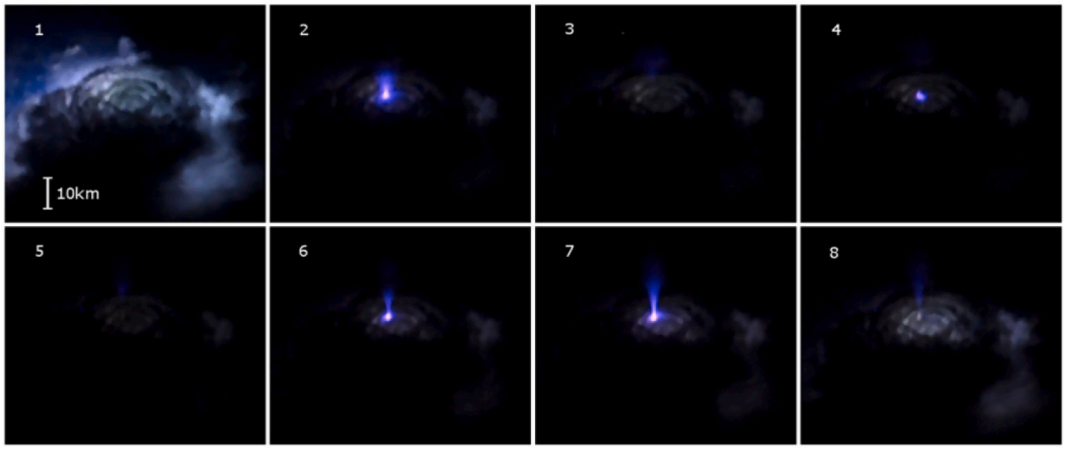

Fig. 17. Eight consecutive images showing the emergence of a pulsating blue jet beginning with the cloud illuminated by lightning deeper inside the cloud. These images were recorded during the Thor experiment conducted from the International Space Station (ISS) from 2 to 11 September 2015 (Chanrion et al., 2017). The first pulse reaches a length of ~13.25 km (2) after which it fades, leaving faint emissions up to ~17.5 km (3). Then a second pulse appears at the base of the original discharge, with faint emissions reaching even higher to 10.5–20 km; these are disconnected from the activity at the root and may be the remains of the first pulse (4). The discharge then fades, with blue emissions remaining at the top (5). The discharge finally rebrightens a third time to 18.5 km (6), reaching its maximum extent of ~21.5 km (7–8) before fading completely. These images were recorded with a Nikon D4 camera at 6400 ISO and recording 24 frames per second at 1920 × 1080 pixels, downscaled from 4928 × 2768 pixels of the sensor. It was mounted with a 58 mm/f1.2 lens, giving a 34.4° × 19.75° field of view corresponding to 1.070/ pixel. With these settings, the camera resolution was 130 m at nadir, 728 m at the limb, and 203 m for the discharge events shown. Image and caption reproduced from Chanrion et al. (2017).

experimentally obtained input for kinetic simulations of the streamer-induced air plasma chemistry. The radial and temporal computed distribution of electrons, ground vibrational levels of the radiative states involved in the radiative transitions analyzed (337.1 nm and 391.5 nm), ground and electronically excited atomic ($O(^3P)$, $O(^1D)$) and molecular (O_2 ($a\ ^1\Delta_g$), O_2 ($b\ ^1\Sigma_g^+$)) oxygen, excited nitrogen atoms ($N(^2P)$, $N(^2D)$), nitric oxide (NO) and ozone (O_3) were calculated by using experimentally measured streamer head electric fields.

The species concentrations found in laboratory produced blue jet streamer analogs at 37 km altitude were consistent with those resulting from the model of Winkler and Notholt (2015). An interesting feature in the work of Hoder et al. (2016) is that $O(^1D)$ is larger and last longer than $N(^2D)$. However, the model of Winkler and Notholt (2015) predicts that $O(^1D)$ (not shown in any figure) is below 3×10^{10} cm^{-3} (the peak concentration of $O(^1S)$ and $N(^2D)$ at 27 km) and, consequently, it is smaller than $N(^2D)$ at 27 km. This $O(^1D)$ chemical trail of the streamer head ($O(^1D)$ is a metastable species) could have some influence on the efficient hot leader chemistry occurring at lower altitudes (when the leader produced N_2O is larger) right afterwards blue jet streamers when thermal NO could be produced by $N_2O + O(^1D) \rightarrow 2\ NO$ (and a blue jet leader Zeldovich mechanism). A subsequent work of Hoder et al. (2020) reported experimental evidence of the emergence of a streamer from an ionisation wave in 1.3 kPa air (equivalent to an altitude of ~25 km), a laboratory analogue of early–stage streamers appearing in blue starters and jets. The radially and temporally resolved electric field patterns of an expanding streamer were determined by sub–nanosecond optical emission spectroscopy. As the emerged streamer expanded, the electric field decreased by a factor of 1.4 in 1 ns. Hoder et al. (2020) quantified the radial expansion of the streamer head and its axial acceleration, reaching the velocity of 10^7 m s^{-1}.

Finally, a new model for investigating the blue jet streamer chemistry was published in 2020 (Xu et al., 2020). This model is based on a previous atmospheric model used to interpret stratospheric ozone measurements by balloons and satellites. The model included an extensive set of chemical reactions (> 1700) and species (> 100) with the plasma chemistry reactions taken from the work of Winkler and Notholt (2015). The idea of the model of Xu et al. (2020) was to compare the model of Winkler and Notholt (2015) that used a prescribed box–like streamer head electric field with a more "rigorous" (though not really self-consistent) streamer electric field pulse shape resulting from an external streamer fluid model. The blue jet streamer chemistry model of Xu et al. (2020) produced slightly different (approximately a factor of two) results in ozone (O_3) and nitric oxide (NO) production at 27 km (the only altitude investigated) in a time scale of 100 s.

The model of Xu et al. (2020) also investigated the chemical effects of blue jet streamers in the atmosphere within a time scale of 2 days. The 2–day simulation revealed that the O_3 volume mixing ratio (vmr) is destroyed through the NO_x catalytic cycle in the middle stratosphere. After two days the ozone vmr decreases to lower vmr than in the no–discharge scenario.

More than 25 years after the discovery of blue jets and blue starters their full chemical impact in the atmosphere remains elusive. It is now known however that blue jets are the second most frequent type of TLE (Chen et al., 2019) after elves. More detailed microphysical self–consistent simulations are needed coupling the electrodynamics with appropriate kinetic schemes able to unveil the complete impact of blue jet streamers and leaders in the concentrations of key atmospheric species such as ozone (O_3), nitric oxide (NO_x) and nitrous oxide (N_2O) in the lower and middle stratosphere. Microphysical models are an indispensable and fundamental tool to extrapolate their results in the form of well designed global parameterizations able to grassp the essence of blue jet chemistries (streamer + leader) so that their implementation in general circulation atmospheric chemistry models (GC–ACM) could provide hints on their possible global chemistry influence in the present and in a foreseen warmer world scenario.

3.6. *Troposphere: atmospheric chemistry of cloud streamer corona discharges*

So far we have limited our discussion to classical TLEs occurring in the upper atmosphere and that, in any case, take place above thunderclouds and/or emanate (blue jets / starters) from their tops. However, lightning themselves initiate inside thunderclouds and their precise inception mechanisms remain unclear (Rison et al., 2016) due to the extreme complexity and variety of electrical activity inside thunderclouds. What do we know about the types of in-cloud electrical discharges? Do they influence the atmospheric chemistry?

Le Vine (1980) first detected strong radio-frequency (RF) sources

from intra-cloud electrical discharges characterized by short-duration (10–20 μs) bipolar sferic radio waveforms recorded in the range of very low frequency (VLF) / low frequency (LF) usually also accompanied by very high frequency (VHF) radiation. This class of cloud electrical process is nowadays called a Narrow Bipolar Event (NBE) and was hypothesized to be formed by a system of streamers (Jacobson and Light, 2012; Jacobson et al., 2013; Rison et al., 2016; Tilles et al., 2019). This has been recently confirmed by Soler et al. (2020) analyzing concurrent cloud corona streamer 337 nm optical emissions recorded by ASIM and VLF / LF radio signals from NBEs, which near ultraviolet blue optical manifestation was detected by ASIM. Radio detection shows that NBEs are very common in many thunderstorms and are considered responsible for the inception of about 10% of intra-cloud lightning (Lyu et al., 2019). NBEs can also appear in relative time isolation (tens of milliseconds) with respect to the occurrence of lightning strokes.

At the edge of the XXI century the Severe Thunderstorm Electrification and Precipitation Study (STEPS) was conducted on the high plains of Colorado and Kansas during the summer of year 2000. This was a multiorganization (and multi–instrument) field program investigating the coevolving dynamical, microphysical, and electrical characteristics of high plains thunderstorms. During STEPS 3D Lightning Mapping Arrays (LMA) were used in coordination with ultrablue sensitive (350–890) low light TV (LLTV) cameras, radars and the National Lightnng Detection Network (NLDN) (Lyons et al., 2003).

During a 20–minute period at 06:12–06:33 UTC on July 22, 2000 17 upward–propagating discharges called “gnomes” were filmed arising out of the convective dome of a high plains supercell storm. This so–called “gnomes” were brief (33–136 ms duration) and estimated to be less than 200 m wide and did not grow more than 1 km above the cloud top. Their color was not determined since the LLTV cameras were monochrome (Lyons et al., 2003). During this same 20−minute period, a series of 83 distinctive, very small but intense dots of light appeared, also scattered about upon the surface of the convective dome. They were also estimated to be on the order of 100 m in size and none of them persisted beyond 16 ms (a single frame of the LLTV camera). These points of light named “pixies” were present in the video frames but were difficult to see and their color could not determined from the video record (Lyons et al., 2003).

Using the LLTV video, the “gnomes” and “pixies” could neither be temporally nor spatially associated with specific cloud–to–ground (CG) or intra-cloud (IC) lightning flashes. No evidence and/or visual connection was found between lightning strokes and the appearance of “gnomes” and “pixies” (Lyons et al., 2003).

In 2011, Edens (2011) reported what the author called a small blue starter (see Fig. 18) that occurred on 4 August 2010 over an active thunderstorm in west–central New Mexico at a range of 114 km to the camera at 297.5° in azimuth and 5.5° in elevation. The storm was of normal polarity with an upper positive charge over a midlevel negative charge distribution. The event was visually observed and photographed, and mapped by the Lightning Mapping Array (LMA) at Langmuir Observatory. The blue luminous discharge occurred during a seven stroke negative cloud–to–ground (–CG) flash concurrent with the blue event. The negative CG strokes were detected by the NLDN about 5 km to the north east of the event. The data from the LMA showed that it initiated between upper positive charge and inferred negative screening charge at the cloud top. The second and third strokes to ground of this parent negative CG flash had the highest peak currents of the seven -CG strokes at 25.8 and 25.2 kA; negative breakdown from the small blue starter initiated 133 ms after the third stroke to ground and 346 ms after the first stroke. Upward positive streamers of the blue starter emerged from the cloud top at 15.2 km altitude (see Fig. 18) and reached a terminal altitude of about 17 km (Edens, 2011). According to Edens (2011) this observation confirmed that blue starters can be initiated by the electric field changes associated with —CG flashes, which enhanced the electric field between upper positive charge and the negative screening charge layer above the cloud top. Krehbiel et al. (2008) suggested that blue–jet

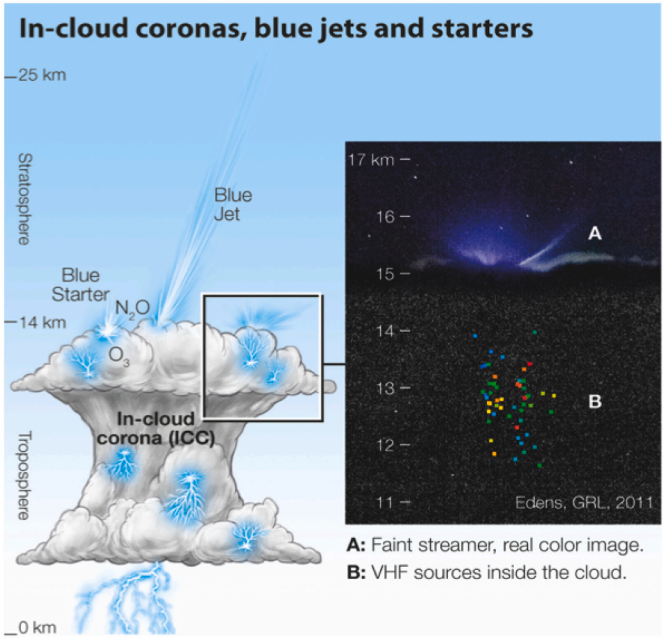

Fig. 18. Representation of cloud corona activity in a thundercloud together with possible concurrent Blue Jet and/or Blue Starter (left). Real color image of a Blue Starter (right). Faint streamers are visible together with VHF sources–colored in time from blue (earlier) to red (later) – inside the cloud recorded by the LMA at Langmuir Observatory (NM). Real color image of the blue starter reproduced from Edens (2011). Note that in-cloud corona discharges, blue starters and blue jets formed by streamers are an unquantified upper troposphere and lower stratosphere source of greenhouse gases such as nitrous oxide (N_2O) and ozone (O_3).

phenomena may initiate during or shortly after the occurrence of a normal —CG flash. Normal —CG flashes remove negative charges from midlevel negative charge region, effectively adding positive charges. This enhances the vertical electric field in the upper part of the storm and it seems that this same mechanism could also explain the inception of blue starters. Interestingly, while —CG flashes enhance the probability of blue jets and starters to occur, typical bilevel IC flashes (Shao and Krehbiel, 1996) (occurring between the main mid-level (~ 7–8 km) negative and upper positive charge region of thunderstorms) prevent them to happen. IC flashes discharge the upper positive charge region reducing the electric field between the upper positive charge region and negative screening charge (Edens, 2011).

The LMA only mapped the negative breakdown of intracloud strokes in upper positive charge, which was centered at 10–12 km altitude. Negative cloud–to–ground (CG) strokes were not mapped because the LMA did not have line–of–sight to the lower regions of the storm that was distant. Thus the blue discharge occurred over the general area of most IC flashes at the upper boundary of the storm’s upper positive charge region. The VHF sources from negative breakdown associated with the cloud top blue discharge were located (using a point–projection method to transform VHF source coordinates to the camera coordinate frame as mentioned in Edens (2011)) in a region of 1.5 × 3 × 2.5 km in azimuth, range and elevation, respectively. The located VHF sources, occurred during a time interval of 92 milliseconds, took place within the 4.3 s exposure time interval of the photograph. The highest VHF sources were located at 13.9 km altitude, 1.3 km below the base of the blue visible part at 15.2 km altitude (see Fig. 18). The downward propagation of negative breakdown extended into the upper positive charge region of the storm to 11.4 km altitude. According to Edens (2011), the absence of located VHF sources above 14 km altitude was suggestive of undetected positive breakdown that propagated upward to emerge from the cloud top at 15.2 km altitude. Together with the presence of negative

breakdown from IC flashes in the upper positive charge region, the LMA also detected a negative breakdown from the blue starter that took place above the area of highest intracloud activity, near the upper boundary of the positive charge region. This blue starter negative breakdown could have been connected to a positive NBE consisting in corona streamers propagating for hundreds of meters (Rison et al., 2016; Soler et al., 2020). However, no VLF / LF sferics were analysed and, consequently, this possibility was not suggested by Edens (2011).

Though once considered a rarity, both blue jets and blue starters have been recently found to be the second most common type of TLE after elves, being more than twice the number of sprites globally. The ISUAL team has recently communicated these new TLE global frequencies as a result of the 12–year ISUAL global survey (Chen et al., 2019).

In 2015, transient blue luminous events were detected just above cloud tops with ISUAL (Kuo et al., 2015). On 18 February 2008, the 427.8 nm–filtered imager of ISUAL recorded a series of blue luminous events north of Australia. One blue starter and nine smaller blue discharges were recorded in 2 min and 34 s in a localized region with the radius less than 4 km over the cloud top. The average time interval between subsequent blue luminous events was about 17 s. The occurrence rate of blue luminous events was of approximately 3.5 events per minute in this short time range. It was slightly lower than the occurrence rate of pixies (4.2 events per minute) but higher than the occurrence rate of gnomes and blue jets in previous observations. The recorded first blue starter lasted up to 60–90 milliseconds and extended its altitude about 8 km with a width of about 2–4 km over the cloud top. After the first blue starter, subsequent nine smaller blue discharges had the decreased heights of about 2–4 km, and their optical duration was shorter. Their major emissions were due to the second positive system of N_2 and first negative system of N_2^+, without lightning OI 777.4 optical emissions (Kuo et al., 2015).

More recently, in 2017, Chanrion et al. (2017) recorded color video images (see Fig. 19) showing profuse activity of blue electrical discharges at the top of thunderstorms. The images were recorded over the Bay of Bengal (India) from the International Space Station (ISS) during the course of the Thor Experiment from 2 to 11 September 2015. The observations showed a multitude of blue, kilometer–scale, discharges at the cloud top layer at about 18 km altitude. Some of the recorded optical emissions were related to possible pixies.

The cloud–top blue discharges reported in Chanrion et al. (2017) occurred at a rate of about 90 per minute since during the 160 s of video recording, 245 discharges were observed. They appeared in different locations of the cloud-top, had spatial areas of 4–9 km^2 with durations of

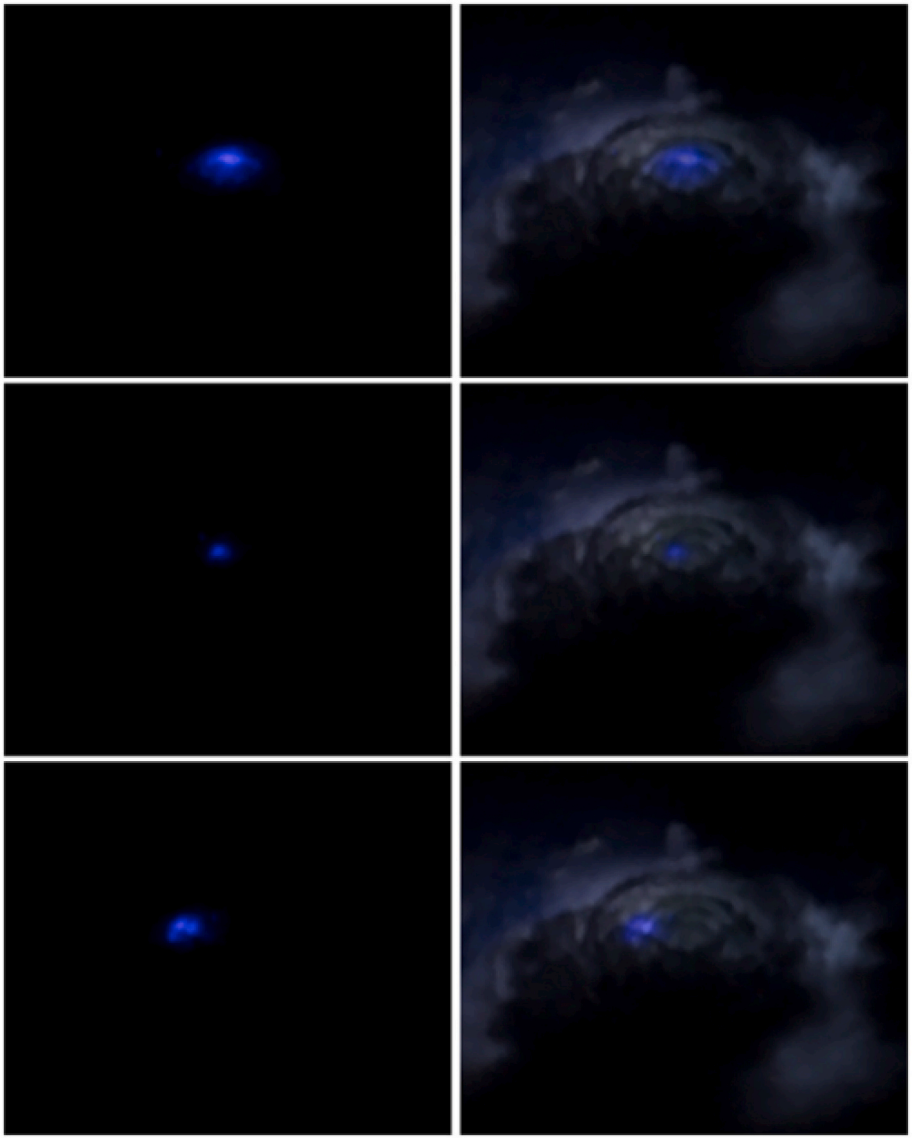

Fig. 19. (Left column) Blue discharges with spatial dimensions of 4–9 km^2 observed at the very top of the cloud and that may last for more than one frame (42 ms). These blue discharges appear unrelated to lightning activity deeper in the thundercloud. (Right column) The blue discharges superimposed on an image of the thundercloud. The blue discharges were photographed during the Thor experiment conducted from the International Space Station in September 2015. Image reproduced from Chanrion et al. (2017).

about 42 ms (the duration of a video frame). The authors reported that no clear relation could be found with lightning activity taking place deeper in the thundercloud (Chanrion et al., 2017). These types of cloud-top electrical activity with durations between 83 ms and 125 ms could be similar to the gnomes reported by Lyons et al. (2003) during STEPS and that lasted 33–136 ms and grew about 1 km above the top of the clouds.

Chanrion et al. (2017) reported that the rate of blue discharges increased from 60 to 180 per minute (1 to 3 per second) before a blue jet occurred and decreased to an average of 120 per minute (2 per second) after it. In addition a strong negative CG lightning with a peak current of −167.5 kA occurred 1.16 s before the pulsating blue jet, which supports the mechanism proposed by Krehbiel et al. (2008) and that was commented above. Thus negative CG lightning plays the role of unbalancing the cloud charge, that is, −CG removes negative charge from the mid-level negative charge region, effectively adding positive charge. This enhances the vertical electric field in the upper part of the storm and increases the chance of blue jet occurrence.

The chemical impact of streamer corona discharges involved in fast cloud breakdown phenomena (Rison et al., 2016; Tilles et al., 2019; Cummer, 2020; Soler et al., 2020) is presently not known. It is not known either what is the atmospheric chemical influence of the streamers in blue starters and of streamers and leaders in blue jets (see Fig. 18). More research is needed to unveil their global occurrence worldwide, their size and chemical efficiency. It is known that laboratory produced streamer corona discharges produced significant amounts of greenhouse gases such as nitrous oxide (N_2O) and ozone (O_3). It is thus possible that cloud corona discharges could play an unexpected role in greenhouse gas production and be a nonneglegible atmospheric (tropospheric) source of N_2O to be taken into consideration. N_2O is a long lifetime gas (> 100 years) in the troposphere, the most important ozone depleting gas in the atmosphere and the third most important greenhouse gas (after CO_2 and methane) with a global warming power (GWP) 300 times that of CO_2.

4. Space, balloon, aircraft and ground based instruments

Most TLE instruments (normal rate (30 frames per second) and high speed cameras, and photometers) based on optical recordings have been specifically designed and used to detect TLEs and to understand their inception mechanisms, propagation dynamics and relationship with lightning. Therefore, the focus was seldom placed on the study of the possible chemical influence of TLEs on the atmosphere.

The detection of optical emissions from TLEs inform about the capacity of TLEs to promote excitation of optically emitting chemical species in the atmosphere. For example, sprite streamers produce significant excitation of N_2(B $^3\prod_g$, v) and N_2(C $^3\prod_u$, v), which radiatively decay emitting red and blue flashes of light, respectively. This suggests that the non-equilibrium electric-field mediated atmospheric chemistry triggered by sprite streamers also produce other excited electronic states of N_2 and O_2 that take longer to produce (or do not produce at all) optical emissions like, for instance, N_2(A $^3\Sigma_u^+$, v), and O_2 (a $^1\Delta_g$, v) and O_2(b $^1\Sigma_g^+$, v), which are metastable species. Consequently, we will restrict this section to those instruments which results could have, in our opinion, implications in the study of the chemical influence of TLEs.

4.1. Space based instruments

An international consortium designed, built and operated during 12 years (2004–2016) the Imager of Sprites and Upper Atmospheric Lightning (ISUAL) instrument on board the FORMOSAT–2 satellite (Chern et al., 2003). ISUAL was composed of a suite of cameras, photometers and spectrophotometers aimed at studying TLEs and their relationship with lightning. Similarly the Japanese Experiment Module – Global LIghtning and sprite MeasurementS (JEM-GLIMS) instrument was on board the ISS and operated in nadir geometry between 2012 and 2015 (Ushio et al., 2011; Sato et al., 2015). JEMS-GLIMS was focused in identifying different types of TLEs with cameras, photometers, very high frequency (VHF) and very low frequency (VLF) radio receivers. In September 2015, the Thor mission on board the ISS took impressive images (see Fig. 17) and videos of the enormous variety of blue luminous events taking place on the cloud tops with a detailed analysis of their frequency, sizes and correlation with nearby occurring regular lightning (Chanrion et al., 2017). There were also other important short period space missions aimed at observing TLEs from space such as the early Lightning and Sprite Observation (LSO) experiment on board the ISS (Blanc et al., 2004; Farges and Blanc, 2016), the sprite observation campaign from the space shuttle during the Mediterranean Israeli dust experiment (MEIDEX) (Yair et al., 2003), and the recording of color images of sprites from the ISS in the framework of the NASA Crew Earth Observation (Jehl et al., 2013) and during the JAXA Cosmic Shore program (Yair et al., 2013).

The Atmosphere Space Interaction Monitor (ASIM) was launched in April 2018 and it is placed on the ISS to study the occurrence of TLEs and Terrestrial Gamma–ray Flashes (TGF) with an optical instrument (so–called MMIA) and a high–energy detector (so–called MXGS). MMIA is composed of two cameras (337 nm and 777.4 nm) and three fast (100 kHz) photometers (180–230 nm, 337 nm, 777.4 nm) (Neubert et al., 2019; Chanrion et al., 2019).

In November 17, 2020 a new research satellite named Tool for the Analysis of Radiation from lightning and Sprites (TARANIS) (Blanc et al., 2007; Lefeuvre et al., 2008) – a nadir-pointing instrument – was launched but suffered a rocket failure and the mission was unfortunately lost. By late November 2020, CNES was reconsidering a new TARANIS-2 mission with similar objectives as TARANIS with reduced costs through the use of spare parts and the expertise acquired by engineers and scientists over many years preparing the mission. TARANIS was designed to investigate TLEs, TGFs and their link using a combination of optical (Farges et al., 2017), high energy photons and electrons, and radio detectors. TARANIS counted with a very complete suite of scientific instruments including two microcameras (762 and 777 nm), four fast (20 kHz) photometers (160–260 nm, 337 ± 5 nm, 762 ± 5 nm and 600–900 nm), a low frequency (LF, from DC to 1 MHz) and high and very high frequency (HF/VHF from 100 kHz to 35 MHz) electric field detectors, magnetic field detectors in VLF (5 Hz to 20 kHz) and mid frequencies (MF, 10 kHz to 1 MHz), detectors for high energy X and gamma photons in the 10 keV – 10 MeV range, and a relativistic electrons and positrons detector in 1–10 MeV range. Finally, TARANIS also included an energetic electron sensor in the 80 keV - 5 MeV range.

Optical emissions are regularly used to detect chemical changes in the atmosphere due to large scale atmospheric phenomena usually exhibiting changes at the time scales of days, weeks, months or seasons. However, conventional limb and/or nadir spectrometers on board low earth orbit satellites have a limited (usually low) time resolution that makes them not very suitable for studying transient atmospheric phenomena occurring in the millisecond time scale. In spite of this some space spectrometers (not specifically designed for the study of TLEs) like MIPAS and GOMOS (see Section 3.1.6) were used in coordination with ground and/or space lightning detectors to search for chemical traces of sprites in the upper atmosphere with unconclusive results (Arnone et al., 2008) or no evidence at all of chemical atmospheric impact of sprites (Rodger et al., 2008). It is very possible that the chemical atmospheric influence of some TLEs (sprites, halos, blue jets) is local (as models predict). However, it could also be possible that some TLEs (sprites and blue jets) have a global chemical influence below the range of detectability of present on orbit spectrometers not developed to extract chemical changes due to transient electrical discharges in the atmosphere. This would require ultrasensitive spectrometers with sufficient time resolution.

The instrument SMILES, an extremely sensitive limb view submillimiter spectrometer with low time resolution, on board the ISS has

recently shown that sprites promote the formation of HO_2 radicals locally and could even contribute to 1% globally (Yamada et al., 2020). Single limb scan HO_2 spectra were observed using SMILES with full local time coverage. The SMILES instrument HO_2 single–scan detection limit was on the order of 1 ppbv in the nighttime mesosphere, which was an order of magnitude better than previous microwave / submillimeter limb instruments (Kikuchi Ki et al., 2010; Baron et al., 2011; Kasai et al., 2013; Kreyling et al., 2013).

4.2. Balloon and aircraft based instruments

In 2015, Croize et al. (2015) published a feasibility study of the HALESIS (High-Altitude Luminous Events Studied by Infrared Spectro–imagery) instrument. The purpose of this instrument would be to measure the atmospheric perturbation in the minutes following the occurrence of TLEs from a stratospheric balloon in the altitude range of 20–40 km. The idea was to show the feasibility of using a infrared spectro-imager in a pointing balloon gondola to detect the local perturbations caused by TLEs on the main vibrational energy level populations of CO_2, CO, NO, O_3 and H_2O. It was concluded that it is necessary to use an instrument with high sensitivity and acquisition frequency.

The first color picture of sprites was recorded from a plane at about 12 km altitude (Sentman et al., 1995). They showed that sprites produce red and blue light emissions. Due to atmospheric absorptiom, blue sprite optical emissions are difficult to detect. They were the first to reveal that different electronic states of molecular nitrogen were involved in sprite optical emissions. From this moment on, several other aircraft campaigns were designed to record sprite spectra at normal and high speed in the blue and near ultraviolet regions (Heavner et al., 2010; Kanmae et al., 2010a, 2010b).

4.3. Ground based instruments

The ground–based instrument, known as Photometric Imaging of Precipitation of Electron Radiation (PIPER), combined high sensitivity (noise level of ~1 R at 100 fps), high time resolution (up to 25,000 fps), and continuous recording (no buffering) with relatively limited spatial resolution (16 × 16 pixels). PIPER was able to simultaneously image at multiple wavelengths using either narrowband optical interference filters or broadband filters (Marshall et al., 2008). PIPER consisted of four 16 – channel multianode Photomultiplier tube (PMT) arrays combined in pairs responding from 185 nm to 900 nm and filtered with different optical filters to cover optical emissions from TLEs or other atmospheric phenomena such as airglow or electron precipitation. PIPER was in used since January 2006. The relatively wide spatial resolution provided by the 18 × 18 degree field of view of PIPER could contribute with valuable information to evaluate the extension of the chemical influence of certain TLEs. However, the limited spatial resolution of its predecessor, an array of horizontally spaced photometers named Fly's Eye (sensitive in the range 185 nm to 800 nm), had in our opinion less chemical-related implications though it served to confirm the radial expandion of elves and lightning produced electromagnetic pulses as the driving mechanism (Inan et al., 1997).

Finally, the ground-based instrument GRAnada Sprite Spectrograph and Polarimeter (GRASSP) was specifically designed for systematic TLE (not only sprites) remote imaging and spectroscopy with spectral resolution of 0.25 nm and a variable spectral range from 400 nm to 900 nm (Passas et al., 2016b). GRASSP has been in operation since 2012 in Europe where different imaging and spectroscopy TLE campaigns have been run (Mende et al., 1995; Hampton et al., 1996; Kanmae et al., 2007). More details about spectroscopic studies of TLEs are discussed in Section 3.1.7.

5. Challenges in the microphysical modeling

In this section we describe details about what we consider challenges in the microphysical modeling of some TLEs. This topic is somehow connected to the atmospheric chemical effects of TLEs (already discussed in a previous sections) but it has its own peculiarities and it deserves a section apart to develop four points (described below) that are relevant and that we consider should be further investigated in the future.

5.1. Modeling the full chemical influence of halos in the atmosphere

Halos are upper–mesospheric glow discharges triggered by the quasi-electrostatic field produced by lightning strokes (Barrington-Leigh et al., 2001). The most realistic models of halos are cylindrically symmetrical density models for electron transport in the mesosphere and lower ionosphere. The quasi–electrostatic field that triggers the inception of the halo is computed from the electric charge accumulated by lightning strokes under statistic assumptions using the quasi–static approximations of Maxwell's equation (Pérez-Invernón et al., 2016). In this type of model, the electrodynamical equations are coupled with a set of chemical reactions to calculate the temporal evolution of some chemical species.

The minimal chemical scheme that is necessary to self–consistently simulate a halo includes impact ionization, dissociative attachment and associative detachment. However, other chemical processes, such as impact excitation, electronic quenching and radiative decay are necessary to estimate the optical emissions of halos. The production of ions and electronically excited molecules in the mesosphere triggers a cascade of chemical reactions that, ultimately, leads to a local increase in the concentration of some atmospheric chemical species, such as NO_x and N_2O. As a consequence, it is necessary to include a consistent set of chemical reactions that describes the evolution of all the species involved in the cascade of chemical reactions produced in the halo.

Current models of halos are capable of self–consistently simulate the complete evolution and chemical impact of halos triggered by low Charge Moment Change (CMC) strokes ($\leq$ 200 C km) that do not produce ionization in the mesosphere, dissapearing about 4 ms after the onset of the halo. However, for higher CMCs the models predict a long-lasting halo (tens of milliseconds (Pérez-Invernón et al., 2018a) that is in disagreement with observations Marshall and Inan (2006); Kuo et al. (2013). This limitation is closely related with the different spatial resolutions that are necessary to simulate the inception of the halo (scale of hundreds of kilometers) and its full descent through the mesosphere (scales of meters) (Luque and Ebert, 2009; Pérez-Invernón et al., 2018a).

Strokes with CMCs larger than ~200 C km produce a descending screening–ionization wave in the halo. The ionization wave sharpens during its descent, until it reaches the width of the simulation domain cells and collapse (Pérez-Invernón et al., 2018b) (see Fig. 20). Luque and Ebert (2009) modeled the inception of sprite streamers from the sharpening screening-ionization wave of a halo. Qin and Pasko (2015) demonstrated that pre-existing plasma irregularities in the D – region ionosphere are associated with the inception of sprite–streamers from the screening–ionization wave produced in halos. Although halo models can reproduce the sharpening of the screening–ionization wave, the simulation is no longer self–consistent after the screening-ionization wave collapses or triggers the inception of sprite streamers.

5.2. Interacting sprite streamers

Sprites are formed by fast–propagating bright plasma filaments known as streamers traveling between 40 km and 90 km altitude (Pasko et al., 1998). They are followed by long-standing (1–100 milliseconds) luminous structures called beads and glows (McHarg et al., 2007).

As we mentioned before, sprites are triggered as a consequence of the quasi–electrostatic electric field produced by a lightning discharge and

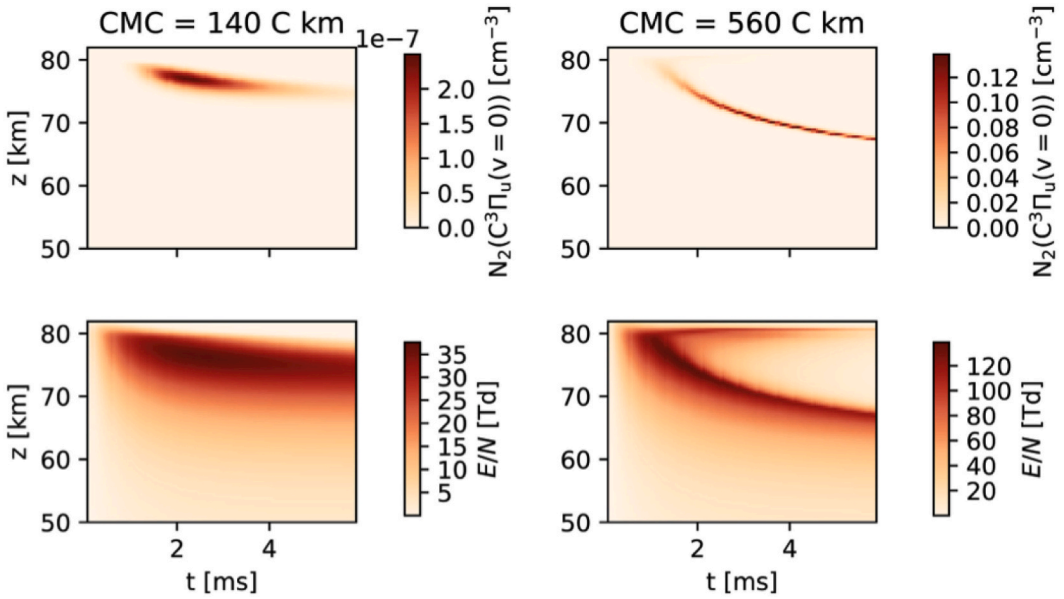

Fig. 20. Predicted temporal evolution of the density of the emitting species N_2 ($C\ ^3\prod_u$ (v = 0)) (top panels) and the reduced electric field (bottom panels) in a halo produced above lightning. Panels in the first and second columns correspond to two different lightning discharges with charge moment changes of 140 and 560 C km, respectively. Image reproduced from Pérez-Invernón et al. (2018a).

pre-existing plasma irregularities in the D region of the ionosphere. Sprites emerge as one or several streamer(s) traveling downward. During their descent, streamers branch and interact through electrostatic effects. The high value of the peak reduced electric field (hundreds of Townsends) in the streamer tip and channel liberate and accelerate large quantities of electrons, producing local enhancements of some chemical species and fast (millisecond) optical emissions.

After the passage of the streamer tip or head through a column of air, the electric current flowing through the streamer channel tends to be homogeneous (Luque et al., 2016). However, as demonstrated by Luque et al. (2016), the temporal evolution of the electric field in different points of the streamer channel can be different, leading to intricate patterns of alternating bright and dark regions within a channel.

The long–lasting, localized spots of optical emissions that appear in the streamer channel are known as glows and beads (Luque and Ebert, 2010; Liu, 2010). As proposed by Luque et al. (2016), the attachment instability can explain the inception of glows and beads. The attachment instability contributes to a decrease in the conductivity of the streamer channel and an increase in the value of the electric field, leading to a production of optical emissions and chemical species. Furthermore, as demonstrated by Malagón-Romero et al. (2020), the attachment instability can also produce the launch of negative streamers from sprite glows (see Fig. 21), as observationally reported by several researchers (McHarg et al., 2007).

The high peak reduced electric field in the streamer heads produce a high rate of ionization and excitation of molecules and atoms by electron impact. In particular, streamer heads produce a large increase of electronically and vibrationally excited states of N_2 and N, a high concentration of O^- and an enhancement in the density of O and N with respect to background values. After the passage of the streamer head, these chemical species participate in cascades of chemical reactions that lead to a production of NO, N_2O and other excited states of O, such as $O(^1S)$. Simultaneously with the development of the streamer head, the long lasting (ten to hundred milliseconds) high electric field produced by the attachment instability in glows and beads contributes to the production of chemical species. The production of O^- by attachment of electrons to molecular oxygen leads to a significant density enhancement of N_2O, while chemical reactions involving molecular oxygen and electronically excited states of N contributes to the production of NO molecules.

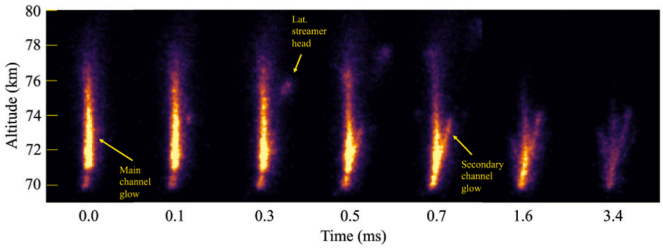

Fig. 21. Time series from high-speed video observations of a sprite showing the emergence of an upward streamer from a glowing sprite segment. Also shown is the propagation and the optical extinction of the glow. The time origin was set in the first frame prior to the launch of the upward streamer. To emphasize the main milestones of the evolution, intervals between the snapshots are not uniform. This event occurred on 5 July 2011 at 08:54:14 UTC and was associated with a large thunderstorm complex over north eastern South Dakota, USA. The event was observed with a Phantom high-speed imager recording at 10000 frames per second on board an aircraft flying at 14.4 km altitude over south-eastern South Dakota about 180 km north of the storm. Image reproduced from Malagón-Romero et al. (2020).

In 2008, four independent novel 0D chemical models of sprite streamers significantly contributed to our understanding of the chemical influence and optical emissions of sprite streamers (Enell et al., 2008; Hiraki et al., 2008; Sentman et al., 2008b; Gordillo-Vázquez, 2008). The models of Sentman et al. (2008b) and Gordillo-Vázquez (2008) imposed the temporal evolution of the electric field in a point of space affected by the passage of a streamer head. Gordillo-Vázquez (2010) reported an extended chemical scheme including a detailed vibrational kinetic model of air plasma produced by sprites. In 2015, Parra-Rojas et al. (2015) developed a 1D self–consistent model of a single sprite streamer in the mesosphere including the temporal evolution of the conductivity in the streamer channel and the current density in the parent-lightning based on previous studies (Luque and Gordillo-Vázquez, 2011a). Both 0D and 1D models of sprite streamers are useful to predict the long–term temporal evolution of the chemical influence of streamer heads at different altitudes. However, these models are limited to simulate the temporal evolution of the concentration of chemical species in the center of streamer heads and do not have the ability to estimate the radius of

streamers or the inception of glows and beads.

Modeling the high complexity of a complete sprite composed by tens to thousand interacting streamer heads and streamer channels and their chemical influence in the atmosphere is far beyond current computational capabilities. Simultaneously with the improvement of chemical models of sprite streamer, several authors reported self-consistent models of sprites streamers. Most of current streamer models are plasma fluid type including transport of electrically charged particles and chemical reactions ((Bagheri et al. (2018) and references herein). These streamer models are successful in the simulation of the first milliseconds of streamers and the inception of glows and beads in the streamer channel (Celestin and Pasko, 2010; Luque et al., 2016; Malagón-Romero et al., 2019). Some 3D models of streamers are able to simulate the inception, propagation and interaction of two or three streamers (Teunissen and Ebert, 2017). However, current microphysical models of streamers are not able to simulate the high complexity of systems of streamers or coronas. Some authors have reported simplified models of several interacting streamers or coronas (Naidis, 1996; Akyuz et al., 2003; Luque and Ebert, 2014; Ihaddadene and Celestin, 2015; Luque et al., 2017). However, these mesoscale physical models do not allow (as they are presently designed) the computation of the chemical influence of streamers in the atmosphere.

5.3. Possible mesospheric source of N_2O due to sprite streamers

Recently, Pérez-Invernón et al. (2020) reported a self-consistent 2D sprite streamer model coupled with the kinetic scheme proposed by Gordillo-Váquez (2008) and extended with vibrational kinetics (Gordillo-Vázquez, 2010) and additional water cluster reactions (Luque et al., 2017). The simulations provided the full chemical influence of one streamer head during about 1 millisecond after its onset. They reported a significant enhancement in the concentration of NO and N_2O molecules in the mesosphere–lower thermosphere (67 km – 74 km) due to the influence of the streamer head and an emerging glow. According to their results, the chemical effect of sprites seems to be not enough to explain the disagreement between the concentration of N_2O in the 60 km – 80 km region of the mesosphere-lower thermosphere over mid and low latitudes measured by ACE-FTS (Sheese et al., 2016) (see Fig. 22) and simulations with general circulation models (Kelly et al., 2018). Inspection of the ACE-FTS N_2O satellite plots shows patchy regions of N_2O throughout the midlatitude and low-latitude mesosphere, which are not reproduced by general circulation models like WACCM (Kelly et al., 2018). Instead, a smooth N_2O distribution is simulated across all latitudes over the whole year. According to Sheese et al. (2016) the patchiness could be attributed to sampling frequency, as there are typically over a factor of 10 fewer occultations at lower latitudes (as the majority of ACE-FTS measurements are made at high latitudes), combined with a weaker signal at high altitude. The majority of stratospheric enhancements can be attributed to surface sources distributed via the Brewer-Dobson circulation. In contrast, N_2O above the stratopause is produced in situ via reactions $N_2(A\,^3\Sigma_u^+) + O_2 \rightarrow N_2O + O$ and $N(^4S) + NO_2 \rightarrow N_2O + O$. The latter reaction involving $N(^4S)$ appears to be less important than previously suggested (Funke et al., 2008; Semeniuk et al., 2008), contributing to no more than 20% of the overall N_2O simulated at any altitude or latitude band in WACCM (Kelly et al., 2018). The only region showing obvious disagreement between ACE-FTS measurements and global model predictions is the mesosphere between 60 and 80 km, particularly over midlatitudes and low latitudes, where less N_2O is simulated than observed (Kelly et al., 2018).

Finally, it also must be said that present microphysical computational capabilities do not allow more extensive spatio–temporal simulations with present 2D sprite streamer models (that self–consistently couple the electrodynamics with full air kinetic schemes including electronic and vibrational nonequilibrium chemistry). Further simulations are clearly needed. Future improvements in computing resources will enable the community to expand self–consistent simulations of a number of interacting sprite streamers, allowing the full simulation of the temporal production of chemical species by glows in the mesosphere-lower thermosphere and finally allowing the simulation of an increasing number of streamers interacting and producing chemical species. The first approach would be to try to carry out longer (than 1 ms) self-consistent simulations of one sprite streamer at altitudes closer to the lower mesosphere (60 km).

5.4. Blue starters and jets: Corona discharges and streamer to leader transition

Upward propagating blue jets are triggered by the electrical breakdown produced between the storm upper charge layer and the screening charge attracted to the cloud top (Krehbiel et al., 2008). Chou et al. (2018) and Liu et al. (2018) reported simultaneous optical and sferic measurements from blue starters and blue jets, providing evidence that blue starters are formed by streamer coronas triggered by fast positive breakdown from the cloud tops.

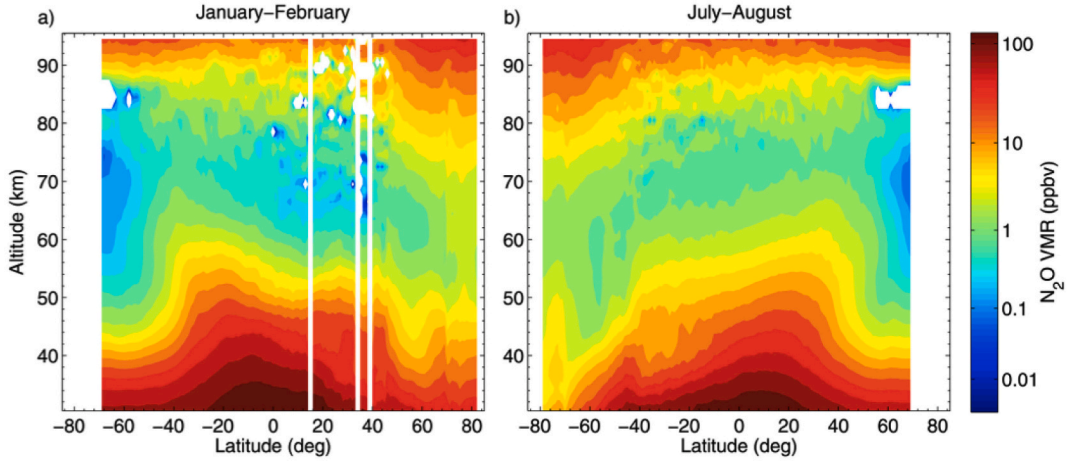

Fig. 22. The 2004–2013 Atmospheric Chemical Experiment - Fourier Transform Spectrograph (ACE-FTS) N_2O volume mixing ratio climatology for (a) January-February and (b) July-August. Values are smoothed. Note that the color scale is logarithmic, white vertical bands represent latitudes that were not sampled, and white regions indicate negative mean values. Inspection of these satellite plots shows patchy regions of N_2O throughout the midlatitude and low-latitude mesosphere, which are not reproduced by general circulation models like WACCM (Kelly et al., 2018). Instead, a smooth N_2O distribution is simulated across all latitudes over the whole year. Image reproduced from Sheese et al. (2016).

Some blue starters can evolve and form a blue jet (Chanrion et al., 2017; Chou et al., 2018; Liu et al., 2018), which is a leader channel surrounded by a streamer corona traveling between ~16 km and ~ 40 km height. The inception of a leader from a streamer corona is known as streamer to leader transition. This transition is produced when the electrical current in the streamer corona heats the air, increasing the temperature some thousands of Kelvin. As a consequence of the increase in the temperature, the low conductive cold plasma that forms the streamer corona transforms into a high conductive hot plasma, triggering the advance of a bi–leader. The upper leader tip travels upwards guided by the streamer corona and heat the air. The production of chemical species turns from being governed by the electric field in the streamer corona to being determined by the high temperature in the leader channel.

Microphysical modeling of blue starters and blue jets is still a challenge for the scientific community. As mentioned before, the high complexity of a system formed by a high number of interacting streamers prevents the self-consistent modeling of corona discharges. In the case of blue jets, the problem of modeling the streamer to leader transition also arises as a main challenge. Some steps have been taken in this direction. Aleksandrov et al. (2001) proposed a simplified model to study some of the characteristic of the streamer to leader transition based on electrostatic assumptions. da Silva and Pasko (2013) reported a 1D radial model to study the scaling of the streamer to leader transition with air density based on an assumed electrical current passing through the simulated section of the channel. They showed the importance of the fast gas heating mechanism and the vibration–dissociation–vibration coupling in the development of a leader from a corona. The model was used to investigate the scaling of the streamer to leader transition time and leader speed with altitude for different electric currents. Malagoán-Romero and Luque (2019) developed a self–consistent 2D cylindrically symmetric model to study the emergence of space stems ahead of negative leaders. The model provided evidence that the attachment instability could play an important role in the streamer to leader transition. However, despite the advances in the modeling of corona discharges and the streamer to leader transition, modeling the high complexity of the microphysical processes involved in these electrical phenomena is still a physics and computational challenge.

The lack of self–consistent microphysical and chemical models of blue starters and blue jets consequently prevents the determination of their chemical influence in the stratosphere. Winkler and Notholt (2015) reported a 0D model of blue jets. These authors proposed a set of chemical reactions coupling chemical processes driven by the electric field during the streamer phase with chemical processes driven by the temperature in the leader phase. They performed two separate simulations to account for the chemical influence of streamers and leaders. In the case of streamers, they assumed the temporal evolution of the electric field in the streamer channel, while in the case of the leader they imposed the temporal evolution of the temperature at different altitudes as reported by da Silva and Pasko (2013). Winkler and Notholt (2015) obtained a significant enhancement in the density of ozone and NO in the center of streamers and a significant enhancement in the concentration of NO and N_2O in the center of the leader. In addition, they reported a depletion in the local concentration of ozone after the passage of the leader. Recently, Xu et al. (2020) developed a 0D model of streamers in blue jets using a different temporal evolution of the electric field than Winkler and Notholt (2015), obtaining an slightly higher enhancement of NO and ozone. These results suggest that blue starters and blue jets could have a non–negligible influence in the chemistry of the stratosphere.

Ripoll et al. (2014b,a) reported a 2D model of return strokes at low (8 km altitude) and atmospheric (0 km altitude) pressures coupled with an extensive set of chemical reactions. These authors did not simulate the leader phase of blue jets. However, the similarities between the leader phase of blue jets and lightning discharges allow us to compare their results with the model of Winkler and Notholt (2015). Ripoll et al. (2014b) obtained a higher increase of NO_x molecules than N_2O molecules in lightning channel, while Winkler and Notholt (2015) (see Fig. 16) reported a higher increased in the concentration of N_2O molecules than NO_x molecules in blue jets. This apparent disagreement could be due to the use of different reaction rates for the main chemical process producing N_2O in hot air plasma ($N_2 + O_2 \rightarrow N_2O + O$). Winkler and Notholt (2015) used the reaction rate reported by Krivonosova et al. (1987), that is about one order of magnitude larger than the reaction rate used by Ripoll et al. (2014b,a) and reported by Garvin (1974).

Future advances in computational resources will enable us to improve microphysical models of coronas and streamer to leader transition. These advances will provide new methods to develop more reliable simulations of the chemical influence of blue starters and blue jets in the atmosphere. Regarding the chemical processes involved in the production of N_2O, NO_x and other chemical species, more laboratory and in–situ measurements are needed to get a better understanding of the chemical reactions that influence the production of chemical species in coronas and hot plasma. SImultaneously, detailed models should be validated and verified (against chemical measurements).

6. Global modeling

Lightning discharges contribute to about 10–15% of the production of NO_x in the troposphere (Schumann and Huntrieser, 2007) and plays an important role in the concentration of ozone and other chemical species in the upper troposphere (Grewe, 2007; Gordillo-Vázquez et al., 2019). Vigorous convection in lightning-producing thunderstorms can also contribute to the injection of lightning–produced NO_x in the stratosphere. It is currently accepted that lightning discharges can produce between 2 and 8 Tg N per year globally (Schumann and Huntrieser, 2007).

Despite significant advances during the last two decades, reducing the uncertainty of the chemical impact of lightning discharges in the atmosphere is still a challenge. Aircraft and satellite measurements have significantly contributed to set the role of lightning discharges in the chemistry of the atmosphere (Huntrieser et al., 2016; Pickering et al., 2016). However, current limitation of satellite measurements in the upper troposphere together with the high variability in the production of NO_x among thunderstorms (Bucsela et al., 2019) introduce large uncertainties in the determination of the amount of NO_x produced per flash.

Measuring the chemical impact of TLEs in the stratosphere and mesosphere poses an even greater challenge (see Section 3). For instance, Arnone et al. (2008) reported a local enhancement of about 1 ppbv (10% above the background value) in the concentration of NO_2 at 52 km height in a 500 km wide horizontal region in coincidence with lightning activity 60 min before.

Recently, Yamada et al. (2020) combined optical measurements of three sprites reported by ISUAL together with spectra reported by SMILES and centered at the 649.701 GHz transition line of HO_2. The measurements showed a local enhancement in the background concentration of HO_2 in the interval of altitudes between 75 and 80 km of about 10^{25} molecules due to the occurrence of one or several sprites. These results suggest that sprites could contribute to about 1% of the total nighttime concentration of HO_2 at 75–80 km height globally. However, these results are not reproduced by current local chemical models of sprites.

General Circulation Models (GCM) coupled with chemistry models (or simply Earth System Models (ESM)) with parameterized convection have been proven to be a powerful tool to investigate the role of lightning discharges in the chemistry of the atmosphere. The occurrence of lightning discharges is introduced in ESMs as sub – grid phemonema using meteorological variables as proxies (Price and Rind, 1992), while the injection of NO_x by lightning is parameterized using a prescribed number of NO_x molecules produced per flash discharge (Tost et al. (2007); Murray (2016); Gordillo-Vázquez et al. (2019) and references

herein). Some authors have followed this approach to investigate the role of sprites and blue jets in the chemistry of the atmosphere using ESMs (Arnone et al., 2014; Pérez-Invernón et al., 2019). However this approach would ideally require accurate microphysical modeling able to realisticaly predict the local chemical impact of sprites, blue jets and blue starters.

6.1. Global modeling of sprite chemical impact

In 2014, Arnone et al. (2014) developed the first sprite–NO_x parameterization and implemented it in the Whole Atmosphere Community Climate Model (WACCM). The occurrence rate of sprites in the model was prescribed in 2–3 sprites per minute globally, in agreement with estimations based on observed climatology of sprites (Sato and Fukunishi, 2003; Ignaccolo et al., 2006; Chen et al., 2008). In order to satisfy the rate of 2–3 sprites per minute globally and the observed geographical distribution of sprites, Arnone et al. (2014) introduced the occurrence of sprites in the model as one sprite per 1000 lightning flashes. As discussed before, estimations on the total number of NO_x molecules produced by sprites is limited due to the lack of microphysical models to simulate the complete evolution of sprites. The parameterization reported by Arnone et al. (2014) calculates the injection of NO_x by sprites based on vertical profiles from the 0D chemical model by Enell et al. (2008), who reported a NO_x density enhancement in the center of sprite streamers at different altitudes. They assumed different scenarios to extrapolate their results to a complete sprite event based on a filling factor, which depends on the total area filled by streamers. They estimated the climate chemistry sensitivity to sprite–NO_x using the largest typical and the maximal injection of NO_x by single sprites reported by Enell et al. (2008). The simulations in WACCM4 showed a global perturbation of tropical NO_x at 70 km height due to sprites between 0.015 ppbv (buried in the background variability) and 0.15 ppbv (about 20% of the background value).

The parameterization developed by Arnone et al. (2014) was a significant advance in the estimation of the global chemical impact of TLEs regarding NO_x. Even today, it is the only sprite parameterization in global models. However, there are still different approaches that could be carried out to improve it.

The occurrence of sprites in the model introduced by the parameterization of Arnone et al. (2014) is not coupled to the meteorological conditions that favor their inception (Lang et al., 2016). Sprites are triggered by high CMC strokes frequently followed by a long continuing current phase (Reising et al., 1996) that can be detected using Extremely Low Frequency (ELF) and optical measurements (Adachi et al., 2009; Bitzer, 2017). For instance, Sato and Fukunishi (2003) estimated locations and rates of sprite occurrences (720 events per day or 1 every two minutes) on average on a global scale using 1–100 Hz ELF magnetic field waveform data obtained at Syowa station in Antarctica and Onagawa observatory in Japan, and the empirical sprite initiation probability reported by Hu et al. (2002). Additionally, a parameterization of sprites based on the meteorological conditions that favor the occurrence of long continuing current lightning (lasting more than 10 ms) could provide information about possible changes in the occurrence rate of sprites in a changing climate. Bitzer (2017) provided the first tropical and equatorial climatology of long continuing current lightning using the lightning measurements provided by the Lightning Imaging Sensor (LIS) on board the Tropical Rainfall Measuring Mission (TRMM). The analysis of this climatology together with the future long continuing current lightning climatology provided by optical measurements of the Geostationary Lightning Mapper (GLM) over the Americas since 2016, and by the Lightning Imager (LI) on board the future (2022/23) Meteosat Third Generation (MTG) satellite over Europe and Africa will provide new information about the relationships between long continuing current lightning and meteorological variables (Grandell et al., 2009). In addition, the ASIM space mission, equipped with instruments that can detect the optical signature of lightning flashes and different types of TLEs including sprites, can contribute to advance our knowledge about the influence of the continuing current in the discharge and the production of sprites. Future climatology of sprites provided by space-based instruments together with upgraded climatologies provided by ground-based measurements (Arnone et al., 2020) will also advance our knowledge on the global occurrence rate and geographical distribution of sprites worldwide.

Several authors have reported a possible increase in the density of N_2O by sprites based on modeling results (Gordillo-Vázquez, 2008; Parra-Rojas et al., 2015; Pérez-Invernón et al., 2020), as well as a possible production of HO_2 based on space-based chemical measurements (Yamada et al., 2020). The parameterization of Arnone et al. (2014) is limited to the production of NO_x by sprites. Future improvements in the parameterization of sprites introducing sprite–N_2O and sprite–HO_2 could be useful to estimate the chemical influence of this type of TLE in other chemical species. In addition, some authors have demonstrated the role of the streamer trailing glow in the production of chemical species by sprites (e.g., Pérez-Invernón et al. (2020)), showing that further advances in local models of the chemical influence of streamers are still needed to estimate the total number of NO_x, N_2O and other (HO_2, …) molecules produced by sprites.

6.2. Global modeling of blue luminous events

Recently, Chen et al. (2019) reported an updated climatology of TLEs observed by ISUAL from space during its 12 – year mission. ISUAL reported the occurrence of 2626 sprites and 5876 blue luminous events (blue jets/starters), showing that blue luminous events could be the second most frequent type of TLE after elves. According to these measurements, the global occurrence rate of these events would be about 1–2 blue luminous events per minute globally.

In 2019, Pérez-Invernón et al. (2019) developed the first parameterization of blue jets in WACCM4 (see Fig. 23). The parameterization assumed that blue jets occur in thunderclouds that are close to the tropopause. This approach is based on the physical mechanism for the inception of blue jets reported by Krehbiel et al. (2008), who proposed that blue jets escape from thunderstorm when the mixing of the screening charge is low. Pérez-Invernón et al. (2019) set different scenarios for the global occurrence rate of blue jets. On the one hand, they performed simulations assuming prescribed global occurrence rates of blue jets of 0.01 and 1 events per minute. On the other hand, Pérez-Invernón et al. (2019) calculated the global occurrence rate of blue jets assuming that all lightning taking place in thunderstorms whose cloud top is close to the tropopause and with a peak electric current above a given threshold is followed by a blue jet, as the case of the blue jet observed by Chanrion et al. (2017) from the International Space Station (ISS). Pérez-Invernón et al. (2019) assumed that the peak current threshold of the lightning discharge preceding a blue jet is between 60 and 167.5 kA. Following the global distribution of lightning peak currents reported by Said et al. (2013), about 1% of lightning discharges have a peak current above 100 kA and only 0.1% have a peak current above 150 kA. Using this parameterization, Pérez-Invernón et al. (2019) obtained a global occurrence rate of blue jets between 0.14 and 7.2 events per minute.

Pérez-Invernón et al. (2019) assumed different radius of the leader phase and the area covered by streamers in order to calculate the total injection of NO, N_2O and O molecules from the density enhancements in the center of blue jets reported by Winkler and Notholt (2015). According to the more realistic scenarios, Pérez-Invernón et al. (2019) reported that blue jets could inject between 10^{-4} and 7.6 Tg N_2O – N per year into the stratosphere. The average value 3.8 Tg N_2O – N per year corresponds to about 38% of natural sources of N_2O. Simulations in WACCM4 showed that this possible injection of N_2O by blue jets could account for a maximum decrease of ozone in the stratosphere of about 5% in equatorial and polar regions (see Fig. 24). In addition, Pérez-Invernón et al. (2019) reported that blue jets could account for up to 1%

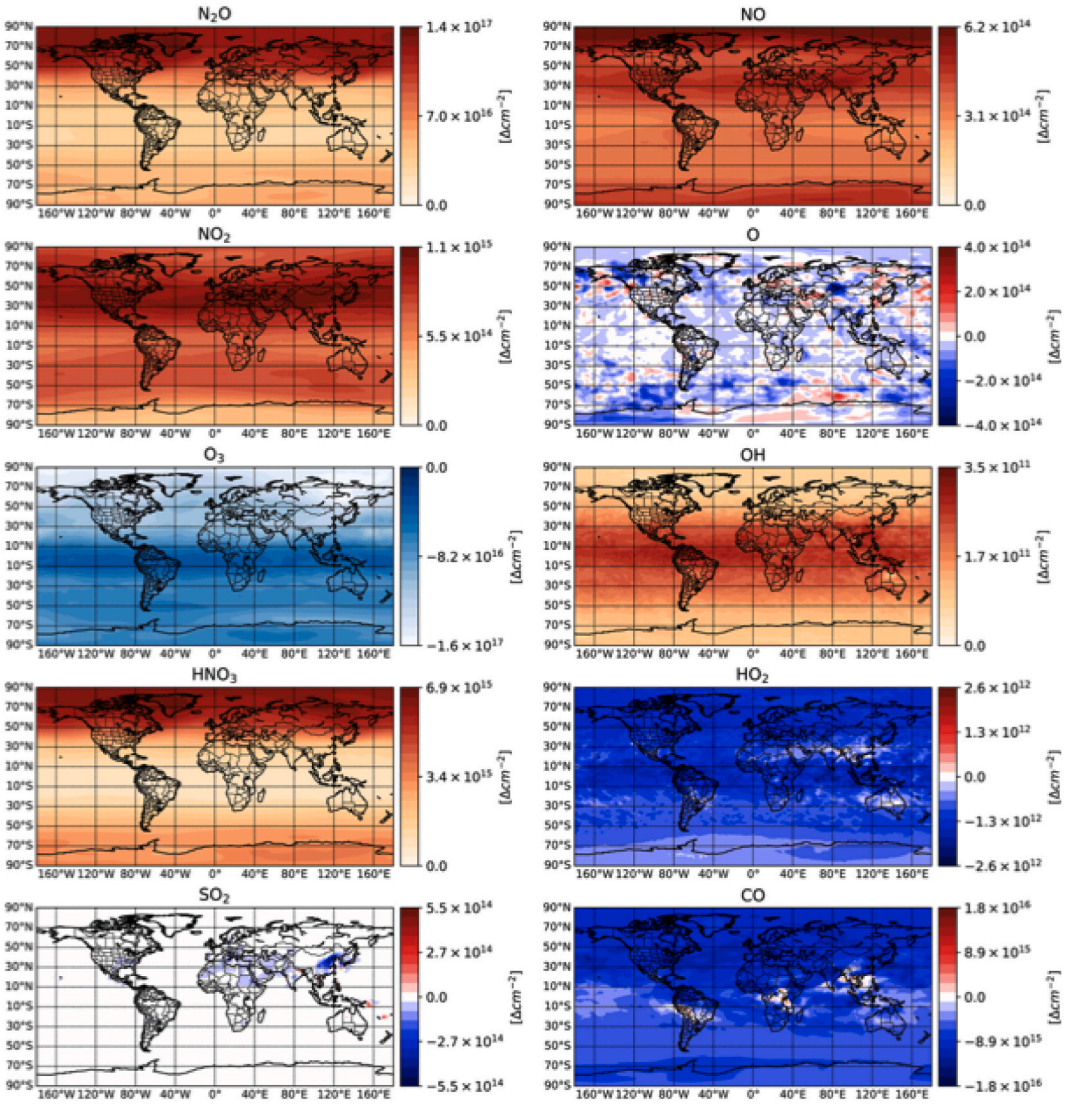

Fig. 23. Differences in the annual average total column density (up to 75 km altitude) of N_2O, NO, NO_2, O, O_3, OH, HNO_3, HO_2, SO_2 and CO between two WACCM4 simulations of 10 years with and without Blue Jets. Positive values correspond to enhancement in densities due to Blue Jets, while negative variations represent density decrease produced by Blue Jets. Image reproduced from Pérez-Invernón et al. (2019).

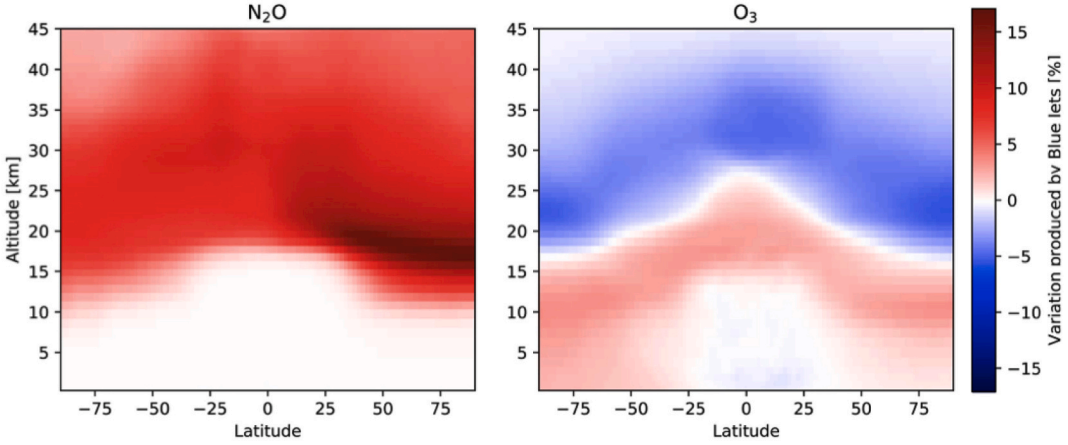

Fig. 24. Latitude-altitude distribution of the differences in the annual average density profile of N_2O and O_3 between two WACCM4 simulations of 10 years with and without Blue Jets. These variations are longitudinally average. Note that N_2O enhancement is very visible in mid and high latitudes of the northern hemisphere. Ozone is predicted to decrease by about 5% above 15 km altitude in high latitudes, and above 20 km and 25 km in mid and tropical latitudes, respectively. Image reproduced from Pérez-Invernón et al. (2019).

of the atmospheric production of NO_x.

The new climatology of blue luminous events reported by Chen et al. (2019) together with the blue jet parameterization developed by Pérez-Invernón et al. (2019) suggest that blue starters/jets could play a non –negligible role in the chemistry of the atmosphere. However, the parameterization of blue jets developed by Pérez-Invernón et al. (2019) and their results on the chemical role of blue jets at a global scale are influenced by several sources of uncertainty. Blue jets are formed by a leader surrounded by streamers, while blue starters are composed by streamer coronas (Chanrion et al., 2017; Chou et al., 2018; Liu et al., 2018). However, the climatology of blue luminous events provided by ISUAL does not distinguish between blue starters and blue jets. As reported by Winkler and Notholt (2015), the leader phase produced a significant enhancement in the density of N_2O that is not present in the streamer phase (though the production of N_2O by blue jet streamers was underestimated in Winkler and Notholt (2015)). Therefore, the ratio of blue starters to blue jets could significantly affect the influence of blue luminous events in the chemistry of the stratosphere. The possible future climatology of blue luminous events provided by JEM-GLIMS and ASIM could enable the scientific community to improve global parameterizations of blue luminous events in global models.

As discussed before, modeling the complete evolution of blue starters and blue jets is still a challenge. Future advances in microphysical models of coronas and streamer to leader transition will provide more reliable results on the production of chemical species in the upper–troposphere and stratosphere by blue starters and blue jets. In addition, future airborne in–situ measurements of the concentration of NO_x, N_2O, ozone and other chemical species in the upper troposphere near thunderstorms could contribute to establish new constrains on their role in the chemistry of the atmosphere.

7. Conclusions and future directions

In this paper, we have given an overview of a body of work carried out over the last 30 years aiming at understanding the atmospheric chemical impact of TLEs. This is, however, tightly linked to our present understanding of the intrinsic nature of TLEs, their inception and time propagation dynamics as well as the their global occurrence rate in the atmosphere. For the latter we only started to have some information in 2008 after the first global surveys of TLEs were published with ISUAL data. Most efforts until now have been oriented towards modeling the expected chemical fingerprints of elves, halos and sprites in the mesosphere, and blue jets and starters in the lower stratosphere and upper troposphere region. The different known TLEs are all connected with the electrical activity in thunderclouds. In particular the quasi–electrostatic and radiation electric fields associated with lightning are responsable of the generation of sprites and halos, and elves, respectively. While elves and halos exhibit a glow-like appearance, sprites combine an upper (above 75–80 km) glowing region with a lower (below 80–75 km) region where extremely complex filamentary structures are formed by many streamers that can branch and interact among them and, depending on the type of sprite, can propagate upwards, downwards or in both directions at the same time.

Energetic electrons generated under the action of electric fields leading to elves, halos and sprites generate locally significant amounts of ground state nitrogen and metastable molecular species such as $N_2(A^3\Sigma_u^+)$. These species and specifically N_2 $(A^3\Sigma_u^+)$ could contribute to the minor high altitude production source of nitrous oxide (N_2O) recently observed by the Atmospheric Chemistry Experiment-Fourier Transform Spectrometer (ACE–FTS) in the mesosphere lower thermosphere (MLT) between 60 km and 80 km and not yet explained by the global atmospheric simulations (Sheese et al., 2016; Kelly et al., 2018). According to recent results the mesospheric N_2O source is due to electron energy precipitation (EEP) near the poles, whereas photoelectrons are most significant in the extrapolar regions, contributing twice as much as EEP to the global N_2O budget (Kelly et al., 2018). A recent work by Pérez-Invernón et al. (2020) has explored the possible connection between mesospheric sprite N_2O production and the layer of enhanced N_2O in the MLT. Self-consistent electrodynamic and kinetic sprite streamer simulations up to 0.85 ms (and between ~74 km and ~ 69 km) indicate that the injection of N and N_2O per sprite streamer in the MLT over mid and low latitudes are about 10^{21} and 10^{18} atoms and molecules, respectively. These values do not seem to be yet enough to account for the discrepancy between satellite observations and simulations in mid and low latitudes (Kelly et al., 2018; Pérez-Invernón et al., 2020). Longer (tens of miliseconds) and at lower altitude in the mesosphere self–consistent sprite streamer kinetic simulations would be needed to fully discard sprites as a contributor to the MLT layer of enhanced N_2O. Longer sprite streamer simulations are important because the streamer trailing glows have been observed to last up to 100 milliseconds due to the existence of a relatively high electric field of about 100 Td (close to the conventional breakdown field) that also keeps active the chemical activity of the sprite streamer trailing glow region. While the chemical reactivity of the sprite streamer head is presently well described and understood, it is not the same with the trailing glow region of sprite streamers that remains an open question (Luque et al., 2016). As we mention in this review, it is not yet clear what chemical reactions (that should include electron detachment) maintain the sprite trailing glow electric field for tens of milliseconds (Luque et al., 2016).

The chemistry of the atmospheric electrical activity occurring in the stratosphere and upper troposphere (blue jets and blue starters) and inside thunderclouds (corona discharges) is presently far from being understood. Blue jets combine the hot chemistry of an upward leader with the (cold) nonequilibrium chemistry of streamers. Blue starters seem to be almost completely formed by streamers and, consequently, the understanding of blue starters chemical output is linked with our current knowledge of streamer physics and chemical reactivity. Finally, the contribution of cloud corona discharges formed by streamers to the atmospheric chemistry has been suspected for a long time but global quantitative determination has not yet been fully investigated. Blue jets, starters and incloud corona discharges are difficult to observe from the ground since they occur close to the thundercloud tops (blue jets and starters) and inside them (cloud corona discharges). For discharges fully composed by streamers like blue starters and cloud coronas we consider that a four action approach is needed in the future for quantifying their atmospheric chemical contribution: First, detailed self–consistent modeling linking streamer electrodynamics and chemical reactivity. Second, controled laboratory experiments to calibrate microphysical models against accurate chemical and optical laboratory measurements. Third, appropriate space missions to determine global occurrence rate. Four, development of appropriate parameterization of blue starters and cloud corona discharges (based on steps one, two and three) and implementation in general atmospheric chemistry circulation model to predict possible global chemical contribution.

The study of blue jets is even more complex because it requires new type of models (not yet available) where the streamer to leader transition naturally emerges and fully coupling electrodynamics and chemical reactivity involving hot chemistry for blue jet leaders and cold (nonequilibrium) chemistry driven by blue jet streamers.

There are still a considerable amount of research needed to fully accomplish the true impact of sprites, blue jets, starters and cloud corona discharges in the chemistry of the atmosphere. The ASIM space research mission and other prospective space missions in the near future with a focus on the chemistry of atmospheric electricity phenomena could contribute to widen our understanding of the chemical contribution of TLEs and corona discharges in thunderclouds.

Credit author statement

Francisco J. Gordillo-Vázquez: Conceptualization, Methodology, Writing - Original and Final draft preparation, Reviewing and Editing, Supervision, Figure Selection. Francisco J. Pérez-Invernón:

Methodology, Writing - Original draft of several sections, Writing - Reviewing, Figure Selection.

Declaration of Competing Interest

The authors declare that they have no known competing financial interests or personal relationships that could have appeared to influence the work reported in this paper.

Acknowledgments

This work was supported by the Spanish Ministry of Science and Innovation (AEI) under projects ESP2017-86263-C4-4-R, PID2019-109269RB-C43 and the FEDER program. FJPI acknowledges the sponsorship provided by the Federal Ministry for Education and Research of Germany through the Alexander von Humboldt Foundation. FJGV acknowledges financial support from the State Agency for Research of the Spanish MCIU through the "Center of Excellence Severo Ochoa" award for the Instituto de Astrofísica de Andalucía (SEV-2017-0709).

References

Abdel-Salam, M., Nakano, M., Mizuno, A., 2007. Electric fields and corona currents in needle-to-meshed plate gaps. J. Phys. D. Appl. Phys. 40 (11), 3363.

Adachi, T., Fukunishi, H., Takahashi, Y., Hiraki, Y., Hsu, R.R., Su, H.T., Chen, A.B., Mende, S.B., Frey, H.U., Lee, L.C., 2006. Electric field transition between the diffuse and streamer regions of sprites estimated from ISUAL/array photometer measurements. Geophys. Res. Lett. 33, L17803. https://doi.org/10.1029/2006GL026495.

Adachi, T., Cummer, S.A., Li, J., Takahashi, Y., Hsu, R.R., Su, H.T., Chen, A.B., Mende, S.B., Frey, H.U., 2009. Estimating lightning current moment waveforms from satellite optical measurements. Geophys. Res. Lett. 36, L18808. https://doi.org/10.1029/2009GL039911.

Akyuz, M., Larsson, A., Cooray, V., Strandberg, G., 2003. 3D simulations of streamer branching in air. J. Electrost. 59 (2), 115–141. https://doi.org/10.1016/S0304-3886(03)00066-4.

Aleksandrov, N., Bazelyan, E., Konchakov, A., 2001. Plasma parameters in the channel of a long leader in air. Plasma Phys. Rep. 27 (10), 875–885.

Allen, D., Pickering, K., Duncan, B., Damon, M., 2010. Impact of lightning NO emissions on North American photochemistry as determined using the Global Modeling Initiative (GMI) model. J. Geophys. Res.-Atmos. 115 (D22).

Andersson, M., Verronen, P., Rodger, C., Clilverd, M., Seppälä, A., 2014. Missing driver in the sun–earth connection from energetic electron precipitation impacts mesospheric ozone. Nat. Commun. 5 (1), 1–5.

Armstrong, R., Lyons, W., 2000. Satellite and ground-based data exploitation for nudet discrimination. In: Characterizing atmospheric electrodynamic emissions from lightning, sprites, jets and elves. Final Report, DOE Contract# DE-AC04-98AL79469, 213.

Armstrong, R., Shorter, J., Taylor, M.J., Suszcynsky, D., Lyons, W., Jeong, L., 1998. Photometric measurements in the sprites'95 &'96 campaigns of nitrogen second positive (399.8 nm) and first negative (427.8 nm) emissions. J. Atmos. Sol. Terr. Phys. 60 (7–9), 787–799.

Armstrong, R.A., Suszcynsky, D.M., Lyons, W.A., Williams, E.R., 2001. Optical signatures, energy deposition, ionization and chemical dynamics in lightning-induced transient electrodyanamic middle and upper atmospheric events (sprites). Boulder, CO: Paper presented at National Radio Science Meeting. Union Radio-Sci Int.

Arnone, E., Kero, A., Dinelli, B.M., Enell, C.F., Arnold, N.F., Papandrea, E., Rodger, C.J., Carlotti, M., Ridolfi, M., Turunen, E., 2008. Seeking sprite-induced signatures in remotely sensed middle atmosphere NO_2. Geophys. Res. Lett. 35, L05807. https://doi.org/10.1029/2007GL031791.

Arnone, E., Smith, A., Enell, C.F., Kero, A., Dinelli, B., 2014. WACCM climate chemistry sensitivity to sprite perturbations. J. Geophys. Res.-Atmos. 119 (11), 6958–6970.

Arnone, E., Bór, J., Chanrion, O., Barta, V., Dietrich, S., Enell, C.F., Farges, T., Füllekrug, M., Kero, A., Labanti, R., et al., 2020. Climatology of transient luminous events and lightning observed above europe and the mediterranean sea. Surv. Geophys. 41 (2), 167–199.

Babaeva, N.Y., Naidis, G.V., 1996. Two-dimensional modelling of positive streamer dynamics in non-uniform electric fields in air. J. Phys. D. Appl. Phys. 29, 2423. https://doi.org/10.1088/0022-3727/29/9/029.

Babaeva, N.Y., Naidis, G.V., 1997. Dynamics of positive and negative streamers in air in weak uniform electric fields. IEEE Trans. Plasma Sci. 25 (2), 375–379.

Bagheri, B., Teunissen, J., Ebert, U., Becker, M.M., Chen, S., Ducasse, O., Eichwald, O., Loffhagen, D., Luque, A., Mihailova, D., et al., 2018. Comparison of six simulation codes for positive streamers in air. Plasma Sources Sci. Technol. 27 (9), 095002.

Baron, P., Urban, J., Sagawa, H., Möller, J., Murtagh, D.P., Mendrok, J., Dupuy, E., Sato, T., Ochiai, S., Suzuki, K., et al., 2011. The level 2 research product algorithms for the superconducting submillimeter-wave limb-emission sounder (SMILES). Atmosph. Meas. Techn. 4 (10), 2105–2124.

Baron, P., Murtagh, D., Urban, J., Sagawa, S., Ochiai, H., Körnich, H., Khosrawi, F., Kikuchi, K., Mizobuchi, S., Sagi, K., et al., 2012. Observation of horizontal winds in the middle-atmosphere between 30 S and 55 N during the northern winter 2009–2010. Atmos. Chem. Phys. 13, 6049–6064.

Barrington-Leigh, C.P., Inan, U.S., 1999. Elves triggered by positive and negative lightning discharges. Geophys. Res. Lett. 26, 683. https://doi.org/10.1029/1999GL900059.

Barrington-Leigh, C.P., Inan, U.S., Stanley, M., Cummer, S.A., 1999. Sprites triggered by negative lightning discharges. Geophys. Res. Lett. 26, 3605. https://doi.org/10.1029/1999GL010692.

Barrington-Leigh, C.P., Inan, U.S., Stanley, M., 2001. Identification of sprites and elves with intensified video and broadband array photometry. J. Geophys. Res. 106, 1741. https://doi.org/10.1029/2000JA000073.

Battye, W., Aneja, V.P., Schlesinger, W.H., 2017. Is nitrogen the next carbon? Earth's Future 5 (9), 894–904.

Bering, E.A., Benbrook, J.R., Garrett, J.A., Paredes, A.M., Wescott, E.M., Moudry, D.R., Sentman, D.D., Stenbaek-Nielsen, H.C., Lyons, W.A., 2002. The electrodynamics of sprites. Geophys. Res. Lett. 29 (5), 1064. https://doi.org/10.1029/2001GL013267.

Bering, E.A., Benbrook, J.R., Bhusal, L., Garrett, J.A., Paredes, A.M., Wescott, E.M., Moudry, D.R., Sentman, D.D., Stenbaek-Nielsen, H.C., Lyons, W.A., 2004a. Observations of transient luminous events (TLEs) associated with negative cloud to ground (-CG) lightning strokes. Geophys. Res. Lett. 31, L05104 https://doi.org/10.1029/2003GL018659.

Bering, E.A., Bhusal, L., Benbrook, J.R., Garrett, J.A., Jackson, A.P., Wescott, E.M., Moudry, D.R., Sentman, D.D., Stenbaek-Nielsen, H.C., Lyons, W.A., 2004b. The results from the 1999 sprites balloon campaign. Adv. Space Res. 34, 1782. https://doi.org/10.1016/j.asr.2003.05.043.

Bitzer, P.M., 2017. Global distribution and properties of continuing current in lightning. J. Geophys. Res.-Atmos. 122 (2), 1033–1041.

Blaes, P.R., Marshall, R.A., Inan, U.S., 2016. Global occurrence rate of elves and ionospheric heating due to cloud-to-ground lightning. J. Geophys. Res. Space Physics 121, 699. https://doi.org/10.1002/2015JA021916.

Blakeslee, R.J., Christian, H.J., Vonnegut, B., 1989. Electrical measurements over thunderstorms. J. Geophys. Res.-Atmos. 94 (D11), 13135–13140.

Blanc, E., Farges, T., Roche, R., Brebion, D., Hua, T., Labarthe, A., Melnikov, V., 2004. Nadir observations of sprites from the International Space Station. J. Geophys. Res. Space Physics 109, A02306. https://doi.org/10.1029/2003JA009972.

Blanc, E., Lefeuvre, F., Roussel-Dupré, R., Sauvaud, J.A., 2007. A microsatellite project dedicated to the study of impulsive transfers of energy between the Earth atmosphere, the ionosphere, and the magnetosphere. Adv. Space Res. 40, 1268. https://doi.org/10.1016/j.asr.2007.06.037.

Boccippio, D.J., Williams, E.R., Heckman, S.J., Lyons, W.A., Baker, I.T., Boldi, R., 1995. Sprites, ELF Transients, and Positive Ground Strokes. Science 269, 1088. https://doi.org/10.1126/science.269.5227.1088.

Boeck, W., Vaughan Jr., O., Blakeslee, R., Vonnegut, B., Brook, M., 1992. Lightning induced brightening in the airglow layer. Geophys. Res. Lett. 19 (2), 99–102.

Boggs, L.D., Liu, N., Peterson, M., Lazarus, S., Splitt, M., Lucena, F., Nag, A., Rassoul, H. K., 2019. First observations of gigantic jets from geostationary orbit. Geophys. Res. Lett. 46 (7), 3999–4006.

Borisov, N., Kozlov, S., Smirnova, N., 1993. Changes in the chemical composition of the middle atmosphere due to a multiple pulsed microwave discharge in air. Kosmicheskie Issledovaniia 31, 63–74.

Bourdon, A., Pasko, V.P., Liu, N.Y., Célestin, S., Ségur, P., Marode, E., 2007. Efficient models for photoionization produced by non-thermal gas discharges in air based on radiative transfer and the Helmholtz equations. Plasma Sources Sci. Technol. 16, 656. https://doi.org/10.1088/0963-0252/16/3/026.

Brandvold, D.K., Martinez, P., Dogruel, D., 1989. Polarity dependence of N_2O formation from corona discharge. Atmosph. Environ. (1967) 23 (9), 1881–1883.

Brandvold, D.K., Martinez, P., Hipsh, R., 1996. Field measurements of O_3 and N_2O produced from corona discharge. Atmos. Environ. 30 (6), 973–976.

Brasseur, G.P., Solomon, S., 2005. Aeronomy of the Middle Atmosphere. 3rd ed. Atmospheric and Oceanographic Sciences LIbrary. Springer, Dordrecht, Holland.

Bucsela, E.J., Morrill, J.S., Heavner, M., Siefring, C., Berg, S., Hampton, D., Moudry, D., Wescott, E., Sentman, D., 2003. $N_2(B^3\Pi_g)$ and $N_2^+(A^2\Pi_u)$ vibrational distributions observed in sprites. J. Atmos. Sol. Terr. Phys. 65, 583. https://doi.org/10.1016/S1364-6826(02)00316-4.

Bucsela, E.J., Pickering, K.E., Allen, D.J., Holzworth, R.H., Krotkov, N.A., 2019. Midlatitude lightning NO_x production efficiency inferred from OMI and WWLLN data. J. Geophys. Res.-Atmos. 124 (23), 13475–13497.

Celestin, S., Pasko, V.P., 2010. Effects of spatial non-uniformity of streamer discharges on spectroscopic diagnostics of peak electric fields in transient luminous events. Geophys. Res. Lett. 37, L07804. https://doi.org/10.1029/2010GL042675.

Chang, S., Kuo, C., Chou, J., Tsai, L., Lee, L., Chen, A.B., Su, H., Hsu, R., Lee, L., 2008. Far-Ultraviolet Emission in ISUAL Recorded TLEs and Lightning Events. AGU Fall Meeting Abstracts, p. A317.

Chanrion, O., Neubert, T., Mogensen, A., Yair, Y., Stendel, M., Singh, R., Siingh, D., 2017. Profuse activity of blue electrical discharges at the tops of thunderstorms. Geophys. Res. Lett. 44 (1), 496–503.

Chanrion, O., Neubert, T., Rasmussen, I.L., Stoltze, C., Tcherniak, D., Jessen, N.C., Polny, J., Brauer, P., Balling, J.E., Kristensen, S.S., et al., 2019. The Modular Multispectral Imaging Array (MMIA) of the ASIM payload on the International Space Station. Space Sci. Rev. 215 (4), 28.

Chen, A.B., Kuo, C.L., Lee, Y.J., Su, H.T., Hsu, R.R., Chern, J.L., Frey, H.U., Mende, S.B., Takahashi, Y., Fukunishi, H., Chang, Y.S., Liu, T.Y., Lee, L.C., 2008. Global distributions and occurrence rates of transient luminous events. J. Geophys. Res. Space Physics 113, A08306. https://doi.org/10.1029/2008JA013101.

Chen, A.B., Hsu, R.R., Su, H.T., Lee, Y.J., Wu, Y.J., Chou, J.K., Lee, L.J., Chuang, C.W., Liu, T.Y., Frey, H.U., et al., 2019. The global distributions, occurrence rates and climatology of transient luminous events by a 12-year space-borne survey. AGUFM 2019, AE23A-04.

Chern, J.L., Hsu, R.R., Su, H.T., Mende, S.B., Fukunishi, H., Takahashi, Y., Lee, L.C., 2003. Global survey of upper atmospheric transient luminous events on the ROCSAT-2 satellite. J. Atmos. Sol. Terr. Phys. 65, 647. https://doi.org/10.1016/S1364-6826(02)00317-6.

Chern, J.S., Wu, A.M., Lin, S.F., 2014. Globalization extension of transient luminous events from FORMOSAT-2 observation. Acta Astron. 98, 64–70.

Chou, J.K., Kuo, C.L., Tsai, L.Y., Chen, A.B., Su, H.T., Hsu, R.R., Cummer, S.A., Li, J., Frey, H.U., Mende, S.B., Takahashi, Y., Lee, L.C., 2010. Gigantic jets with negative and positive polarity streamers. J. Geophys. Res. Space Physics 115, A00E45. https://doi.org/10.1029/2009JA014831.

Chou, J.K., Hsu, R.R., Su, H.T., Chen, A.B., Kuo, C.L., Huang, S.M., Chang, S.C., Peng, K. M., ISUAL-Observed Blue, Wu Y.J., 2018. Luminous Events: The Associated Sferics. J. Geophys. Res. Space Physics 123 (4), 3063–3077.

Christian, H.J., Blakeslee, R.J., Boccippio, D.J., Boeck, W.L., Buechler, D.E., Driscoll, K. T., Goodman, S.J., Hall, J.M., Koshak, W.J., Mach, D.M., et al., 2003. Global frequency and distribution of lightning as observed from space by the Optical Transient Detector. J. Geophys. Res.-Atmos. 108 (D1), ACL-4.

Croize, L., Payan, S., Bureau, J., Duruisseau, F., Thieblemont, R., Huret, N., 2015. Effect of Blue Jets on Atmospheric Composition: Feasibility of Measurement From a Stratospheric Balloon. IEEE J. Select. Top. Appl. Earth Observ. Remote Sens. 8 (6), 3183–3192. https://doi.org/10.1109/JSTARS.2014.2381556.

Crutzen, P.J., 1970. The influence of nitrogen oxides on the atmospheric ozone content. Q. J. R. Meteorol. Soc. 96 (408), 320–325.

Cummer, S.A., 2020. Indirectly measured ambient electric fields for lightning initiation in fast breakdown regions. Geophys. Res. Lett. 47 (4), e2019GL086089.

Cummer, S.A., Füllekrug, M., 2001. Unusually intense continuing current in lightning produces delayed mesospheric breakdown. Geophys. Res. Lett. 28, 495. https://doi.org/10.1029/2000GL012214.

Cummer, S.A., Lyons, W.A., 2005. Implications of lightning charge moment changes for sprite initiation. J. Geophys. Res. Space Physics 110, A04304. https://doi.org/10.1029/2004JA010812.

Cummer, S.A., Inan, U.S., Bell, T.F., Barrington-Leigh, C.P., 1998. Radiation produced by electrical currents in sprites. Geophys. Res. Lett. 25, 1281. https://doi.org/10.1029/98GL50937.

Cummer, S.A., Jaugey, N., Li, J., Lyons, W.A., Nelson, T.E., Gerken, E.A., 2006. Submillisecond imaging of sprite development and structure. Geophys. Res. Lett. 33, L04104. https://doi.org/10.1029/2005GL024969.

Cummer, S.A., Briggs, M.S., Dwyer, J.R., Xiong, S., Connaughton, V., Fishman, G.J., Lu, G., Lyu, F., Solanki, R., 2014. The source altitude, electric current, and intrinsic brightness of terrestrial gamma ray flashes. Geophys. Res. Lett. 41, 8586. https://doi.org/10.1002/2014GL062196.

da Silva, C.L., Pasko, V.P., 2012. Simulation of leader speeds at gigantic jet altitudes. Geophys. Res. Lett. 39, L13805 https://doi.org/10.1029/2012GL052251.

da Silva, C.L., Pasko, V.P., 2013. Dynamics of streamer-to-leader transition at reduced air densities and its implications for propagation of lightning leaders and gigantic jets. J. Geophys. Res.-Atmos. 118, 13. https://doi.org/10.1002/2013JD020618.

de Larquier, S., Pasko, V.P., Stenbaek-Nielsen, H.C., Wilson, C.R., Olson, J.V., 2010. Finite-difference time-domain modeling of infrasound from pulsating auroras and comparison with recent observations. Geophys. Res. Lett. 37, L06804 https://doi.org/10.1029/2009GL042124.

de Urquijo, J., Gordillo-Vázquez, F.J., 2010. Comment on "NOx production in laboratory discharges simulating blue jets and red sprites" by Harold Peterson et al. J. Geophys. Res. Space Physics 115 (A12).

de Urquijo, J., Bekstein, A., Ruiz-Vargas, G., Gordillo-Vázquez, F.J., 2013. Drift and clustering of daughter negative ions of H_2O in parent gas. J. Phys. D. Appl. Phys. 46 (3), 035201 https://doi.org/10.1088/0022-3727/46/3/035201.

DeCaria, A.J., Pickering, K.E., Stenchikov, G.L., Ott, L.E., 2005. Lightning-generated NO_x and its impact on tropospheric ozone production: A three-dimensional modeling study of a Stratosphere-Troposphere Experiment: Radiation, Aerosols and Ozone (STERAO-A) thunderstorm. J. Geophys. Res.-Atmos. 110 (D14).

Dhali, S.K., Williams, P.F., 1987. Two-dimensional studies of streamers in gases. J. Appl. Phys. 62, 4696. https://doi.org/10.1063/1.339020.

Dowden, R., Rodger, C., Brundell, J., Clilverd, M., 2001. Decay of whistler-induced electron precipitation and cloud-ionosphere electrical discharge Trimpis: Observations and analysis. Radio Sci. 36, 151. https://doi.org/10.1029/1999RS002297.

Dubrovin, D., Nijdam, S., van Veldhuizen, E.M., Ebert, U., Yair, Y., Price, C., 2010. Sprite discharges on Venus and Jupiter-like planets: A laboratory investigation. J. Geophys. Res. Space Physics 115, A00E34. https://doi.org/10.1029/2009JA014851.

Edens, H., 2011. Photographic and lightning mapping observations of a blue starter over a New Mexico thunderstorm. Geophys. Res. Lett. 38 (17).

Enell, C.F., Verronen, P., Seppala, A., Ulich, T., Turunen, E., 2005. Possibility of $_x$ production by transient luminous events studied in acoupled ion-neutral chemical model, paper G3 presented at IAMAS Meeting. Int. Assoc. of Meteorol. and Atmos. Sci. Beijing, China, 2–11 Aug.

Enell, C.F., Arnone, E., Adachi, T., Chanrion, O., Verronen, P.T., Seppälä, A., Neubert, T., Ulich, T., Turunen, E., Takahashi, Y., Hsu, R.R., 2008. Parameterisation of the chemical effect of sprites in the middle atmosphere. Ann. Geophys. 26, 13. https://doi.org/10.5194/angeo-26-13-2008.

Evtushenko, A.A., Mareev, E.A., 2011. Simulation of mesospheric-composition disturbances under the action of highaltitude discharges (sprites). Radiophys. Quantum Electron. 54 (2), 111.

Evtushenko, A.A., Kuterin, F.A., Mareev, E.A., 2013. A model of sprite influence on the chemical balance of mesosphere. J. Atmos. Sol. Terr. Phys. 102, 298. https://doi.org/10.1016/j.jastp.2013.06.005.

Evtushenko, A.A., Gushchin, M.E., Korobkov, S.V., Strikovskiy, A.V., Mareev, E.A., 2020. Simulation of High-Altitude Discharges in a Large Plasma Facility. Geomagn. Aeron. 60 (3), 345–354.

Farges, T., Blanc, E., 2010. Characteristics of infrasound from lightning and sprites near thunderstorm areas. J. Geophys. Res. Space Physics 115, A00E31. https://doi.org/10.1029/2009JA014700.

Farges, T., Blanc, E., 2016. Characteristics of lightning, sprites, and human-induced emissions observed by nadir-viewing cameras on board the International Space Station. J. Geophys. Res.-Atmos. 121, 3405. https://doi.org/10.1002/2015JD024524.

Farges, T., Blanc, E., Le Pichon, A., Neubert, T., Allin, T.H., 2005. Identification of infrasound produced by sprites during the Sprite2003 campaign. Geophys. Res. Lett. 32, L01813 https://doi.org/10.1029/2004GL021212.

Farges, T., Blanc, E., Tanguy, M., 2007. Experimental evidence of D region heating by lightning-induced electromagnetic pulses on MF radio links. J. Geophys. Res. Space Physics 112, A10302. https://doi.org/10.1029/2007JA012285.

Farges, T., Blanc, E., Hébert, P., Le Mer-Dachard, F., Ravel, K., Gaillac, S., 2017. Microcameras and photometers (mcp) on board taranis satellite. EGUGA 6024.

Finney, D., Doherty, R., Wild, O., Abraham, N.L., 2016. The impact of lightning on tropospheric ozone chemistry using a new global lightning parametrisation. Atmos. Chem. Phys. 16 (12), 7507–7522.

Franz, R.C., Nemzek, R.J., Winckler, J.R., 1990. Television image of a large upward electrical discharge above a thunderstorm system. Science 249, 48. https://doi.org/10.1126/science.249.4964.48.

Frey, H.U., Mende, S.B., Cummer, S.A., Li, J., Adachi, T., Fukunishi, H., Takahashi, Y., Chen, A.B., Hsu, R.R., Su, H.T., Chang, Y.S., 2007. Halos generated by negative cloud-to-ground lightning. Geophys. Res. Lett. 34, L18801. https://doi.org/10.1029/2007GL030908.

Fukunishi, H., Takahashi, Y., Kubota, M., Sakanoi, K., Inan, U.S., Lyons, W.A., 1996. Elves: Lightning-induced transient luminous events in the lower ionosphere. Geophys. Res. Lett. 23, 2157. https://doi.org/10.1029/96GL01979.

Funke, B., López-Puertas, M., Garcia-Comas, M., Stiller, G., von Clarmann, T., Glatthor, N., 2008. Mesospheric N_2O enhancements as observed by MIPAS on Envisat during the polar winters in 2002–2004. Atmos. Chem. Phys. 8 (19), 5787–5800. https://doi.org/10.5194/acp-8-5787-2008.

Gallimberti, I., 1979. The mechanism of the long spark formation. Le J. Phys. Colloq. 40, C7):C7–193.

Gamerota, W.R., Cummer, S.A., Li, J., Stenbaek-Nielsen, H.C., Haaland, R.K., McHarg, M. G., 2011. Comparison of sprite initiation altitudes between observations and models. J. Geophys. Res. Space Physics 116, A02317. https://doi.org/10.1029/2010JA016095.

Ganot, M., Yair, Y., Price, C., Ziv, B., Sherez, Y., Greenberg, E., Devir, A., Yaniv, R., 2007. First detection of transient luminous events associated with winter thunderstorms in the eastern Mediterranean. Geophys. Res. Lett. 34, L12801. https://doi.org/10.1029/2007GL029258.

Garipov, G., Khrenov, B., Klimov, P., Klimenko, V., Mareev, E., Martines, O., Mendoza, E., Morozenko, V., Panasyuk, M., Park, I., et al., 2013. Global transients in ultraviolet and red-infrared ranges from data of universitetsky-tatiana-2 satellite. J. Geophys. Res.-Atmos. 118 (2), 370–379.

Garvin, D., 1974. Chemical Kinetics Data Survey VII: Tables of Rate and Photochemical Data for Modelling of the Stratosphere, 13. US Department of Commerce, National Bureau of Standards.

Gerken, E.A., 2002. Inan US. A survey of streamer and diffuse glow dynamics observed in sprites using telescopic imagery. J. Geophys. Res. Space Physics 107, 1344. https://doi.org/10.1029/2002JA009248.

Gerken, E.A., Inan, U.S., 2003. Observations of decameter-scale morphologies in sprites. J. Atmos. Sol. Terr. Phys. 65, 567. https://doi.org/10.1016/S1364-6826(02)00333-4.

Gerken, E.A., Inan, U.S., Barrington-Leigh, C.P., 2000. Telescopic imaging of sprites. Geophys. Res. Lett. 27, 2637. https://doi.org/10.1029/2000GL000035.

Glukhov, V.S., Pasko, V.P., Inan, U.S., 1992. Relaxation of transient lower ionospheric disturbances caused by lightning-whistler-induced electron precipitation bursts. J. Geophys. Res. 97, 16971. https://doi.org/10.1029/92JA01596.

Gordillo-Váquez, F.J., 2008. Air plasma kinetics under the influence of sprites. J. Phys. D. Appl. Phys. 41 (23), 234016 https://doi.org/10.1088/0022-3727/41/23/234016.

Gordillo-Vázquez, F.J., 2007. Preliminary kinetic simulations of the transient electron driven air plasma chemistry stimulated by Sprites: impact on the formation of nitride oxides. In: IUGG XXIV General Assembly "Earth, Our Changing Planet".

Gordillo-Vázquez, F.J., 2010. Vibrational kinetics of air plasmas induced by sprites. J. Geophys. Res. Space Physics 115, A00E25. https://doi.org/10.1029/2009JA014688.

Gordillo-Vázquez, F.J., Donkó, Z., 2009. Electron energy distribution functions and transport coefficients relevant for air plasmas in the troposphere: impact of humidity and gas temperature. Plasma Sources Sci. Technol. 18 (3), 034021 https://doi.org/10.1088/0963-0252/18/3/034021.

Gordillo-Vázquez, F.J., Luque, A., Simek, M., 2011. Spectrum of sprite halos. J. Geophys. Res. Space Physics 116, A09319. https://doi.org/10.1029/2011JA016652.

Gordillo-Vázquez, F.J., Luque, A., Simek, M., 2012. Near infrared and ultraviolet spectra of TLEs. J. Geophys. Res. Space Physics 117, A05329.

Gordillo-Vázquez, F.J., Luque, A., Haldoupis, C., 2016. Upper D region chemical kinetic modeling of LORE relaxation times. J. Geophys. Res. Space Physics 121, 3525. https://doi.org/10.1002/2015JA021408.

Gordillo-Vázquez, F.J., Passas, M., Luque, A., Sánchez, J., Velde, O., Montanyá, J., 2018. High spectral resolution spectroscopy of sprites: A natural probe of the mesosphere. J. Geophys. Res.-Atmos. 123 (4), 2336–2346.
Gordillo-Vázquez, F.J., Pérez-Invernón, F., Huntrieser, H., Smith, A., 2019. Comparison of six lightning parameterizations in cam5 and the impact on global atmospheric chemistry. Earth Space Sci. 6 (12), 2317–2346.
Gordillo-Vázquez, F.J., Luque, A., 2010. Electrical conductivity in sprite streamer channels. Geophys. Res. Lett. 37, L16809 https://doi.org/10.1029/2010GL044349.
Grandell, J., Finke, U., Stuhlmann, R., 2009. The eumetsat meteosat third generation lightning imager (mtg-li): Applications and product processing. ems. EMS2009–551.
Green, B.D., Fraser, M.E., Rawlins, W.T., Jeong, L., Blumberg, W.A.M., Mende, S.B., Swenson, G.R., Hampton, D.L., Wescott, E.M., Sentman, D.D., 1996. Molecular excitation in sprites. Geophys. Res. Lett. 23, 2161. https://doi.org/10.1029/96GL02071.
Grewe, V., 2007. Impact of climate variability on tropospheric ozone. Sci. Total Environ. 374 (1), 167–181.
Haldoupis, C., Amvrosiadi, N., Cotts, B.R.T., van der Velde, O.A., Chanrion, O., Neubert, T., 2010. More evidence for a one-to-one correlation between Sprites and Early VLF perturbations. J. Geophys. Res. Space Physics 115, A07304. https://doi.org/10.1029/2009JA015165.
Haldoupis, C., Cohen, M., Cotts, B.R., Arnone, E., Inan, U., 2012. Long lasting D-region ionospheric modifications, caused by intense lightning in association with elve and sprite pairs. Geophys. Res. Lett. 39, L16801 https://doi.org/10.1029/2012GL052765.
Haldoupis, C., Cohen, M., Arnone, E., Cotts, B.R., Dietrich, S., 2013. Step-like and long-recovery VLF perturbations caused by EM pulses radiated by powerful ± CG lightning discharges. J. Geophys. Res. Space Physics 118. https://doi.org/10.1002/jgra.50489.
Hale, L.C., 1994. Coupling of ELF/VLF energy from lightning and MeV particles to the middle atmosphere, ionosphere, and global circuit. J. Geophys. Res.-Atmos. 99 (D10), 21089–21096.
Hale, L.C., Croskey, C.L., Mitchell, J.D., 1981. Measurements of middle-atmosphere electric fields and associated electrical conductivities. Geophys. Res. Lett. 8 (8), 927–930.
Hallinan, T.J., Stenbaek-Nielsen, H.C., Deehr, C.S., 1985. Enhanced Aurora. J. Geophys. Res. 90, 8461–8475. https://doi.org/10.1029/JA090iA09p08461.
Hampton, D.L., Heavner, M.J., Wescott, E.M., Sentman, D.D., 1996. Optical spectral characteristics of sprites. Geophys. Res. Lett. 23, 89. https://doi.org/10.1029/95GL03587.
Hauglustaine, D., Emmons, L., Newchurch, M., Brasseur, G., Takao, T., Matsubara, K., Johnson, J., Ridley, B., Stith, J., Dye, J., 2001. On the role of lightning NO_x in the formation of tropospheric ozone plumes: A global model perspective. J. Atmos. Chem. 38 (3), 277–294.
Hayakawa, M., Nakamura, T., Hobara, Y., Williams, E., 2004. Observation of sprites over the Sea of Japan and conditions for lightning-induced sprites in winter. J. Geophys. Res. Space Physics 109, A01312. https://doi.org/10.1029/2003JA009905.
Heavner, M.J., 2000. Optical Spectroscopic Observations of Sprites, Blue Jets, and Elves: Inferred Microphysical Processes and their Macrophysical Implications. Ph.D. thesis.
Heavner, M.J., Morrill, J.S., Siefring, C., Sentman, D.D., Moudry, D.R., Wescott, E.M., Bucsela, E.J., 2010. Near-ultraviolet and blue spectral observations of sprites in the 320–460 nm region: N_2 (2PG) emissions. J. Geophys. Res. Space Physics 115, A00E44. https://doi.org/10.1029/2009JA014858.
Hill, R.D., Rahmim, I., Rinker, R.G., 1988. Experimental study of the production of nitric oxide, nitrous oxide, and ozone in a simulated atmospheric corona. Ind. Eng. Chem. Res. 27 (7), 1264–1269.
Hiraki, Y., Tong, L., Fukunishi, H., Nanbu, K., Kasai, Y., Ichimura, A., 2004. Generation of metastable oxygen atom O(1D) in sprite halos. Geophys. Res. Lett. 31, L14105 https://doi.org/10.1029/2004GL020048.
Hiraki, Y., Kasai, Y., Fukunishi, H., 2008. Chemistry of sprite discharges through ion-neutral reactions. Atmos. Chem. Phys. 8, 3919.
Hoder, T., Simek, M., Bonaventura, Z., Prukner, V., Gordillo-Vázquez, F.J., 2016. Radially and temporally resolved electric field of positive streamers in air and modelling of the induced plasma chemistry. Plasma Sources Sci. Technol. 25 (4), 045021.
Hoder, T., Bonaventura, Z., Prukner, V., Gordillo-Vázquez, F.J., Simek, M., 2020. Emerging and expanding streamer head in low-pressure air. Plasma Sources Sci. Technol. 29 (3), 03LT01.
Hu, W., Cummer, S.A., Lyons, W.A., Nelson, T.E., 2002. Lightning charge moment changes for the initiation of sprites. Geophys. Res. Lett. 29 (8), 1279. https://doi.org/10.1029/2001GL014593.
Hu, W., Cummer, S.A., Lyons, W.A., 2007. Testing sprite initiation theory using lightning measurements and modeled electromagnetic fields. J. Geophys. Res.-Atmos. 112, D13115 https://doi.org/10.1029/2006JD007939.
Huntrieser, H., Lichtenstern, M., Scheibe, M., Aufmhoff, H., Schlager, H., Pucik, T., Minikin, A., Weinzierl, B., Heimerl, K., Pollack, I., et al., 2016. Injection of lightning-produced NO_x, water vapor, wildfire emissions, and stratospheric air to the UT/LS as observed from DC3 measurements. J. Geophys. Res.-Atmos. 121 (11), 6638–6668.
Ignaccolo, M., Farges, T., Mika, A., Allin, T.H., Chanrion, O., Blanc, E., Neubert, T., Fraser-Smith, A.C., Füllekrug, M., 2006. The Planetary rate of sprite events. Geophys. Res. Lett. 33, L11808 https://doi.org/10.1029/2005GL025502.
Ihaddadene, M.A., Celestin, S., 2015. Increase of the electric field in head-on collisions between negative and positive streamers. Geophys. Res. Lett. 42, 5644. https://doi.org/10.1002/2015GL064623.
Ihaddadene, M.A., Celestin, S., 2017. Determination of sprite streamers altitude based on N_2 spectroscopic analysis. J. Geophys. Res. Space Physics 122, 1000. https://doi.org/10.1002/2016JA023111.
Inan, U.S., Bell, T.F., Rodriguez, J.V., 1991. Heating and ionization of the lower ionosphere by lightning. Geophys. Res. Lett. 18, 705. https://doi.org/10.1029/91GL00364.
Inan, U.S., Pasko, V.P., Bell, T.F., 1996a. Sustained heating of the ionosphere above thunderstorms as evidenced in "early/fast" VLF events. Geophys. Res. Lett. 23, 1067. https://doi.org/10.1029/96GL01360.
Inan, U.S., Reising, S.C., Fishman, G.J., Horack, J.M., 1996b. On the association of terrestrial gamma-ray bursts with lightning and implications for sprites. Geophys. Res. Lett. 23, 1017. https://doi.org/10.1029/96GL00746.
Inan, U.S., Barrington-Leigh, C., Hansen, S., Glukhov, V.S., Bell, T.F., Rairden, R., 1997. Rapid lateral expansion of optical luminosity in lightning-induced ionospheric flashes referred to as 'elves'. Geophys. Res. Lett. 24, 583. https://doi.org/10.1029/97GL00404.
Inan, U.S., Cummer, S.A., Marshall, R.A., 2010. A survey of ELF and VLF research on lightning-ionosphere interactions and causative discharges. J. Geophys. Res. Space Physics 115, A00E36. https://doi.org/10.1029/2009JA014775.
Iwagami, N., Inomata, S., Ogawa, T., 1998. Doppler detection of hydroxyl column abundance in the middle atmosphere: 2. Measurement for three years and comparison with a 1D model. J. Atmos. Chem. 29 (2), 195–216.
Jacobson, A., Light, T., 2012. Revisiting "Narrow Bipolar Event" intracloud lightning using the FORTE satellite. In: Annales Geophysicae. Copernicus GmbH 30, 389.
Jacobson, A., Light, T., Hamlin, T., Nemzek, R., 2013. Joint radio and optical observations of the most radio-powerful intracloud lightning discharges. In: Annales Geophysicae. Copernicus GmbH, 31, pp. 563–580.
Jehl, A., Farges, T., Blanc, E., 2013. Color pictures of sprites from non-dedicated observation on board the international space station. J. Geophys. Res. Space Physics 118 (1), 454–461.
Kanmae, T., Stenbaek-Nielsen, H.C., McHarg, M.G., 2007. Altitude resolved sprite spectra with 3 ms temporal resolution. Geophys. Res. Lett. 34, L07810. https://doi.org/10.1029/2006GL028608.
Kanmae, T., Stenbaek-Nielsen, H.C., McHarg, M.G., Haaland, R.K., 2010a. Observation of blue sprite spectra at 10,000 fps. Geophys. Res. Lett. 37, L13808 https://doi.org/10.1029/2010GL043739.
Kanmae, T., Stenbaek-Nielsen, H.C., McHarg, M.G., Haaland, R.K., 2010b. Observation of sprite streamer head's spectra at 10,000 fps. J. Geophys. Res. Space Physics 115, A00E48. https://doi.org/10.1029/2009JA014546.
Kanmae, T., Stenbaek-Nielsen, H., McHarg, M., Haaland, R., 2012. Diameter-speed relation of sprite streamers. J. Phys. D. Appl. Phys. 45 (27), 275203.
Kasai, Y., Sagawa, H., Kreyling, D., Dupuy, E., Baron, P., Mendrok, J., Suzuki, K., Sato, T., Nishibori, T., Mizobuchi, S., et al., 2013. Validation of stratospheric and mesospheric ozone observed by SMILES from International Space Station. Atmosph. Meas. Techn. 6 (9), 2311–2338.
Kelly, C., Chipperfield, M., Plane, J.M., Feng, W., Sheese, P., Walker, K.A., Boone, C.D., 2018. An explanation for the nitrous oxide layer observed in the mesopause region. Geophys. Res. Lett. 45 (15), 7818–7827.
Khrenov, B., Garipov, G., Zotov, M.Y., Klimov, P., Panasyuk, M., Petrov, V., Sharakin, S., Shirokov, A., Yashin, I., Grebenyuk, V., et al., 2020. A study of atmospheric radiation flashes in the near-ultraviolet region using the tus detector aboard the lomonosov satellite. Cosm. Res. 58 (5), 317–329.
Kikuchi Ki, Nishibori T., Ochiai, S., Ozeki, H., Irimajiri, Y., Kasai, Y., Koike, M., Manabe, T., Mizukoshi, K., Murayama, Y., et al., 2010. Overview and early results of the Superconducting Submillimeter-Wave Limb-Emission Sounder (SMILES). J. Geophys. Res.-Atmos. 115 (D23).
Kochkin, P., Lehtinen, N., van Deursen, A.P.J., Østgaard, N., 2016. Pilot system development in metre-scale laboratory discharge. J. Phys. D. Appl. Phys. 49, 425203. https://doi.org/10.1088/0022-3727/49/42/425203.
Kochkin, P.O., Nguyen, C.V., van Deursen, A.P.J., Ebert, U., 2012. Experimental study of hard X-rays emitted from metre-scale positive discharges in air. J. Phys. D. Appl. Phys. 45, 425202. https://doi.org/10.1088/0022-3727/45/42/425202.
Kochkin, P.O., van Deursen, A.P.J., Ebert, U., 2014. Experimental study of the spatio-temporal development of metre-scale negative discharge in air. J. Phys. D. Appl. Phys. 47 (14), 145203 https://doi.org/10.1088/0022-3727/47/14/145203.
Kossyi, I.A., Kostinsky, A.Y., Matveyev, A.A., Silakov, V.P., 1992. Kinetic scheme of the non-equilibrium discharge in nitrogen-oxygen mixtures. Plasma Sources Sci. Technol. 1, 207. https://doi.org/10.1088/0963-0252/1/3/011.
Krehbiel, P.R., Riousset, J.A., Pasko, V.P., Thomas, R.J., Rison, W., Stanley, M.A., Edens, H.E., 2008. Upward electrical discharges from thunderstorms. Nat. Geosci. 1, 233. https://doi.org/10.1038/ngeo162.
Kreyling, D., Sagawa, H., Wohltmann, I., Lehmann, R., Kasai, Y., 2013. SMILES zonal and diurnal variation climatology of stratospheric and mesospheric trace gasses: O_3, HCl, HNO_3, ClO, BrO, HOCl, HO_2, and temperature. J. Geophys. Res.-Atmos. 118 (20), 11–888.
Krivonosova, O., Losev, S., Nalivaiko, V., Mukoseev, Y.K., Shatalov, O., 1987. Recommended data on the rate constants of chemical reactions between molecules consisting of N and O atoms. Plasma Chem. 14, 3–31.
Kulikovsky, A.A., 1997. Production of chemically active species in the air by a single positive streamer in a nonuniform field. IEEE Trans. Plasma Sci. 25, 439. https://doi.org/10.1109/27.597258.
Kulikovsky, A.A., 1998. Three-dimensional simulation of a positive streamer in air near curved anode. Phys. Lett. A 245, 445. https://doi.org/10.1016/S0375-9601(98)00415-0.
Kuo, C.L., Hsu, R.R., Chen, A.B., Su, H.T., Lee, L.C., Mende, S.B., Frey, H.U., Fukunishi, H., Takahashi, Y., 2005. Electric fields and electron energies inferred from the ISUAL recorded sprites. Geophys. Res. Lett. 32, L19103 https://doi.org/10.1029/2005GL023389.

Kuo, C.L., Chen, A.B., Lee, Y.J., Tsai, L.Y., Chou, R.K., Hsu, R.R., Su, H.T., Lee, L.C., Cummer, S.A., Frey, H.U., Mende, S.B., Takahashi, Y., Fukunishi, H., 2007. Modeling elves observed by FORMOSAT-2 satellite. J. Geophys. Res. Space Physics 112, A11312. https://doi.org/10.1029/2007JA012407.

Kuo, C.L., Chou, J.K., Tsai, L.Y., Chen, A.B., Su, H.T., Hsu, R.R., Cummer, S.A., Frey, H. U., Mende, S.B., Takahashi, Y., Lee, L.C., 2009. Discharge processes, electric field, and electron energy in ISUAL-recorded gigantic jets. J. Geophys. Res. Space Physics 114, A04314. https://doi.org/10.1029/2008JA013791.

Kuo, C.L., Huang, T.-Y., Chang, S.C., Chou, J.K., Lee, L.J., Wu, Y.J., Chen, A.B., Su, Han-Tzong, Hsu, Rue-Ron, Frey, H.U., Others, 2012. Full-kinetic elve model simulations and their comparisons with the ISUAL observed events. J. Geophys. Res. Space Physics 117 (A7).

Kuo, C.L., Williams, E., Bór, J., Lin, Y.H., Lee, L.J., Huang, S.M., Chou, J.K., Chen, A.B., Su, Han-Tzong, Hsu, Rue-Ron, Others, 2013. Ionization emissions associated with N_2^+ 1N band in halos without visible sprite streamers. J. Geophys. Res. Space Physics 118 (8), 5317–5326.

Kuo, C.L., Su, H.T., Hsu, R.R., 2015. The blue luminous events observed by ISUAL payload on board FORMOSAT-2 satellite. J. Geophys. Res. Space Physics 120 (11), 9795–9804.

Kuo, C.L., Chou, J.K., Wu, Y.J., Williams, E., Chen, A.B.C., Su, H.T., Hsu, R.R., Lee, L.C., 2019. The boltzmann vibrational temperature of N_2 ($B^3\Pi_g$) derived from ISUAL imager multiband measurements of transient luminous events. J. Geophys. Res. Space Physics 124 (12), 10760–10777.

Lang, T.J., Lyons, W.A., Cummer, S.A., Fuchs, B.R., Dolan, B., Rutledge, S.A., Krehbiel, P., Rison, W., Stanley, M., Ashcraft, T., 2016. Observations of two sprite-producing storms in Colorado. J. Geophys. Res.-Atmos. 121 (16), 9675–9695.

Langford, A.O., Portmann, R.W., Daniel, J.S., Miller, H.L., Solomon, S., 2004. Spectroscopic measurements of NO_2 in a Colorado thunderstorm: Determination of the mean production by cloud-to-ground lightning flashes. J. Geophys. Res. 109, D11304 https://doi.org/10.1029/2003JD004158.

Le Vine, D.M., 1980. Sources of the strongest RF radiation from lightning. J. Geophys. Res. Oceans 85 (C7), 4091–4095.

Lee, Y.S., Shepherd, G., 2010. Summer high-latitude mesospheric observations of supersonic bursts and $O(^1S)$ emission rate with the UARS WINDII instrument and the association with sprites, meteors, and lightning. J. Geophys. Res. Space Physics 115 (A5).

Lefeuvre, F., Blanc, E., Pinçon, J.L., Roussel-Dupré, R., Lawrence, D., Sauvaud, J.A., Rauch, J.L., de Feraudy, H., Lagoutte, D., 2008. Taranis—a satellite project dedicated to the physics of tles and tgfs. Space Sci. Rev. 137 (1–4), 301–315.

Lehtinen, N.G., Inan, U.S., 2007. Possible persistent ionization caused by giant blue jets. Geophys. Res. Lett. 34, L08804 https://doi.org/10.1029/2006GL029051.

Levine, J.S., Hughes, R.E., Chameides, W.L., Howell, W.E., 1979. N_2O and CO production by electric discharge: Atmospheric implications. Geophys. Res. Lett. 6 (7), 557–559.

Levine, J.S., Rogowski, R.S., Gregory, G.L., Howell, W.E., Fishman, J., 1981. Simultaneous measurements of NO_x, NO, and O_3 production in a laboratory discharge: Atmospheric implications. Geophys. Res. Lett. 8 (4), 357–360.

Li, J., Cummer, S.A., 2009. Measurement of sprite streamer acceleration and deceleration. Geophys. Res. Lett. 36, L10812. https://doi.org/10.1029/2009GL037581.

Li, J., Cummer, S.A., Lyons, W.A., Nelson, T.E., 2008. Coordinated analysis of delayed sprites with high-speed images and remote electromagnetic fields. J. Geophys. Res.-Atmos. 113, D20206 https://doi.org/10.1029/2008JD010008.

Li, J., Cummer, S.A., Lu, G., Zigoneanu, L., 2012. Charge moment change and lightning-driven electric fields associated with negative sprites and halos. J. Geophys. Res. Space Physics 117 (A9).

Liu, F., Zhu, B., Lu, G., Qin, Z., Lei, J., Peng, K.M., Chen, A.B., Huang, A., Cummer, S.A., Chen, M., et al., 2018. Observations of blue discharges associated with negative narrow bipolar events in active deep convection. Geophys. Res. Lett. 45 (6), 2842–2851.

Liu, N., 2010. Model of sprite luminous trail caused by increasing streamer current. Geophys. Res. Lett. 37, L04102 https://doi.org/10.1029/2009GL042214.

Liu, N., 2012. Multiple ion species fluid modeling of sprite halos and the role of electron detachment of O^- in their dynamics. J. Geophys. Res. Space Physics 117, A03308. https://doi.org/10.1029/2011JA017062.

Liu, N., Pasko, V.P., 2004. Effects of photoionization on propagation and branching of positive and negative streamers in sprites. J. Geophys. Res. Space Physics 109, A04301. https://doi.org/10.1029/2003JA010064.

Liu, N., Pasko, V.P., 2005. Molecular nitrogen LBH band system far-UV emissions of sprite streamers. Geophys. Res. Lett. 32, L05104. https://doi.org/10.1029/2004GL022001.

Liu, N., Pasko, V.P., Burkhardt, D.H., Frey, H.U., Mende, S.B., Su, H.T., Chen, A.B., Hsu, R.R., Lee, L.C., Fukunishi, H., Takahashi, Y., 2006. Comparison of results from sprite streamer modeling with spectrophotometric measurements by ISUAL instrument on FORMOSAT-2 satellite. Geophys. Res. Lett. 33, L01101 https://doi.org/10.1029/2005GL024243.

Liu, N., Pasko, V.P., Frey, H.U., Mende, S.B., Su, H.T., Chen, A.B., Hsu, R.R., Lee, L.C., et al., 2009. J. Geophys. Res. Space Physics 114, A00E02. https://doi.org/10.1029/2008JA013735.

Liu, N., Kosar, B., Sadighi, S., Dwyer, J.R., Rassoul, H.K., 2012. Formation of Streamer Discharges from an Isolated Ionization Column at Subbreakdown Conditions. Phys. Rev. Lett. 109 (2), 025002 https://doi.org/10.1103/PhysRevLett.109.025002.

Liu, N., Dwyer, J.R., Cummer, S.A., 2017. Elves Accompanying Terrestrial Gamma Ray Flashes. J. Geophys. Res. Space Physics 122 (10). https://doi.org/10.1002/2017JA024344.

Loeb, L.B., Meek, J.M., 1940. The Mechanism of Spark Discharge in Air at Atmospheric Pressure. I. J. Appl. Phys. 11, 438. https://doi.org/10.1063/1.1712792.

Lu, G., Yu, B., Cummer, S.A., Peng, K.M., Chen, A.B., Lyu, F., Xue, X., Liu, F., Hsu, R.R., Su, H.T., 2018. On the causative strokes of halos observed by isual in the vicinity of north america. Geophys. Res. Lett. 45 (19), 10–781.

Luque, A., Ebert, U., 2009. Emergence of sprite streamers from screening-ionization waves in the lower ionosphere. Nat. Geosci. 2, 757. https://doi.org/10.1038/ngeo662.

Luque, A., Ebert, U., 2010. Sprites in varying air density: Charge conservation, glowing negative trails and changing velocity. Geophys. Res. Lett. 37, L06806 https://doi.org/10.1029/2009GL041982.

Luque, A., Ebert, U., 2014. Growing discharge trees with self-consistent charge transport: the collective dynamics of streamers. New J. Phys. 16 (1), 013039 https://doi.org/10.1088/1367-2630/16/1/013039.

Luque, A., Gordillo-Vázquez, F.J., 2011a. Mesospheric electric breakdown and delayed sprite ignition caused by electron detachment. Nat. Geosci. 4 https://doi.org/10.1038/ngeo1314.

Luque, A., Gordillo-Vázquez, F.J., 2011b. Modeling and analysis of $N_2(B^3\Pi_g)$ and $N_2(C^3\Pi_u)$ vibrational distributions in sprites. J. Geophys. Res. Space Physics 116, A02306. https://doi.org/10.1029/2010JA015952.

Luque, A., Gordillo-Vázquez, F.J., 2011c. Sprite beads originating from inhomogeneities in the mesospheric electron density. Geophys. Res. Lett. 38, L04808 https://doi.org/10.1029/2010GL046403.

Luque, A., Ebert, U., Montijn, C., Hundsdorfer, W., 2007. Photoionization in negative streamers: Fast computations and two propagation modes. Appl. Phys. Lett. 90 (8), 081501 https://doi.org/10.1063/1.2435934.

Luque, A., Ebert, U., Hundsdorfer, W., 2008a. Interaction of streamer discharges in air and other oxygen-nitrogen mixtures. Phys. Rev. Lett. 101 (7), 075005 https://doi.org/10.1103/PhysRevLett.101.075005.

Luque, A., Ratushnaya, V., Ebert, U., 2008b. Positive and negative streamers in ambient air: modelling evolution and velocities. J. Phys. D. Appl. Phys. 41 (23), 234005. https://doi.org/10.1088/0022-3727/41/23/234005.

Luque, A., Stenbaek-Nielsen, H., McHarg, M., Haaland, R., 2016. Sprite beads and glows arising from the attachment instability in streamer channels. J. Geophys. Res. Space Physics 121 (3), 2431–2449.

Luque, A., González, M., Gordillo-Vázquez, F.J., 2017. Streamer discharges as advancing imperfect conductors: inhomogeneities in long ionized channels. Plasma Sources Sci. Technol. 26 (12), 125006.

Lyons, W.A., 2006. The meteorology of transient luminous events-an introduction and overview. In: Sprites, Elves and Intense Lightning Discharges. Springer, pp. 19–56.

Lyons, W.A., Nelson, T.E., Armstrong, R.A., Pasko, V.P., Stanley, M.A., 2003. Upward electrical discharges from thunderstorm tops. Bull. Am. Meteorol. Soc. 84, 445. https://doi.org/10.1175/BAMS-84-4-445.

Lyu, F., Cummer, S.A., McTague, L., 2015. Insights into high peak current in-cloud lightning events during thunderstorms. Geophys. Res. Lett. 42, 6836. https://doi.org/10.1002/2015GL065047.

Lyu, F., Cummer, S.A., Qin, Z., Chen, M., 2019. Lightning initiation processes imaged with very high frequency broadband interferometry. J. Geophys. Res.-Atmos. 124 (6), 2994–3004.

Maggio, C.R., Marshall, T.C., Stolzenburg, M., 2009. Estimations of charge transferred and energy released by lightning flashes. J. Geophys. Res. 114, D14203. https://doi.org/10.1029/2008JD011506.

Malagoán-Romero, A., Luque, A., 2019. Spontaneous emergence of space stems ahead of negative leaders in lightning and long sparks. Geophys. Res. Lett. 46 (7), 4029–4038.

Malagón-Romero, A., Pérez-Invernón, F.J., Luque, A., Gordillo-Vázquez, F.J., 2019. Analysis of the spatial nonuniformity of the electric field in spectroscopic diagnostic methods of atmospheric electricity phenomena. J. Geophys. Res.-Atmos. 124 (22), 12356–12370.

Malagón-Romero, A., Teunissen, J., Stenbaek-Nielsen, H., McHarg, M., Ebert, U., Luque, A., 2020. On the emergence mechanism of carrot sprites. Geophys. Res. Lett. 47 (1), e2019GL085776.

Marode, E., 1975. The mechanism of spark breakdown in air at atmospheric pressure between a positive point and a plane. i. experimental: Nature of the streamer track. J. Appl. Phys. 46 (5), 2005–2015.

Marshall, R.A., Inan, U.S., 2006. High-speed measurements of small-scale features in sprites: Sizes and lifetimes. Radio Sci. 41, RS6S43 https://doi.org/10.1029/2005RS003353.

Marshall, R.A., Inan, U.S., Lyons, W.A., 2006. On the association of early/fast very low frequency perturbations with sprites and rare examples of VLF backscatter. J. Geophys. Res.-Atmos. 111, D19108 https://doi.org/10.1029/2006JD007219.

Marshall, R.A., Newsome, R., Inan, U., 2008. Fast photometric imaging using orthogonal linear arrays. IEEE Trans. Geosci. Remote Sens. 46, 3885. https://doi.org/10.1109/TGRS.2008.2000824.

Marshall, R.A., Silva, C.L., Pasko, V.P., 2015. Elve doublets and compact intracloud discharges. Geophys. Res. Lett. 42, 6112. https://doi.org/10.1002/2015GL064862.

McHarg, M.G., Stenbaek-Nielsen, H.C., Kammae, T., 2007. Observations of streamer formation in sprites. Geophys. Res. Lett. 34, L06804. https://doi.org/10.1029/2006GL027854.

McHarg, M.G., Harley, J., Maldonado, C., Lane, C.T., Taylor, L.M., Sonnenfeld, R., da Silva, C.L., Jensen, D., Contreras Vidal, L., Haaland, R.K., et al., 2019. Sprite streamer interactions at 100,000 frames per second. AGUFM 2019, AE23A-08.

Mende, S.B., Rairden, R.L., Swenson, G.R., Lyons, W.A., 1995. Sprite spectra; N_2 1 PG band identification. Geophys. Res. Lett. 22, 2633. https://doi.org/10.1029/95GL02827.

Milikh, G.M., Valdivia, J.A., Papadopoulos, K., 1997. Model of red sprite optical spectra. Geophys. Res. Lett. 24, 833. https://doi.org/10.1029/97GL00759.

Milikh, G.M., Usikov, D.A., Valdivia, J.A., 1998. Model of infrared emission from sprites. J. Atmos. Sol. Terr. Phys. 60, 895. https://doi.org/10.1016/S1364-6826(98)80009-6.

Mishin, E.V., 1997. Ozone layer perturbation by a single blue jet. Geophys. Res. Lett. 24, 1919. https://doi.org/10.1029/97GL01890.

Mishin, E.V., Milikh, G.M., 2008. Blue Jets: Upward Lightning. Space Sci. Rev. 137, 473. https://doi.org/10.1007/s11214-008-9346-z.

Moore, R.C., Barrington-Leigh, C.P., Inan, U.S., Bell, T.F., 2003. Early/fast VLF events produced by electron density changes associated with sprite halos. J. Geophys. Res. Space Physics 108, 1363. https://doi.org/10.1029/2002JA009816.

Morrill, J.S., Bucsela, E.J., Pasko, V.P., Berg, S.L., Heavner, M.J., Moudry, D.R., Benesch, W.M., Wescott, E.M., Sentman, D.D., 1998. Time resolved N_2 triplet state vibrational populations and emissions associated with red sprites. J. Atmos. Sol. Terr. Phys. 60, 811. https://doi.org/10.1016/S1364-6826(98)00031-5.

Morrill, J.S., Bucsela, E., Siefring, C., Heavner, M., Berg, S., Moudry, D., Slinker, S., Fernsler, R., Wescott, E., Sentman, D., Osborne, D., 2002. Electron energy and electric field estimates in sprites derived from ionized and neutral N_2 emissions. Geophys. Res. Lett. 29 (10), 1462. https://doi.org/10.1029/2001GL014018.

Moruzzi, J., Ekin Jr., J., Phelps, A., 1968. Electron production by associative detachment of O^--ions with NO, CO, and H_2. J. Chem. Phys. 48 (7), 3070–3076.

Moruzzi, J.L., Price, D.A., 1974. Ionization, attachment and detachment in air and air-CO_2 mixtures. J. Phys. D. Appl. Phys. 7, 1434. https://doi.org/10.1088/0022-3727/7/10/317.

Mosier, A., Kroeze, C., Nevison, C., Oenema, O., Seitzinger, S., van Cleemput, O., 1997. Closing the global atmospheric N_2O budget: nitrous oxide emissions through the agricultural nitrogen cycle.(OECD/IPCC/IEA Phase II Development of IPCC Guidelines for National Greenhouse Gas Inventories). In: Dissipation of N from the human N-cycle, and its role in present and future N_2O emissions to the atmosphere. Int. Workshop, Oslo, Norway, p. 4.

Moudry, D., Stenbaek-Nielsen, H., Sentman, D., Wescott, E., 2003. Imaging of elves, halos and sprite initiation at 1ms time resolution. J. Atmos. Sol. Terr. Phys. 65, 509. https://doi.org/10.1016/S1364-6826(02)00323-1.

Murray, L.T., 2016. Lightning NO_x and impacts on air quality. Curr. Pollut. Rep. 2 (2), 115–133.

Myhre, G., Aas, W., Cherian, R., Collins, W., Faluvegi, G., Flanner, M., Forster, P., Hodnebrog, O., Klimont, Z., Lund, M., et al., 2017. Multi-model simulations of aerosol and ozone radiative forcing due to anthropogenic emission changes during the period 1990–2015. Atmos. Chem. Phys. 17 (4), 2709–2720.

Naidis, G.V., 1996. On streamer interaction in a pulsed positive corona discharge. J. Phys. D. Appl. Phys. 29, 779. https://doi.org/10.1088/0022-3727/29/3/039.

Nault, B.A., Garland, C., Wooldridge, P.J., Brune, W.H., Campuzano-Jost, P., Crounse, J. D., Day, D.A., Dibb, J., Hall, S.R., Huey, L.G., et al., 2016. Observational Constraints on the Oxidation of NO_x in the Upper Troposphere. J. Phys. Chem. A 120 (9), 1468–1478.

Nault, B.A., Laughner, J.L., Wooldridge, P.J., Crounse, J.D., Dibb, J., Diskin, G., Peischl, J., Podolske, J.R., Pollack, I.B., Ryerson, T.B., 2017. others . Lightning NO_x Emissions: Reconciling measured and modeled estimates with updated NO_x chemistry. Geophys. Res. Lett. 44 (18), 9479–9488.

Neubert, T., Allin, T.H., Stenbaek-Nielsen, H., Blanc, E., 2001. Sprites over Europe. Geophys. Res. Lett. 28, 3585. https://doi.org/10.1029/2001GL013427.

Neubert, T., Østgaard, N., Reglero, V., Blanc, E., Chanrion, O., Oxborrow, C.A., Orr, A., Tacconi, M., Hartnack, O., Bhanderi, D.D., 2019. The ASIM mission on the international space station. Space Sci. Rev. 215 (2), 26.

Newsome, R.T., Inan, U.S., 2010. Free-running ground-based photometric array imaging of transient luminous events. J. Geophys. Res. Space Physics 115, A00E41. https://doi.org/10.1029/2009JA014834.

Nijdam, S., van Veldhuizen, E.M., Ebert, U., 2010. Comment on NO_x production in laboratory discharges simulating blue jets and red sprites by H. Peterson et al. J. Geophys. Res. Space Physics 115, A12305. https://doi.org/10.1029/2010JA015861.

Opaits, D.F., Shneider, M.N., Howard, P.J., Miles, R.B., Milikh, G.M., 2010. Study of streamers in gradient density air: Table top modeling of red sprites. Geophys. Res. Lett. 37 (14).

Ott, L.E., Pickering, K.E., Stenchikov, G.L., Huntrieser, H., Schumann, U., 2007. Effects of lightning NO_x production during the 21 July European Lightning Nitrogen Oxides Project storm studied with a three-dimensional cloud-scale chemical transport model. J. Geophys. Res.-Atmos. 112 (D5).

Panasyuk, M., Svertilov, S., Bogomolov, V., Garipov, G., Barinova, V., Bogomolov, A., Veden'kin, N., Golovanov, I., Iyudin, A., Kalegaev, V., et al., 2016a. Experiment on the vernov satellite: Transient energetic processes in the earth's atmosphere and magnetosphere. part i: Description of the experiment. Cosm. Res. 54 (4), 261–269.

Panasyuk, M., Svertilov, S., Bogomolov, V., Garipov, G., Barinova, V., Bogomolov, A., Veden'kin, N., Golovanov, I., Iyudin, A., Kalegaev, V., et al., 2016b. Experiment on the vernov satellite: Transient energetic processes in the earth's atmosphere and magnetosphere. part ii. first results. Cosm. Res. 54 (5), 343–350.

Pancheshnyi, S.V., 2013. Effective ionization rate in nitrogen–oxygen mixtures. J. Phys. D. Appl. Phys. 46 (15), 155201.

Pancheshnyi, S.V., Starikovskii, A.Y., 2003. Two-dimensional numerical modelling of the cathode-directed streamer development in a long gap at high voltage. J. Phys. D. Appl. Phys. 36, 2683. https://doi.org/10.1088/0022-3727/36/21/014.

Pancheshnyi, S.V., Nudnova, M., Starikovskii, A., 2005. Development of a cathode-directed streamer discharge in air at different pressures: Experiment and comparison with direct numerical simulation. Phys. Rev. E 71 (1), 016407. https://doi.org/10.1103/PhysRevE.71.016407.

Parra-Rojas, F.C., Luque, A., Gordillo-Vázquez, F.J., 2013a. Chemical and electrical impact of lightning on the Earth mesosphere: The case of sprite halos. J. Geophys. Res. Space Physics 118, 5190. https://doi.org/10.1002/jgra.50449.

Parra-Rojas, F.C., Passas, M., Carrasco, E., Luque, A., Tanarro, I., Simek, M., Gordillo-Vázquez, F.J., 2013b. Spectroscopic diagnosis of laboratory air plasmas as a benchmark for spectral diagnosis of TLEs. J. Geophys. Res. Space Physics 118, 4649–4661. https://doi.org/10.1002/jgra.50433.

Parra-Rojas, F.C., Luque, A., Gordillo-Vázquez, F.J., 2015. Chemical and thermal impact of sprite streamers in the Earth mesosphere. J. Geophys. Res. Space Physics. https://doi.org/10.1002/2014JA020933.

Pasko, V.P., 2007. Red sprite discharges in the atmosphere at high altitude: the molecular physics and the similarity with laboratory discharges. Plasma Sources Sci. Technol. 16, 13. https://doi.org/10.1088/0963-0252/16/1/S02.

Pasko, V.P., 2008. Blue jets and gigantic jets: transient luminous events between thunderstorm tops and the lower ionosphere. Plasma Phys. Controlled Fusion 50 (12), 124050. https://doi.org/10.1088/0741-3335/50/12/124050.

Pasko, V.P., 2010. Recent advances in theory of transient luminous events. J. Geophys. Res. Space Physics 115, A00E35. https://doi.org/10.1029/2009JA014860.

Pasko, V.P., George, J.J., 2002. Three-dimensional modeling of blue jets and blue starters. J. Geophys. Res. Space Physics 107, 1458. https://doi.org/10.1029/2002JA009473.

Pasko, V.P., Stenbaek-Nielsen, H.C., 2002. Diffuse and streamer regions of sprites. Geophys. Res. Lett. 29 (10), 1440. https://doi.org/10.1029/2001GL014241.

Pasko, V.P., Inan, U.S., Taranenko, Y.N., Bell, T.F., 1995. Heating, ionization and upward discharges in the mesosphere due to intense quasi-electrostatic thundercloud fields. Geophys. Res. Lett. 22, 365. https://doi.org/10.1029/95GL00008.

Pasko, V.P., Inan, U.S., Bell, T.F., 1996a. Blue jets produced by quasi-electrostatic pre-discharge thundercloud fields. Geophys. Res. Lett. 23, 301. https://doi.org/10.1029/96GL00149.

Pasko, V.P., Inan, U.S., Bell, T.F., 1996b. Sprites as luminous columns of ionization produced by quasi-electrostatic thundercloud fields. Geophys. Res. Lett. 23, 649. https://doi.org/10.1029/96GL00473.

Pasko, V.P., Inan, U.S., Bell, T.F., Taranenko, Y.N., 1997. Sprites produced by quasi-electrostatic heating and ionization in the lower ionosphere. J. Geophys. Res. 102, 4529. https://doi.org/10.1029/96JA03528.

Pasko, V.P., Inan, U.S., Bell, T.F., 1998. Spatial structure of sprites. Geophys. Res. Lett. 25, 2123. https://doi.org/10.1029/98GL01242.

Pasko, V.P., Stanley, M.A., Mathews, J.D., Inan, U.S., Wood, T.G., 2002. Electrical discharge from a thundercloud top to the lower ionosphere. Nature 416, 152.

Pasko, V.P., Yair, Y., Kuo, C.L., 2012. Lightning related transient luminous events at high altitude in the Earth's atmosphere: Phenomenology, mechanisms and effects. Space Sci. Rev. 168, 475–516. https://doi.org/10.1007/s11214-011-9813-9.

Passas, M., Sánchez, J., Luque, A., Gordillo-Vázquez, F.J., 2014. Transient Upper Atmospheric Plasmas: Sprites and Halos. IEEE Trans. Plasma Sci. 42, 2664–2665. https://doi.org/10.1109/TPS.2014.2329320.

Passas, M., Madiedo, J.M., Gordillo-Vázquez, F.J., 2016a. High resolution spectroscopy of an Orionid meteor from 700 to 800 nm. Icarus 266, 134–141. https://doi.org/10.1016/j.icarus.2015.11.020.

Passas, M., Sánchez, J., Sánchez-Blanco, E., Luque, A., Gordillo-Vázquez, F.J., 2016b. GRASSP: a spectrograph for the study of transient luminous events. Appl. Opt. 55 (23), 6436–6442. https://doi.org/10.1364/AO.55.006436.

Pérez-Invernón, F.J., Gordillo-Vázquez, F.J., Luque, A., 2016. On the electrostatic field created at ground level by a halo. Geophys. Res. Lett. 43 (13), 7215–7222.

Pérez-Invernón, F.J., Luque, A., Gordillo-Vázquez, F.J., 2017. Three-dimensional modeling of lightning-induced electromagnetic pulses on Venus, Jupiter, and Saturn. J. Geophys. Res. Space Physics 122 (7), 7636–7653.

Pérez-Invernón, F.J., Luque, A., Gordillo-Vázquez, F.J., 2018a. Modeling the chemical impact and the optical emissions produced by lightning-induced electromagnetic fields in the upper atmosphere: the case of halos and elves triggered by different lightning discharges. J. Geophys. Res.-Atmos. 123 (14), 7615–7641.

Pérez-Invernón, F.J., Luque, A., Gordillo-Vázquez, F.J., Sato, M., Ushio, T., Adachi, T., Chen, A.B., 2018b. Spectroscopic diagnostic of halos and elves detected from space-based photometers. J. Geophys. Res.-Atmos. 123 (22), 12–917.

Pérez-Invernón, F.J., Gordillo-Vázquez, F.J., Smith, A.K., Arnone, E., Winkler, H., 2019. Global occurrence and chemical impact of stratospheric Blue Jets modeled with WACCM4. J. Geophys. Res.-Atmos. https://doi.org/10.1029/2018JD029593.

Pérez-Invernón, F.J., Malagón-Romero, A., Gordillo-Vázquez, F.J., Luque, A., 2020. The contribution of sprite streamers to the chemical composition of the mesosphere-lower thermosphere. Geophys. Res. Lett. 47 (n/a), e2020GL088578 https://doi.org/10.1029/2020GL088578.

Peterson, H., Bailey, M., Hallett, J., Beasley, W., 2009. NO_x production in laboratory discharges simulating blue jets and red sprites. J. Geophys. Res. Space Physics 114, A00E07. https://doi.org/10.1029/2009JA014489.

Petrov, N.I., Petrova, G.N., 1999. Physical mechanisms for the development of lightning discharges between a thundercloud and the ionosphere. J. Tech. Phys. 44, 472. https://doi.org/10.1134/1.1259327.

Peyrous, R., Lapeyre, R., 1982. Gaseous products created by electrical discharges in the atmosphere and condensation nuclei resulting from gaseous phase reactions. Atmosph. Environ. (1967) 16 (5), 959–968.

Picard, R.H., Inan, U.S., Pasko, V.P., Winick, J.R., Wintersteiner, P.P., 1997. Infrared glow above thunderstorms? Geophys. Res. Lett. 24, 2635. https://doi.org/10.1029/97GL02753.

Pickering, K.E., Bucsela, E., Allen, D., Ring, A., Holzworth, R., Krotkov, N., 2016. Estimates of lightning NOx production based on OMI NO_2 observations over the Gulf of Mexico. J. Geophys. Res.-Atmos. 121 (14), 8668–8691.

Pinto, O., Saba, M.M.F., Pinto, I.R.C.A., Tavares, F.S.S., Naccarato, K.P., Solorzano, N.N., Taylor, M.J., Pautet, P.D., Holzworth, R.H., 2004. Thunderstorm and lightning characteristics associated with sprites in Brazil. Geophys. Res. Lett. 31, L13103 https://doi.org/10.1029/2004GL020264.

Pontiga, F., Castellanos, A., 2006. Nitrogen oxides generation induced by negative corona discharge in $N_2 + O_2$ mixtures. In: 2006 IEEE Conference on Electrical Insulation and Dielectric Phenomena. IEEE, pp. 264–267.

Portmann, R., Daniel, J., Ravishankara, A., 2012. Stratospheric ozone depletion due to nitrous oxide: influences of other gases. Philosoph. Trans. R. Soc. B: Biol. Sci. 367 (1593), 1256–1264.

Price, C., Rind, D., 1992. A simple lightning parameterization for calculating global lightning distributions. J. Geophys. Res.-Atmos. 97 (D9), 9919–9933.

Price, C., Penner, J., Prather, M., 1997. NO_x from lightning: 1. Global distribution based on lightning physics. J. Geophys. Res.-Atmos. 102 (D5), 5929–5941.

Qin, J., Pasko, V.P., 2015. Dynamics of sprite streamers in varying air density. Geophys. Res. Lett. 42 (6), 2031–2036.

Qin, J., Celestin, S., Pasko, V.P., 2011. On the inception of streamers from sprite halo events produced by lightning discharges with positive and negative polarity. J. Geophys. Res. Space Physics 116, A06305. https://doi.org/10.1029/2010JA016366.

Qin, J., Celestin, S., Pasko, V.P., 2012. Minimum charge moment change in positive and negative cloud to ground lightning discharges producing sprites. Geophys. Res. Lett. 39 (22).

Qin, J., Celestin, S., Pasko, V.P., Cummer, S.A., McHarg, M.G., Stenbaek-Nielsen, H.C., 2013. Mechanism of column and carrot sprites derived from optical and radio observations. Geophys. Res. Lett. 40 (17), 4777–4782.

Qin, J., Pasko, V.P., McHarg, M.G., Stenbaek-Nielsen, H.C., 2014. Plasma irregularities in the D-region ionosphere in association with sprite streamer initiation. Nat. Commun. https://doi.org/10.1038/ncomms4740.

Raether, H., 1939. Die Entwicklung der Elektronenlawine in den Funkenkanal. Z. Phys. 112, 464. https://doi.org/10.1007/BF01340229.

Raizer, Y.P., 1991. Gas Discharge Physics. Springer-Verlag, Berlin, p. 449.

Raizer, Y.P., Simakov, A.N., 1998. Main factors determining the radius of the head of a long streamer and the maximum electric field near the head. Plasma Phys. Rep. 24, 700.

Raizer, Y.P., Milikh, G.M., Shneider, M.N., 2006. On the mechanism of blue jet formation and propagation. Geophys. Res. Lett. 33, L23801. https://doi.org/10.1029/2006GL027697.

Raizer, Y.P., Milikh, G.M., Shneider, M.N., 2007. Leader streamers nature of blue jets. J. Atmosph. Terrestr. Phys. 69, 925. https://doi.org/10.1016/j.jastp.2007.02.007.

Raizer, Y.P., Milikh, G.M., Shneider, M.N., 2010. Streamer- and leader-like processes in the upper atmosphere: Models of red sprites and blue jets. J. Geophys. Res. Space Physics 115, A00E42. https://doi.org/10.1029/2009JA014645.

Rakov, V.A., Uman, M.A., 2003. Lightning Physics and Effects. Cambridge University Press, Cambridge.

Rayment, S.W., Moruzzi, J.L., 1978. Electron detachment studies between O^- ions and nitrogen. Int. J. Mass Spectrom. 26, 321. https://doi.org/10.1016/0020-7381(78)80033-3.

Reising, S.C., Inan, U.S., Bell, T.F., Lyons, W.A., 1996. Evidence for continuing current in sprite-producing cloud-to-ground lightning. Geophys. Res. Lett. 23, 3639. https://doi.org/10.1029/96GL03480.

Ridley, B., Avery, M., Plant, J., Vay, S., Montzka, D., Weinheimer, A., Knapp, D., Dye, J., Richard, E., 2006. Sampling of chemical constituents in electrically active convective systems: Results and cautions. J. Atmos. Chem. 54 (1), 1–20.

Riousset, J.A., Pasko, V.P., Krehbiel, P.R., Thomas, R.J., Rison, W., 2007. Three-dimensional fractal modeling of intracloud lightning discharge in a New Mexico thunderstorm and comparison with lightning mapping observations. J. Geophys. Res.-Atmos. 112, D15203 https://doi.org/10.1029/2006JD007621.

Ripoll, J.F., Zinn, J., Colestock, P.L., Jeffery, C.A., 2014a. On the dynamics of hot air plasmas related to lightning discharges: 2. electrodynamics. J. Geophys. Res.-Atmos. 119 (15), 9218–9235.

Ripoll, J.F., Zinn, J., Jeffery, C.A., Colestock, P.L., 2014b. On the dynamics of hot air plasmas related to lightning discharges: 1. gas dynamics. J. Geophys. Res.-Atmos. 119 (15), 9196–9217.

Rison, W., Krehbiel, P.R., Stock, M.G., Edens, H.E., Shao, X.M., Thomas, R.J., Stanley, M. A., Zhang, Y., 2016. Observations of narrow bipolar events reveal how lightning is initiated in thunderstorms. Nat. Commun. 7, 10721.

Robledo-Martinez, A., Garcia-Villareal, L., 2016. Virtual anode effect in the propagation of positive streamers. Phys. Plasmas 23 (3), 033508.

Robledo-Martinez, A., Garcia-Villarreal, A., Sobral, H., 2017. Comparison between low-pressure laboratory discharges and atmospheric sprites. J. Geophys. Res. Space Physics 122 (1), 948–962.

Rodger, C.J., Seppälä, A., Clilverd, M.A., 2008. Significance of transient luminous events to neutral chemistry: Experimental measurements. Geophys. Res. Lett. 35 (7).

Romand, F., Vialatte, A., Croizé, L., Payan, S., Barthélémy, M., 2018. CO_2 thermal infrared signature following a sprite event in the mesosphere. J. Geophys. Res. Space Physics 123 (9), 8039–8050.

Rudlosky, S.D., Goodman, S.J., Virts, K.S., Bruning, E.C., 2019. Initial geostationary lightning mapper observations. Geophys. Res. Lett. 46 (2), 1097–1104.

Said, R., Cohen, M., Inan, U., 2013. Highly intense lightning over the oceans: Estimated peak currents from global GLD360 observations. J. Geophys. Res.-Atmos. 118 (13), 6905–6915.

Salut, M.M., Abdullah, M., Graf, K.L., Cohen, M.B., Cotts, B.R., Kumar, S., 2012. Long recovery VLF perturbations associated with lightning discharges. J. Geophys. Res. Space Physics 117, A08311. https://doi.org/10.1029/2012JA017567.

Salut, M.M., Cohen, M.B., Ali, M.A.M., Graf, K.L., Cotts, B.R., Kumar, S., 2013. On the relationship between lightning peak current and Early VLF perturbations. J. Geophys. Res. Space Physics 118. https://doi.org/10.1002/2013JA019087.

Sato, M., Fukunishi, H., 2003. Global sprite occurrence locations and rates derived from triangulation of transient Schumann resonance events. Geophys. Res. Lett. 30 (16), 1859.

Sato, M., Ushio, T., Morimoto, T., Kikuchi, M., Kikuchi, H., Adachi, T., Suzuki, M., Yamazaki, A., Takahashi, Y., Inan, U., et al., 2015. Overview and early results of the global lightning and sprite measurements mission. J. Geophys. Res.-Atmos. 120 (9), 3822–3851.

Schumann, U, Huntrieser, H, 2007. The global lightning-induced nitrogen oxides source. Atmos. Chem. Phys. 7 (14), 3823–3907. https://www.atmos-chem-phys.net/7/3823/2007/. https://doi.org/10.5194/acp-7-3823-2007.

Semeniuk, K., McConnell, J., Jin, J., Jarosz, J., Boone, C., Bernath, P., 2008. N_2O production by high energy auroral electron precipitation. J. Geophys. Res.-Atmos. 113 (D16).

Sentman, D.D., Stenbaek-Nielsen, H.C., 2009. Chemical effects of weak electric fields in the trailing columns of sprite streamers. Plasma Sources Sci. Technol. 18 (3), 034012 https://doi.org/10.1088/0963-0252/18/3/034012.

Sentman, D.D., Wescott, E.M., 1995. Red sprites and blue jets: Thunderstorm-excited optical emissions in the stratosphere, mesosphere, and ionosphere. Phys. Plasmas 2, 2514. https://doi.org/10.1063/1.871213.

Sentman, D.D., Wescott, E.M., Osborne, D.L., Hampton, D.L., Heavner, M.J., 1995. Preliminary results from the Sprites94 aircraft campaign: 1. Red sprites. Geophys. Res. Lett. 22, 1205. https://doi.org/10.1029/95GL00583.

Sentman, D.D., Wescott, E.M., Heavner, M.J., Moudry, D.R., 1996. Observations of sprite beads and balls. Eos Trans. AGU 77 (46). Fall–Meet.

Sentman, D.D., Moudry, D.R., Stenbaek-Nielsen, H.C., Wescott, E.M., São Sabbas, F.T., 2000. Electric field effects on chemical reaction rates within sprites. EOS Trans. Abstract A11E–01.

Sentman, D.D., Wescott, E.M., Picard, R.H., Winick, J.R., Stenbaek-Nielsen, H.C., Dewan, E.M., Moudry, D.R., São Sabbas, F.T., Heavner, M.J., Morrill, J., 2003. Simultaneous observations of mesospheric gravity waves and sprites generated by a midwestern thunderstorm. J. Atmos. Sol. Terr. Phys. 65, 537. https://doi.org/10.1016/S1364-6826(02)00328-0.

Sentman, D.D., Stenbaek-Nielsen, H.C., McHarg, M.G., Morrill, J.S., 2008a. Correction to "Plasma chemistry of sprite streamers". J. Geophys. Res.-Atmos. 113, D14399 https://doi.org/10.1029/2008JD010634.

Sentman, D.D., Stenbaek-Nielsen, H.C., McHarg, M.G., Morrill, J.S., 2008b. Plasma chemistry of sprite streamers. J. Geophys. Res.-Atmos. 113, D11112 https://doi.org/10.1029/2007JD008941.

Sentman, D.D., Wescott, E.M., 1993. Observations of upper atmospheric optical flashes recorded from an aircraft. Geophys. Res. Lett. 20 (24), 2857–2860. Wiley Online Library.

Shao, X.M., Krehbiel, P.R., 1996. The spatial and temporal development of intracloud lightning. J. Geophys. Res. 101, 26641. https://doi.org/10.1029/96JD01803.

Sheese, P.E., Walker, K.A., Boone, C.D., Bernath, P.F., Funke, B., 2016. Nitrous oxide in the atmosphere: First measurements of a lower thermospheric source. Geophys. Res. Lett. 43 (6), 2866–2872.

Simek, M., 2002. The modelling of streamer-induced emission in atmospheric pressure, pulsed positive corona discharge: N_2 second positive and NO-γ systems. J. Phys. D. Appl. Phys. 35, 1967. https://doi.org/10.1088/0022-3727/35/16/311.

Simek, M., DeBenedictis, S., Dilecce, G., Babickỳ, V., Clupek, M., Sunka, P., 2002. Time and space resolved analysis of $N_2(C^3\Pi_u)$ vibrational distributions in pulsed positive corona discharge. J. Phys. D. Appl. Phys. 35, 1981. https://doi.org/10.1088/0022-3727/35/16/312.

Smirnova, N., Lyakhov, A., Kozlov, S., 2003. Lower stratosphere response to electric field pulse. Int. J. Geomagn. Aeron. 3 (3), 281–287.

Soler, S., Pérez-Invernón, F.J., Gordillo-Vázquez, F.J., Luque, A., Li, D., Malagón-Romero, A., Neubert, T., Chanrion, O., Reglero, V., Navarro-González, J., Lu, G., Zhang, H., Huang, A., Ostgaard, N., 2020. Blue optical observations of narrow bipolar events by ASIM suggest corona streamer activity in thunderstorms. J. Geophys. Res.-Atmos. https://doi.org/10.1029/2020JD032708.

Sosnin, E.A., Baksht, E.K., Kuznetsov, V.S., Panarin, V.A., Pechenitsin, D.S., Skakun, V.S., Tarasenko, V.F., 2019. Apokamp discharge as a laboratory analogue of the transient luminous events of middle atmosphere. In: XIV International Conference on Pulsed Lasers and Laser Applications. International Society for Optics and Photonics, 11322, p. 1132225.

Stanley, M., Krehbiel, P., Rison, W., Moore, C., Brook, M., Vaughan, O., 1996. Observations of sprites and jets from Langmuir Laboratory, New Mexico. Eos Trans. AGU 77 (F69), A11A–7.

Stanley, M., Krehbiel, P., Brook, M., Moore, C., Rison, W., Abrahams, B., 1999. High speed video of initial sprite development. Geophys. Res. Lett. 26, 3201. https://doi.org/10.1029/1999GL010673.

Stanley, M., Brook, M., Krehbiel, P., Cummer, S.A., 2000. Detection of daytime sprites via a unique sprite ELF signature. Geophys. Res. Lett. 27, 871. https://doi.org/10.1029/1999GL010769.

Stenbaek-Nielsen, H.C., McHarg, G.G., 2007. High time-resolution sprite observations. AGU Fall Meet. Abstr. A7.

Stenbaek-Nielsen, H.C., McHarg, M.G., 2008. High time-resolution sprite imaging: observations and implications. J. Phys. D. Appl. Phys. 41 (23), 234009 https://doi.org/10.1088/0022-3727/41/23/234009.

Stenbaek-Nielsen, H.C., Moudry, D.R., Wescott, E.M., Sentman, D.D., São Sabbas, F.T., 2000. Sprites and possible mesospheric effects. Geophys. Res. Lett. 27, 3829. https://doi.org/10.1029/2000GL003827.

Stenbaek-Nielsen, H.C., McHarg, M.G., Kanmae, T., Sentman, D.D., 2007. Observed emission rates in sprite streamer heads. Geophys. Res. Lett. 34, L11105. https://doi.org/10.1029/2007GL029881.

Stenbaek-Nielsen, H.C., Kanmae, T., McHarg, M.G., Haaland, R., 2013. High-speed observations of sprite streamers. Surv. Geophys. 34 (6), 769–795. https://doi.org/10.1007/s10712-013-9224-4. Springer.

Strikovskiy, A., Evtushenko, A., Gushchin, M., Korobkov, S., Kostrov, A., 2017. Pulsed high-voltage discharge in air with a pressure gradient. Plasma Phys. Rep. 43 (10), 1031–1038.

Su, H.T., Hsu, R.R., Chen, A.B.C., Lee, Y.J., Lee, L.C., 2002. Observation of sprites over the Asian continent and over oceans around Taiwan. Geophys. Res. Lett. 29 (4), 1044. https://doi.org/10.1029/2001GL013737.

Su, H.T., Hsu, R.R., Chen, A.B., Wang, Y.C., Hsiao, W.S., Lai, W.C., Lee, L.C., Sato, M., Fukunishi, H., 2003. Gigantic jets between a thundercloud and the ionosphere. Nature 423, 974.

Sukhorukov, A.I., Mishin, E.V., Stubbe, P., Rycroft, M.J., 1996a. On blue jet dynamics. Geophys. Res. Lett. 23, 1625. https://doi.org/10.1029/96GL01367.

Sukhorukov, A.I., Rudenchik, E.A., Stubbe, P., 1996b. Simulation of the strong lightning pulse penetration into the lower ionosphere. Geophys. Res. Lett. 23, 2911. https://doi.org/10.1029/96GL02881.

Suszcynsky, D.M., Roussel-Dupré, R., Lyons, W.A., Armstrong, R.A., 1998. Blue-light imagery and photometry of sprites. J. Atmos. Sol. Terr. Phys. 60, 801. https://doi.org/10.1016/S1364-6826(98)00027-3.

Suzuki, T., Hayakawa, M., Matsudo, Y., Michimoto, K., 2006. How do winter thundercloud systems generate sprite-inducing lightning in the Hokuriku area of Japan? Geophys. Res. Lett. 33, L10806 https://doi.org/10.1029/2005GL025433.

Taranenko, Y.N., Inan, U.S., Bell, T.F., 1992. Optical signatures of lightning-induced heating of the D region. Geophys. Res. Lett. 19 (18), 1815–1818.

Taranenko, Y.N., Inan, U.S., Bell, T.F., 1993. The interaction with lower ionosphere of electromagnetic pulses from lightning: Excitation of optical emissions. Geophys. Res. Lett. 20, 2675–2678.

Tarasenko, V.F., Beloplotov, D.V., Lomaev, M.I., 2016. Colored diffuse mini jets in runaway electrons preionized diffuse discharges. IEEE Trans. Plasma Sci. 44 (4), 386–392.

Taylor, M., Clark, S., 1996. High resolution CCD and video imaging of sprites and elves in the N_2 first positive band emission. Eos Trans. AGU 77 (F60), A71B–4.

Teunissen, J., Ebert, U., 2017. Simulating streamer discharges in 3D with the parallel adaptive Afivo framework. J. Phys. D. Appl. Phys. 50, 474001 https://doi.org/10.1088/1361-6463/aa8faf.

Tian, H., Yang, J., Lu, C., Xu, R., Canadell, J.G., Jackson, R.B., Arneth, A., Chang, J., Chen, G., Ciais, P., et al., 2018. The global N_2O model intercomparison project. Bull. Am. Meteorol. Soc. 99 (6), 1231–1251.

Tilles, J.N., Liu, N., Stanley, M.A., Krehbiel, P.R., Rison, W., Stock, M.G., Dwyer, J.R., Brown, R., Wilson, J., 2019. Fast negative breakdown in thunderstorms. Nat. Commun. 10 (1), 1648.

Tost, H., Jöckel, P., Lelieveld, J., 2007. Lightning and convection parameterisations–uncertainties in global modelling. Atmos. Chem. Phys. 7 (17), 4553–4568.

Turunen, E., Matveinen, H., Tolvanen, J., Ranta, H., 1996. D-region ion chemistry model. STEP handbook of ionospheric models, pp. 1–25.

Ushio, T., Sato, M., Morimoto, T., Suzuki, M., Kikuchi, H., Yamazaki, A., Takahashi, Y., Hobara, Y., Inan, U., Linscott, I., et al., 2011. The global lightning and sprite measurement (glims) mission on international space station. IEEJ Trans. Fundam. Mater. 131 (12), 971–976.

van der Velde, O.A., Montanyà, J., López, J.A., Cummer, S.A., 2019. Gigantic jet discharges evolve stepwise through the middle atmosphere. Nat. Commun. 10 (1), 1–10.

van der Velde, O.A., Montanyà, J., 2016. Statistics and variability of the altitude of elves. Geophys. Res. Lett. 43, 5467–5474. https://doi.org/10.1002/2016GL068719.

Vitello, P.A., Penetrante, B.M., Bardsley, J.N., 1994. Simulation of negative-streamer dynamics in nitrogen. Phys. Rev. E 49, 5574. https://doi.org/10.1103/PhysRevE.49.5574.

Walker, T.D., Christian, H.J., 2019. Triggered lightning spectroscopy: 2. a quantitative analysis. J. Geophys. Res.-Atmos. 124 (7), 3930–3942.

Wang, Y., DeSilva, A., Goldenbaum, G., Dickerson, R., 1998. Nitric oxide production by simulated lightning: Dependence on current, energy, and pressure. J. Geophys. Res.-Atmos. 103 (D15), 19149–19159.

Watson, S.S., Marshall, T.C., 2007. Current propagation model for a narrow bipolar pulse. Geophys. Res. Lett. 34, L04816. https://doi.org/10.1029/2006GL027426.

Wescott, E.M., Sentman, D., Osborne, D., Hampton, D., Heavner, M., 1995. Preliminary results from the Sprites94 aircraft campaign: 2. Blue jets. Geophys. Res. Lett. 22, 1209. https://doi.org/10.1029/95GL00582.

Wescott, E.M., Sentman, D.D., Heavner, M.J., Hampton, D.L., Osborne, D.L., Vaughan, O. H., 1996. Blue starters: Brief upward discharges from an intense Arkansas thunderstorm. Geophys. Res. Lett. 23, 2153. https://doi.org/10.1029/96GL01969.

Wescott, E.M., Sentman, D.D., Stenbaek-Nielsen, H.C., Huet, P., Heavner, M.J., Moudry, D.R., 2001a. New evidence for the brightness and ionization of blue starters and blue jets. J. Geophys. Res. 106, 21549. https://doi.org/10.1029/2000JA000429.

Wescott, E.M., Stenbaek-Nielsen, H.C., Sentman, D.D., Heavner, M.J., Moudry, D.R., Sabbas, F.T.S., 2001b. Triangulation of sprites, associated halos and their possible relation to causative lightning and micrometeors. J. Geophys. Res. 106, 10467. https://doi.org/10.1029/2000JA000182.

Wiens, K.C., Hamlin, T., Harlin, J., Suszcynsky, D.M., 2008. Relationships among narrow bipolar events, "total" lightning, and radar-inferred convective strength in great plains thunderstorms. J. Geophys. Res.-Atmos. 113 (D5).

Williams, E.R., 2001. Sprites, elves, and glow discharge tubes. Phys. Today 54 (11), 110000. https://doi.org/10.1063/1.1428435.

Williams, E.R., 2006. Problems in lightning physics–the role of polarity asymmetry. Plasma Sources Sci. Technol. 15, 91. https://doi.org/10.1088/0963-0252/15/2/S12.

Williams, E.R., Valente, M., Gerken, E., Golka, R., 2006. Calibrated radiance measurements with an air-filled glow discharge tube: Application to sprites in the mesosphere. In: Sprites, Elves and Intense Lightning Discharges. Springer, pp. 237–251.

Williams, E.R., Kuo, C.L., Bór, J., Sátori, G., Newsome, R.T., Adachi, R., Boldi, R., Chen, A., Downes, E., Hsu, R.R., Lyons, W., Saba, M.M.F., Taylor, M., 2012. Su HT. Resolution of the sprite polarity paradox: The role of halos. Radio Sci. 47 (2) https://doi.org/10.1029/2011RS004794.

Wilson, C.T.R., 1924. The electric field of a thundercloud and some of its effects. Proc. Phys. Soc. Lond. 37 (1), 32D.

Winkler, H., Notholt, J., 2014. The chemistry of daytime sprite streamers–a model study. Atmos. Chem. Phys. 14 (7), 3545–3556.

Winkler, H., Notholt, J., 2015. A model study of the plasma chemistry of stratospheric blue jets. J. Atmos. Sol. Terr. Phys. 122, 75–85.

Xu, C., Huret, N., Garnung, M., Celestin, S., 2020. A new detailed plasma-chemistry model for the potential impact of blue jet streamers on atmospheric chemistry. J. Geophys. Res.-Atmos. 125 (6), e2019JD031789.

Yair, Y., Price, C., Levin, Z., Joseph, J., Israelevitch, P., Devir, A., Moalem, M., Ziv, B., Asfur, M., 2003. Sprite observations from the space shuttle during the Mediterranean Israeli dust experiment (MEIDEX). J. Atmos. Sol. Terr. Phys. 65, 635. https://doi.org/10.1016/S1364-6826(02)00332-2.

Yair, Y., Rubanenko, L., Mezuman, K., Elhalel, G., Pariente, M., Glickman-Pariente, M., Ziv, B., Takahashi, Y., Inoue, T., 2013. New color images of transient luminous events from dedicated observations on the international space station. J. Atmos. Sol. Terr. Phys. 102, 140–147.

Yamada, T., Sato, T., Adachi, T., Winkler, H., Kuribayashi, K., Larsson, R., Yoshida, N., Takahashi, Y., Sato, M., Chen, A., et al., 2020. HO Generation Above Sprite-Producing Thunderstorms Derived from Low-Noise SMILES Observation Spectra. Geophys. Res. Lett. 47 (3), e60090.

Yang, J., Qie, X., Guangshu, Z., Yang, Z., Tong, Z., 2008. Red sprites over thunderstorms in the coast of Shandong Province, China. Chin. Sci. Bull. 53 (7), 1079–1086.

Yang, J., Qie, X., Zhong, L., He, Q., Lu, G., Wang, Z., Wang, Y., Liu, N., Liu, F., Peng, K. M., et al., 2020. Analysis of a gigantic jet in southern china: morphology, meteorology, storm evolution, lightning, and narrow bipolar events. J. Geophys. Res.-Atmos. 125 (15), e2019JD031538.

Zahn, A., Brenninkmeijer, C., Crutzen, P., Parrish, D., Sueper, D., Heinrich, G., Güsten, H., Fischer, H., Hermann, M., Heintzenberg, J., 2002. Electrical discharge source for tropospheric "ozone-rich transients". J. Geophys. Res.-Atmos. 107 (D22), ACH-16.

Zhang, X., Yin, Y., van der A, R., Lapierre, J.L., Chen, Q., Kuang, X., Yan, S., Chen, J., He, C., Shi, R., 2020. Estimates of lightning NO_x production based on high-resolution OMI NO_2 retrievals over the continental US. Atmosph. Meas. Techn. 13 (4).

Zhelezniak, M.B., Mnatsakanian, A.K., Sizykh, S.V., 1982. Photoionization of nitrogen and oxygen mixtures by radiation from a gas discharge. Teplofizika Vysokikh Temp. 20, 423.